
A REPORT
ON
DESIGN, DEVELOPMENT & INTEGRATION
OF AOTF BASED NIR SPECTROPHOTOMETER

Authored by

R.Govindaraj, Senior Principal Scientist
G.Ganesh, Formerly Research Intern

*Central Electronics Engineering Research Institute
Chennai Centre
CSIR Madras Complex, Taramani
Chennai - 600113*



JANUARY 2015

Copyright © 2016

PUBLISHED BY

CSIR - CENTRAL ELECTRONICS ENGINEERING RESEARCH INSTITUTE, INDIA



This work is licensed under a Creative Commons Attribution-NonCommercial 4.0 International License (the “License”); you may not use this file except in compliance with the License. You may obtain a copy of the License at <http://creativecommons.org/licenses/by-nc/4.0/>. See the License for the governing permissions and limitations under the License.

First printing, January 2015

Acknowledgement

We sincerely thank our Director, CEERI, Pilani for approving the AOTF based spectrophotometer activity under supra institutional project programme and supported us with necessary financial sanctions to carry out the R&D works at CEERI Chennai Centre.

We are also thankful to Shri K.Subrahmanyam, retired Scientist-in-charge, CEERI Chennai Centre and Dr.ASV.Sarma, Scientist-in-charge, CEERI Chennai Centre for their constant support and encouragement in executing the activity.

We would like to thank Shri.P.K.Anil, retired Principal Technical Officer, CEERI Chennai Centre, for his constant technical support in interfacing AOTF signal processing circuits with embedded hardware. We are thankful to Shri T.Chinnu, Senior Technician, CEERI Chennai Centre for the technical support provided in testing the electronic circuit modules.

We acknowledge the efforts put by the student project trainees viz. Shri Aditya Rajaraman, Shri V.P.Bhaskar and Shri Debanjum Singh Solanky of Birla Institute of Technology & Science [BITS], Pilani for their software development support towards this activity.

Our thanks are also due to IPLG team, drawing and mechanical sections, staff of stores and secretariat, CEERI Chennai Centre for their support at various stages of project activity execution.

About the Report

This technical report records the development history of an Acousto-Optic Tunable Filter based Near Infrared Spectrophotometer undergone at CSIR-CEERI Chennai centre. Elucidation of general systems architecture, integration, testing and updating the system with better technologies is also included. It also reports about the various testing experiments undertaken and their results throughout the stable development stages.

Fundamental theoretical aspects of the Spectroscopy in general and principles behind the operation of acousto-optic tunable filter is included in detail. A thorough understanding of the instrument design and development with their corresponding systems visualization are explained. The report contains the required specifications of the submodules procured and integrated together for constructing the instrument which are listed in the appendices.

It especially presents a documentation for generalized programming interface to facilitate further additions in the software domain of the instrument. Eventhough the report details about the development of the NIR-AOTF spectrophotometer, it necessitates data analytics solution with the inclusion of chemometrics to analyze the spectral data.

This report records the updates made in embedded system & supervisory software system from proprietary tool chain to free hardware and software tool chain. Realizing the enhancement has further encouraged us to update possible modules of the instrument by utilizing publicly licensed designs and tools. As a pragmatic proof this report itself has been completely compiled using Copyleft - GPL(general public license) based tools and packages such as, inkscape, gimp, & L^AT_EX. We have not only witnessed a great improvement in publishing quality but also had a splendid documentation experience in preparing this technical report.

Contents

Introduction to Spectroscopy	1
What is Spectroscopy	1
Origin of Electromagnetic Radiation	3
Interaction of Electromagnetic energy with Matter	3
Electromagnetic Spectrum	5
Wavefunction & Schrodinger Equation	6
Potential Energy, Harmonic Oscillation & Molecular Vibration	7
Quantum Harmonic Oscillator	8
Quantum Anharmonic Oscillator	10
Energy Associated with a Molecule	11
Molecular Vibration	12
Internal Coordinates	13
Measured Spectrum and Uncertainty	14
Beer-Lambert's Law	16
 Acousto-Optics	 21
Acousto-Optic Theory	22
Bragg diffraction	23
Characteristic Parameters	25
Acoustic-Optic Tunable Filter	26
Working Principle	27
Advantages of Acousto-optic Tunable Filter	29
Mechanical Issues	30
Temperature Issues	30
 AOTF System Integration - I	 31
Non-linear characteristics of AOTF & Radio Frequency Driver	36
Implementation of Prototype Analog Signal Processing Unit	39
 AOTF System Integration - II	 47
Prototyping Microcontroller based Embedded System	47
The Mechanism : Embedded Task	49
Implementation through Proprietary System	49
Implementation through Free System	50

Prototyping Supervisory System	51
Implementation through Proprietary System	52
Implementation through Free System	53
Testing	55
RF Driver Test	55
Spectral Test Output from the Spectrophotometer	57
List of Necessary Conceptual/Implementation Updates	63
Generalized Instrumentation Platform Specification & Updates	63
Updating the Analog Signal Processing System	63
Hardware that supports simple firmware and whole operating system	63
Software platform that completely covers Desktop, Embedded and Web Technologies	64
Inclusion of Machine Learning, Data Analytics and Visualization Capability	64
Attempting to form Instrument Grid	65
Spectroscopy Specific Updates	65
Spectral Manipulation	65
Data Handling	66
Data Analysis	66
Quantitative Analysis	66
Spectral Library Search	67
Scripting, Programming and Automation	67
Supported File Formats for Saving Data (Try only for which are open)	67
Appendix A	69
Complete AOTF instrument Integrated Setup	69
Appendix B	71
Acousto Optic Tunable Filter Specification	71
NOTE	72
Appendix C	73
InGaAs Detector Specification	73
InGaAs Detector Spectral Response	74
Appendix D	75
TE Cooler Specification	75
Appendix E	77
TE Cooling - Temperature Controller	77
Electrical functionality of TEC controller	77
Features	78
Appendix F	79
Pre Amplifier Specification	79
Equivalent circuit of Transimpedance Preamplifier	80

Appendix G	81
Circuit Schematic for the Analog Signal Processing Unit	81
Appendix H	83
LookUp Table(LUT) - Matched for Nonlinear Characteristics of RF Driver-AOTF tuning curve	83
NOTE	87
Bibliography	89
Index	93
Published Works	95
About the Authors	97

List of Figures

1	3D representation of Electromagnetic wave and its Propagation	1
2	A plot of the amplitude of the electric vector of a light wave versus time.	2
3	Oscillators in an Atom and a Molecule	3
4	Absorption of Electromagnetic Radiation	4
5	Electromagnetic Spectrum	5
6	Comparison of Harmonic and Anharmonic potential functions of a diatomic oscillator	8
7	Harmonic potential functions for a diatomic oscillator	8
8	Anharmonic potential functions for a diatomic oscillator	10
9	Energy level diagram for a molecule, showing rotational, vibrational and electronic energy levels	12
10	Normal mode of vibration for a simple diatomic molecule	13
11	Types of Internal Coordinates	14
12	A line spectrum of Transmission and Absorption	15
13	Line broadening phenomenon of Absorption Spectra	15
14	Beer's law experimental setup	16
15	Elastic Collision between a Photon and a CH_4 molecule	17
16	InElastic Collision between a Photon and a CH_4 with change in direction of photon	17
17	InElastic Collision between a Photon and a CH_4 with absorbance	18
18	Interaction of light and solid material	23
19	Diffraction in Bragg Cell	23
20	Variation of Refractive index in Bragg cell for an acoustic wave	24
21	Refractive index profile in Bragg cell created by an acoustic wave	25
22	AOTF anatomy and Diffraction process	27
23	Wave-vector diagram of an Acousto-optic(AO) crystal	29
24	Layered abstract view of the Spectrophotometer system	31
25	Block Schematic of NIR-AOTF Spectrophotometer	32
26	Signal flow Schematic of NIR-AOTF Spectrophotometer	34
27	Voltage - Frequency characteristic curve of RF Driver	36
28	Output Power characteristics of RF Driver	36
29	Frequency - Wavelength tuning characteristics of AOTF	37
30	Filtering process involved with RF Driver and AOTF	37
31	Interpretation of Tuning curve into lookuptable(LUT) involved with filtering process	38
32	Analog Signal Processing Chain Block Schematic	39

33	First Stage - Voltage Amplifier Unit	40
34	Notch Filter Unit	41
35	AC - Voltage Amplifier Unit	41
36	RMS to DC Converter Unit	42
37	Final Stage DC Amplification before ADC	42
38	PWM Clipper Stage	43
39	DAC to VCO Signal Conditioning Unit	43
40	Pre-amplifier Output with 1× CRO probe Setting	44
41	Amplified AC component of the Reference signal with 10× CRO probe Setting	44
42	Pulse Width Modulation Signal applied to RF driver with 1× CRO probe Setting	44
43	Amplified AC component of the Sample signal with 10× CRO probe setting during scan	45
44	Fabricated electronic ASPU board	45
45	Generic Microcontroller with an embedded task interfaced with ASPU and Supervisory system	47
46	Flowchart of the embedded task	48
47	Integration using proprietary embedded microcontroller	49
48	Integration using free microcontroller platform	50
49	DAC output from MCP 4725 interfaced with Arduino	51
50	Supervisory system designed for the spectrophotometer	51
51	GUI based on Visual Basic	52
52	Trilayer approach of integrating embedded and supervisory layers	53
53	GUI based on HTML5 & JavaScript	54
54	RF rise time test output captured with MSO	55
55	RF fall time test output captured with MSO	56
56	Constructed plot of RF power for change in modulation voltage	56
57	Experimental observation of RF power Vs. modulation voltage	57
58	Single scan NIR-spectra of PET sample	58
59	Overlaid spectral scan of PET sample with different lamp power	58
60	Spectral test output of NIR-AOTF Spectrophotometer with different samples	59
61	NIR spectra of Oil sample with no change in modulation voltage and frequency	60
62	NIR spectra of Oil sample with change in modulation frequency	60
63	NIR spectra of Oil sample with change in both modulation voltage and frequency	61
64	Completely Integrated NIR-AOTF Spectrometer Unit (Present Status)	70
65	TE cooler and its Heat Sink assembly	76
66	Complete Assembly of TE Cooler and its Controller	76
67	Electrical block diagram of TEC controller unit	77
68	TE cooling - Temperature Controller unit with its Heat Sink Assembly	78
69	TE cooler and its assembly	80
70	Circuit Schematic of designed ASPU - page 1	81
71	Circuit Schematic of designed ASPU - page 2	82

Glossary

AC Alternating Current. [40, 41](#)

AO Acousto-Optics. [xi, 23, 24, 28, 30](#)

AOTF Acousto-Optic Tunable Filter. [26, 29, 31, 49, 52, 69](#)

ARM Advanced RISC Machines. [49](#)

ASPU Analog Signal Processing Unit. [xii, 43, 48, 69](#)

BNC Bayonet Neill-Concelman Coaxial RF Connector. [75](#)

CSS Cascading Style Sheets. [54](#)

DAQ Data Acquisition. [30, 35](#)

DC Direct Current. [41](#)

FSV Full Scale Voltage. [48](#)

FWHM Full Width Half Maximum. [29, 39](#)

GNU GNU is Not Unix. [50](#)

GUI Graphical User Interface. [xii, 52, 54](#)

HTML Hyper Text Markup Language. [xii, 54](#)

IDE Integrated Development Environment. [50, 52](#)

InGaAs Indium Gallium Arsenide. [39, 40, 69](#)

LED Light Emitting Diode. [78](#)

LUT LookUp Table. [ix, xi, 38, 55, 83](#)

NIR Near Infrared. [31](#), [52](#)

PA Pre-amplifier. [40](#)

PWM Pulse Width Modulation. [42](#)

RF Radio Frequency. [26](#), [36](#)

SMA Sub Miniature Version-A Coaxial RF Connector. [71](#), [75](#)

SMB Sub Miniature Version-B Coaxial RF Connector. [71](#)

TEC Thermoelectric Cooler. [40](#), [77](#), [78](#)

VIS Visualization. [52](#)

Introduction to Spectroscopy

What is Spectroscopy

Spectroscopy is the study of the interaction of light with matter. The fundamental measurement obtained in spectroscopy is a spectrum, which is a plot of measured light intensity versus some property of light. An instrument used to measure a spectrum electronically is called a spectrophotometer, or sometimes simply a spectrometer. There are many different kinds of spectrophotometers in the world, and they use many different types of light to obtain spectra. The details of how these instruments work are beyond the scope of this report. Literature are available [1] [2] [3] [4] that deals with the architecture and instrumentation of the spectrophotometers.

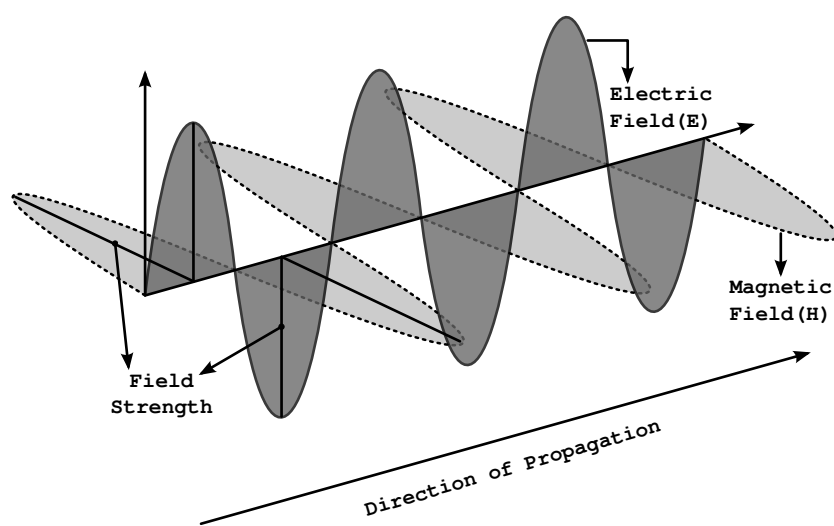


Figure 1: 3D representation of Electromagnetic wave and its Propagation.

To understand how a molecule absorbs light, we must first understand something about the properties of light. Light can be thought of as being a wave or a particle, depending upon the particular property of light under consideration. This wave-particle duality is an inherent feature of light. For now, we will consider light as a wave. Light beams are composed of electric and magnetic waves that undulate in planes perpendicular to each other. Light is properly called electromagnetic radiation because it contains electric and magnetic waves. According to electromagnetic theory, electromagnetic radiation is a form of energy that is composed

of oscillating electric and magnetic fields acting in planes that are perpendicular to each other and to the direction of propagation [5] as shown in Figure 1.

The light wave traverses through space in a direction defined by the line where the two planes containing the waves intersect. The interaction of the electric wave of light, the electric vector, with matter is what is usually measured to obtain absorbance spectra. The amplitude of the electric vector changes over time and has the form of a sine wave, as shown in Figure 2.

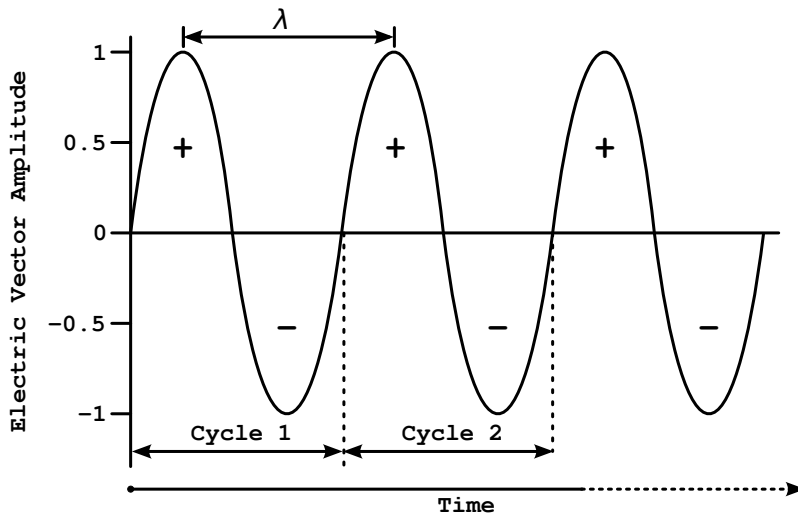


Figure 2: A plot of the amplitude of the electric vector of a light wave versus time.

One of the properties used to distinguish between different types of light is the light's wavelength. A wavelength is the distance between adjacent crests or troughs of a wave, as seen in Figure 2. Wavelength is denoted by the lowercase Greek letter λ . Different types of light have different wavelengths. For example, infrared radiation is longer in wavelength than visible light, which is longer in wavelength than X-rays. Another property of a light beam is its frequency. Frequency is denoted by the Greek letter ν , and equals the number of cycles a wave undergoes per second.

A cycle is considered complete when a light wave starts at zero and then crosses the x-axis twice. The wave in Figure 2 undergoes three cycles. Frequency is measured in cycles/s or Hertz (Hz). Frequency is a measure of the number of cycles of a light wave per unit time. The frequency, wavelength, and speed of a light beam are related to each other via the following equation

$$c = \nu\lambda$$

where,

c = the speed of light (3×10^8 m/s)

ν = frequency in Hertz s^{-1}

λ = wavelength in metres

Origin of Electromagnetic Radiation

The flux of energy of an electromagnetic radiation along the direction of propagation is equally divided between electric and magnetic fields. Electromagnetic radiations are produced by accelerating electric charges and electric charge accelerations are produced when electromagnetic radiations are absorbed. Electromagnetic radiations of different energies are produced when the energy involved in the acceleration of electric charges is different [6]. The origin of electromagnetic radiation varies widely. A system that emits radiation is also capable of absorbing that radiation. An example of this is the absorption and emission of yellow light by sodium atoms by which sodium is quantitatively determined by atomic spectrometry. We use a sodium lamp that emits energy at a particular frequency which is produced when an excited electron relaxes from an excited state to the ground state, exciting another sodium atom's electron from a ground state to the same corresponding excited state.

Interaction of Electromagnetic energy with Matter

Matter is composed of molecules or atoms. Atoms are composed of nuclei containing protons, neutrons and electrons surrounding the nucleus. This means that matter is full of *oscillators* of very different dimensions. Any of these can be excited to a higher level using electromagnetic radiation of appropriate energy. For example, vibration in a molecule containing two atoms is equivalent to a simple oscillator. This vibration can be excited to the next vibrational level by irradiating the molecule with infrared radiation of appropriate energy (i.e. appropriate frequency).

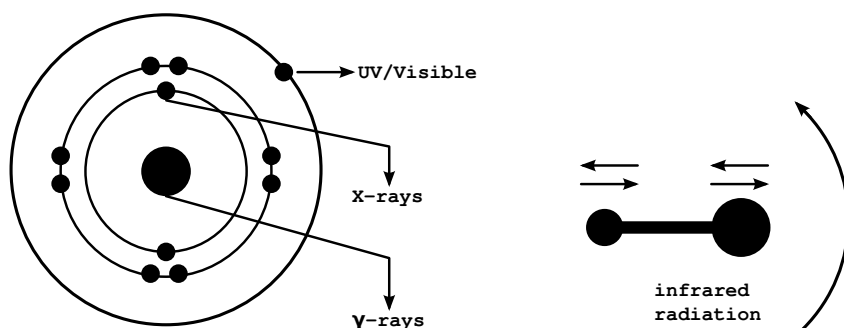


Figure 3: Oscillators in an Atom and a Molecule

As mentioned earlier, electromagnetic radiations originate from oscillators arising from the acceleration of electric charges. As depicted in Figure 3, γ -rays are produced by the oscillators in the atomic nuclei; x-rays are produced by the oscillators arising from the tightly bound electrons in the vicinity of the nucleus of atoms; visible and ultraviolet radiations are produced by the oscillators arising from the outer electrons in the molecules and atoms; infrared radiation is produced by the oscillators arising from the vibration and rotation of molecules. Now we should be able to understand why electromagnetic radiations of different dimensions are used in studying nuclear, electronic, vibrational and rotational transitions in matter.

If the energy of the radiation does not match the energy difference between the excited and ground states of the molecule, no absorption will take place as shown in Figure 4. If the frequency of the radiation that is absorbed by the molecule is ν , then the energy difference between the ground state and excited state is given by the equation

$$\Delta E = E_e - E_g = h\nu = h\frac{c}{\lambda} = h\bar{\nu}c$$

where,

E_e, E_g are absolute energies of the excited and ground states.

h is the planck's constant.

$\bar{\nu}$ is wavenumber in cm^{-1} .

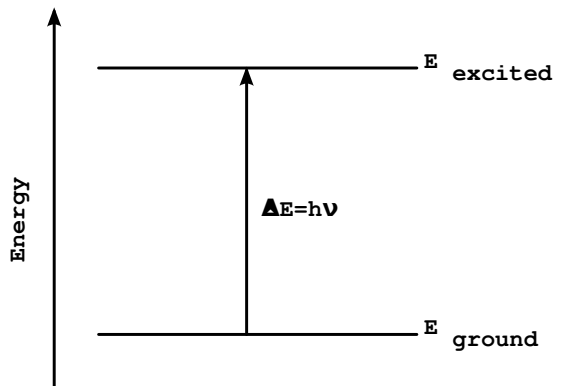


Figure 4: Absorption of Electromagnetic Radiation

Chemical bonds between atoms in a molecule form because they make the situation more stable for the involved atoms, which generally means the sum of the energy levels for the involved atoms in the molecule is lower than if the atoms were not so bonded. As separate atoms approach each other to covalently bond, their orbitals affect each other's energy levels to form *bonding and antibonding molecular orbitals*. An antibonding orbital is a type of molecular orbital that, if occupied by electrons, weakens the bond between two atoms and helps to raise the energy of the molecule relative to the separated atoms. Such an orbital has one or more nodes in the bonding region between the nuclei. The density of the electrons in the orbital is concentrated outside the bonding region and acts to pull one nucleus away from the other and tends to cause mutual repulsion between the two atoms.

The energy level of the bonding orbitals is lower, and the energy level of the antibonding orbitals is higher [7]. For the bond in the molecule to be stable, the covalent bonding electrons occupy the lower energy bonding orbital, which may be signified by such symbols as σ or π depending on the situation. Corresponding anti-bonding orbitals can be signified by adding an asterisk to get σ^* or π^* orbitals. A non-bonding orbital in a molecule is an orbital with electrons in outer shells which do not participate in bonding and its energy level is the same as that of the constituent atom. Such orbitals can be designated as n orbitals. The electrons in an n orbital are typically lone pairs. In polyatomic molecules, different vibrational and rotational energy levels are also involved.

Electromagnetic Spectrum

ELECTROMAGNETIC RADIATION had been first linked to electromagnetism in 1845, when Michael Faraday noticed that the polarization of light traveling through a transparent material responded to a magnetic field (see Faraday effect). During the 1860s James Maxwell developed four partial differential equations for the electromagnetic field. Two of these equations predicted the possibility of, and behavior of, waves in the field. Analyzing the speed of these theoretical waves, Maxwell realized that they must travel at a speed that was about the known speed of light. This startling coincidence in value led Maxwell to make the inference that light itself is a type of electromagnetic wave.

Maxwell's equations predicted an infinite number of frequencies of electromagnetic waves, all traveling at the speed of light. This was the first indication of the existence of the entire electromagnetic spectrum. Maxwell's predicted waves included waves at very low frequencies compared to infrared, which in theory might be created by oscillating charges in an ordinary electrical circuit of a certain type. Attempting to prove Maxwell's equations and detect such low frequency electromagnetic radiation, in 1886 the physicist Heinrich Hertz built an apparatus to generate and detect what is now called radio waves. Hertz found the waves and was able to infer (by measuring their wavelength and multiplying it by their frequency) that they travelled at the speed of light. Hertz also demonstrated that the new radiation could be both reflected and refracted by various dielectric media, in the same manner as light. For example, Hertz was able to focus the waves using a lens made of tree resin. In a later experiment, Hertz similarly produced and measured the properties of microwaves.

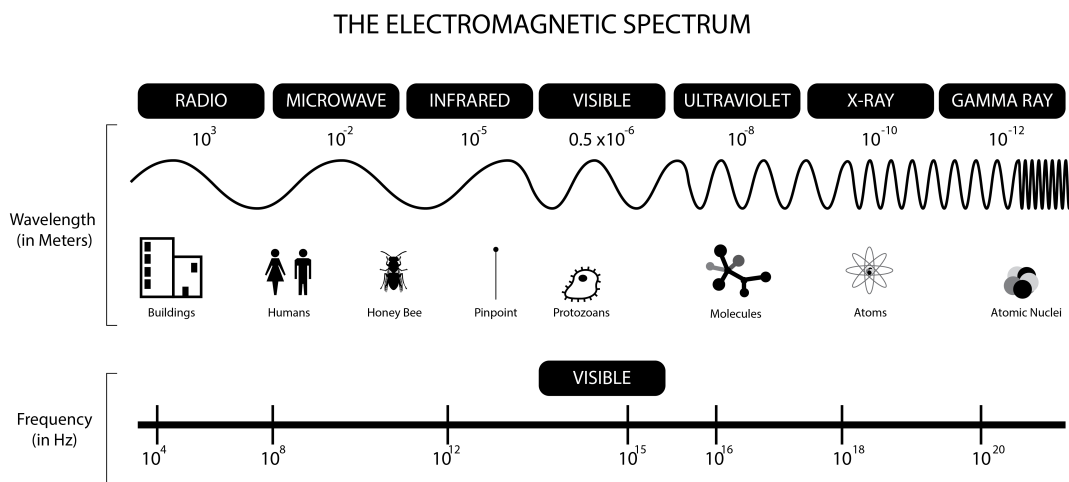


Figure 5: Electromagnetic Spectrum

Electromagnetic waves are typically described by any of the following three physical properties: the frequency ν , wavelength λ , or photon energy E . Frequencies observed in astronomy range from 2.4×10^{23} Hz (1 GeV gamma rays) down to the local plasma frequency of the ionized interstellar medium (≈ 1 kHz) [8]. Wavelength is inversely proportional to the wave frequency, so gamma rays have very short wavelengths that are fractions of the size of atoms, whereas wavelengths on the opposite end of the spectrum can be as long as

the universe. Photon energy is directly proportional to the wave frequency, so gamma ray photons have the highest energy (around a billion electron volts), while radio wave photons have very low energy (around a femtoelectronvolt). These relations are illustrated by the following equations:

$$\nu = \frac{c}{\lambda}, \text{ or } \nu = \frac{E}{h}$$

$$E = \frac{hc}{\lambda}$$

where,

$c = 299,792,458 \text{ m/s}$ is the speed of light in vacuum

$h = 6.62606896 \times 10^{-34} \text{ Js} = 4.13566733(10)10^{15} \text{ eV s}$ is Planck's constant.

Whenever electromagnetic waves exist in a medium with matter, their wavelength is decreased. Wavelengths of electromagnetic radiation, no matter what medium they are traveling through, are usually quoted in terms of the vacuum wavelength, although this is not always explicitly stated.

Generally, electromagnetic radiation is classified by wavelength into radio wave, microwave, terahertz (or sub-millimeter) radiation, infrared, the visible region is perceived as light, ultraviolet, X-rays and gamma rays as illustrated in Figure 5. The behavior of EM radiation depends on its wavelength. When EM radiation interacts with single atoms and molecules, its behavior also depends on the amount of energy per quantum (photon) it carries.

Spectroscopy can detect a much wider region of the EM spectrum than the visible range of 400 nm to 700 nm. A common laboratory spectroscope can detect wavelengths from 2 nm to 2500 nm. Detailed information about the physical properties of objects, gases, or even stars can be obtained from this type of device. Spectroscopes are widely used in astrophysics. For example, many hydrogen atoms emit a radio wave photon that has a wavelength of 21.12 cm. Also, frequencies of 30 Hz and below can be produced by and are important in the study of certain stellar nebulae[10] and frequencies as high as 2.9×10^{27} Hz have been detected from astrophysical sources.

Wavefunction & Schrodinger Equation

IT IS ONE OF THE POSTULATES of quantum mechanics that for a physical system consisting of a particle there is an associated wavefunction [9] [10] [11]. This wavefunction determines everything that can be known about the system. The wavefunction is assumed here to be a single-valued function of position and time, since that is sufficient to guarantee an unambiguous value of probability of finding the particle at a particular position and time. The wavefunction may be a complex function, since it is its product with its complex conjugate which specifies the real physical probability of finding the particle in a particular state.

The Schrodinger equation [12] plays the role of Newton's laws and conservation of energy in classical mechanics - i.e., it predicts the future behavior of a dynamic system. It is a **wave equation** in terms of the **wavefunction** which predicts analytically and precisely the probability of events or outcome. The detailed outcome is not strictly determined, but given a large number of events, the Schrodinger equation will predict the distribution of results. Each particle is represented by a wavefunction $\psi(\text{position, time})$ such that $\psi^* \psi =$ probability of finding the particle at that position at that time.

$\psi(x, y, z, t)$ = probability amplitude

$\psi^*\psi$ = probability

The properties [13] of a wavefunction are :

- It contains all the measurable information about the particle.
- $\psi^*\psi$ summed over all space = 1 (if the particle exists, the probability of finding it somewhere must be one).
- It is continuous.
- allows Energy calculations using Schrodinger equation.
- Establishes probability distribution in three dimensions.
- Permits calculation of effective average value (expectation value) of a given variable.
- wavefunction for a free particle is sine wave, implying precisely determined momentum and totally uncertain position(uncertainty principle).

In order to represent a physically observable system, the wavefunction must satisfy certain constraints [14]:

- Must be a solution of the Schrodinger equation.
- Must be a continuous function of x i.e., $\psi(x)$ must be continuous at all x.
- Must be normalizable. This implies that the wavefunction approaches zero as x approaches infinity.
- The slope of the function in x must be continuous and specifically $\frac{\partial\psi(x)}{\partial x}$ must be continuous.

The time dependent Schrodinger equation for one spatial dimension is of the form :

$$\frac{\hbar^2}{2m} \frac{\partial^2 \psi(x,t)}{\partial x^2} + U\psi(x,t) = i\hbar \frac{\partial \psi(x,t)}{\partial t}$$

Potential Energy, Harmonic Oscillation & Molecular Vibration

The Morse potential, which is the most popular potential energy function used for fitting spectroscopic data named after physicist Philip M. Morse, is a convenient interatomic interaction model for the potential energy of a diatomic molecule [15] [16].

It is a better approximation for the vibrational structure of the molecule than the *QHO (quantum harmonic oscillator)* because it explicitly includes the effects of bond breaking, such as the existence of unbound states. It also *accounts for the anharmonicity of real bonds and the non-zero transition probability for overtone and combination bands*. The Morse potential can also be used to model other interactions such as the interaction between an atom and a surface [9] [17].

Unlike the energy levels of the harmonic oscillator potential, which are evenly spaced by $\hbar\nu$, the Morse potential level spacing decreases as the energy approaches the dissociation energy as shown in Figure 6. The dissociation energy D_e is larger than the true energy required for dissociation D_0 due to the zero point energy of the lowest $n = 0$ vibrational level.

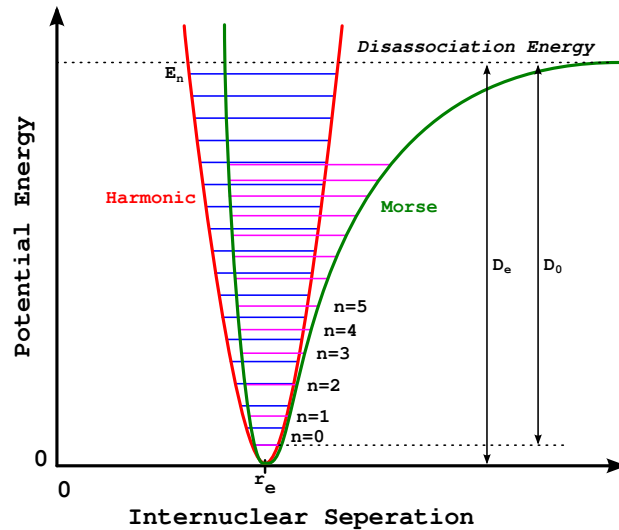


Figure 6: Comparison of Harmonic and Anharmonic potential functions of a diatomic oscillator

Quantum Harmonic Oscillator

A diatomic molecule vibrates somewhat like two masses on a spring with a potential energy that depends upon the square of the displacement from equilibrium. But the energy levels are quantized at equally spaced values. In this case, the potential energy V contains a single quadratic term:

$$V = \frac{1}{2}k(r - r_0) = \frac{1}{2}kx^2$$

where, k is the force constant of the bond, r is the internuclear distance, r_0 is the equilibrium internuclear distance and $x = (r - r_0)$ is the displacement coordinate.

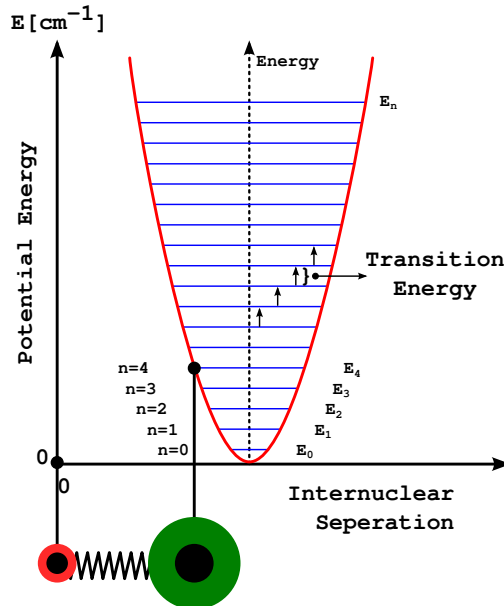


Figure 7: Harmonic potential functions for a diatomic oscillator

The potential energy curve is parabolic in shape and symmetrical about the equilibrium bond length, r_0 as shown in Figure 7. The vibrating mechanical model for a diatomic molecule leads to the classical vibrational frequency, ν

$$\nu = \frac{1}{2\pi} \sqrt{\frac{k}{\mu}}$$

where μ is the reduced molecular mass, such that: $\mu = \frac{m_1 m_2}{m_1 + m_2}$ and m_1 and m_2 are the masses of the two nuclei.

A quantum mechanical treatment (Schrodinger equation for Quantum Harmonic Oscillator) [18] shows that the energy of the oscillator may only have certain discrete values called *energy levels* that are *equally spaced*. For the harmonic oscillator, these energy levels are given by:

$$E_{vib} = h\nu(n + \frac{1}{2})$$

where h is the Planck's constant, ν is the classical vibrational frequency defined above and n is the vibrational quantum number which can only have integer values 0, 1, 2, 3...

The quantum harmonic oscillator has implications far beyond the simple diatomic molecule. It is the foundation for the understanding of complex modes of vibration in larger molecules, the motion of atoms in a solid lattice, the theory of heat capacity, etc. In real systems, energy spacings are equal only for the lowest levels where the potential is a good approximation of the "mass on a spring" type harmonic potential. The anharmonic terms which appear in the potential for a diatomic molecule are useful for mapping the detailed potential of such systems.

The energy levels $G(n)$, are expressed in wavenumber units (cm^{-1}) by the expression:

$$G(n) = \frac{E_{vib}}{hc} = \bar{\nu}(n + \frac{1}{2})$$

where $\bar{\nu}$ being the wavenumber of the vibrational transition. The selection rules that state which transitions are active or allowed can be deduced from the examination of the transition moment given by the expression:

$$P_{v''} = \int \psi_{v'}^* \epsilon \psi_{v''} d\tau$$

where $\psi_{v'}^*$ and $\psi_{v''}$ are the wave functions of the v' and v'' states ϵ is the dipole moment which may be expressed as a linear function of x for small displacements about the equilibrium configuration :

$$\epsilon = \epsilon_0 + \left(\frac{d\epsilon}{dx}\right)_e x$$

where ϵ_0 is the dipole moment at the equilibrium internuclear distance. The transition moment for the transition $v' \rightarrow v''$ may be calculated by substituting the appropriate wave functions and dipole moment. Transitions are allowed for a nonzero value of the transition moment. This occurs if the vibration is accompanied by a dipole-moment change; this implies that only heteronuclear, diatomic molecules will exhibit vibrational-spectral transitions.

Qualitatively, we can picture the dipole moment as an oscillating dipole coupled with the electric field of the incident radiation in such a way that the energy can be exchanged between the molecule and the radiation. In the quantum mechanical harmonic oscillator, a further restriction concerns the vibrational quantum number which can only change by one unit. Thus, transitions across more than one energy level are forbidden in the harmonic oscillator. Therefore, transitions are allowed only if:

$$\left(\frac{d\epsilon}{dx}\right)_e \neq 0$$

$$\Delta n = \pm 1$$

Quantum Anharmonic Oscillator

Two experimental observations give evidence that molecules are not ideal oscillators. Firstly, the vibrational energy levels are not equally spaced, so the transitions originating from vibrationally excited levels for $n \neq 0$ do not have exactly the same frequency as the fundamental transition energy. Secondly, overtone transitions such as $n = 0$ to $n = 2, 3, 4, \dots$ are allowed. This departure from harmonic behaviour may be expressed by two effects .

The first effect, called *mechanical anharmonicity* [2] [19], arises from the effect of cubic and higher terms in the potential-energy expression:

$$V = \frac{1}{2}kx^2 + k'x^3 + \dots k' \ll k$$

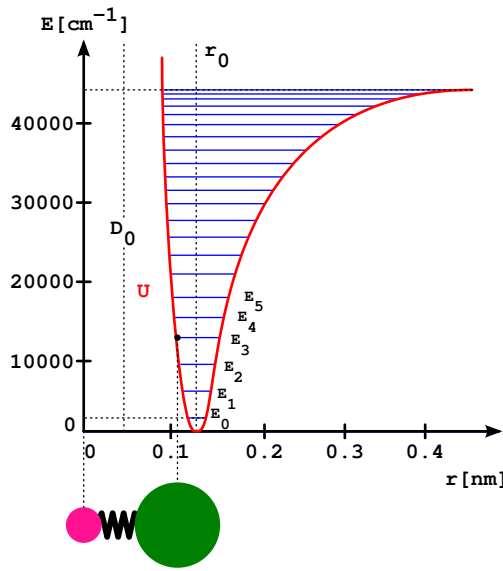


Figure 8: Anharmonic potential functions for a diatomic oscillator

The above expression is used in the Schrodinger equation to deduce the energy levels of the allowed states of the anharmonic oscillator. The solution is obtained by an approximation or perturbation method and leads to an energy level (in cm^{-1}) that can be written as.

$$\begin{aligned} G(n) &= \frac{E_{vib}}{\hbar c} = \bar{v}(n + \frac{1}{2}) - x_e \bar{v}(n + \frac{1}{2})^2 \\ G(n) &= \frac{E_{vib}}{\hbar c} = \bar{v}(n + \frac{1}{2}) - X(n + \frac{1}{2})^2 \end{aligned}$$

Here x_e is the *anharmonicity constant* and $X = x_e \bar{v}$. Unlike the harmonic oscillator, energy levels are not longer equally spaced as shown in Figure 8. An emperical equation called the *Morse function*, as illustrated in Figure 8, has often been used for the harmonic potential function:

$$V = D_e(1 - e^{-\beta x})^2$$

where β is a constant and D_e is the dissociation energy measured from the equilibrium position, which is the minimum of the curve. In terms of this potential, D_e is given by:

$$D_e = \frac{\bar{v}}{4x_e}$$

The second effect, called *electrical anharmonicity* [2] [20], is responsible for the appearance of overtones corresponding to transitions between energy levels that differ by two or three vibrational quantum number units ($\Delta n = +2, +3\dots$) in the infrared spectra. The electrical anharmonicity arises from the effect of square and higher terms in the *dipole-moment* expression.

$$\epsilon = \epsilon_0 + (\frac{d\epsilon}{dx})_e x + \frac{1}{2}(\frac{d^2\epsilon}{dx^2})_e x^2 + \dots$$

As can be seen, for the anharmonic oscillator, the frequencies of the overtone absorptions are not exactly $2, 3, \dots$ times that of the fundamental absorption. On the contrary, on account of the mechanical anharmonicity, the frequency of the hot bands is less than that of the fundamental transition.

Energy Associated with a Molecule

The energy associated with the absorption bands of a molecule is given by :

$$E = E_{electronic} + E_{vibrational} + E_{rotational}$$

where, $E_{rotational}$ denotes the rotation energy of the molecule, $E_{vibrational}$ the vibrational energy and $E_{electronic}$ the electronic energy. The number of rotational levels in a molecule is much larger than the number of vibrational states and the number of vibrational states is in turn larger than the number of electronic levels. These facts are also related to the differences in energy among the different states [21], where:

$$E_{electronic} > E_{vibrational} > E_{rotational}$$

Hence for a given molecule a number of electronic energy states exists, an even larger number of vibrational levels and also more rotational levels as shown in Figure 9.

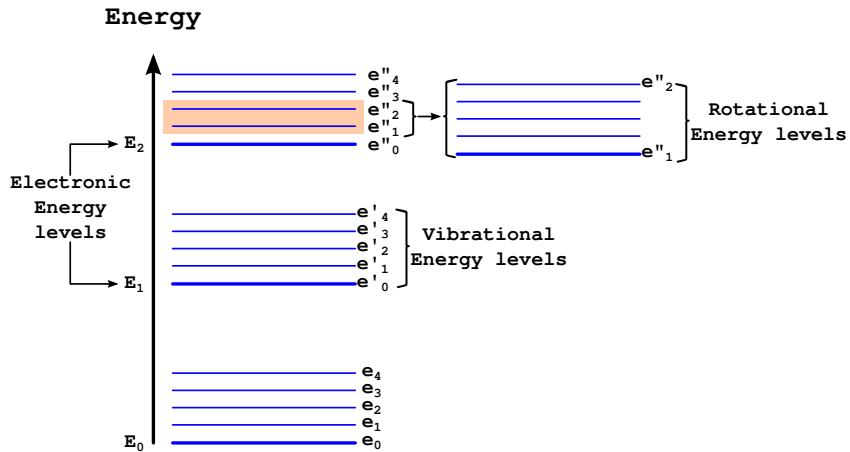


Figure 9: Energy level diagram for a molecule, showing rotational, vibrational and electronic energy levels

Molecular Vibration

MOLECULAR VIBRATION occurs when atoms in a molecule are in periodic motion while the molecule as a whole has constant translational and rotational motion. The frequency of the periodic motion is known as a vibration frequency, and the typical frequencies of molecular vibrations range from less than 10^{12} to approximately 10^{14} Hz. These frequencies correspond to radiation in the infrared region of the electromagnetic spectrum. At any given instant, each molecule in a sample has a certain amount of vibrational energy [22]. However, the amount of vibrational energy that a molecule has continually changes due to collisions and other interactions with other molecules in the sample.

At room temperature, most molecules are in the lowest energy state known as the ground state. A few molecules are in higher energy states known as excited states. The fraction of molecules occupying a given vibrational mode at a given temperature can be calculated using the Boltzmann distribution. Performing such a calculation shows that, for relatively low temperatures (such as those used for most routine spectroscopy), most of the molecules occupy the ground vibrational state. Such a molecule can be excited to a higher vibrational mode through the direct absorption of a photon of the appropriate energy.

In general, a molecule with N atoms has $3N - 6$ normal modes of vibration [2] [23], but a linear molecule has $3N - 5$ such modes, as rotation about its molecular axis cannot be observed. A diatomic molecule has one normal mode of vibration. The normal modes of vibration of polyatomic molecules are independent of each other but each normal mode will involve simultaneous vibrations of different parts of the molecule such as different chemical bonds.

The internal degrees of freedom for a molecule define n as the number of atoms in a molecule and define each atom with 3 degrees of freedom of motion in the X , Y , and Z directions resulting in $3n$ degrees of motional freedom. Here, three of these degrees are translation, while three describe rotations. The remaining $3n - 6$ degrees (non-linear molecule) are motions, which change the distance between atoms, or the angle between bonds. A simple example of the $3n - 6$ non-linear molecule is water (H_2O) which has $3(3) - 6 = 3$

degrees of freedom. The three vibrations include an in-phase and out-of-phase stretch and a deformation (bending) vibration. Simple examples of $3n - 5$ linear molecules include H_2 , N_2 , and O_2 which all have $3(2) - 5 = 1$ degree of freedom. The only vibration for these simple molecules is a simple stretching vibration. The more complicated CO_2 molecule has $3(3) - 5 = 4$ degrees of freedom and therefore four vibrations. The four vibrations include an in-phase and out-of-phase stretch and two mutually perpendicular deformation (bending) vibrations.

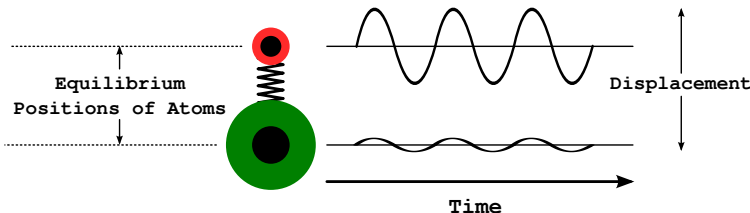


Figure 10: Normal mode of vibration for a simple diatomic molecule

For the normal mode of vibrations, Cartesian displacements of each atom in molecule change periodically with the same frequency and go through equilibrium positions simultaneously. The center of the mass does not move and the molecule does not rotate. Thus in the case of harmonic oscillator, the Cartesian coordinate displacements of each atom plotted as a function of time is a sinusoidal wave. The relative vibrational amplitudes may differ in either magnitude or direction. Figure 10 shows the normal mode of vibration for a simple diatomic such as HCl .

The vibrational states of a molecule can be probed in a variety of ways. The most direct way is through infrared spectroscopy, as vibrational transitions typically require an amount of energy that corresponds to the infrared region of the spectrum. Raman spectroscopy, which typically uses visible light, can also be used to measure vibration frequencies directly. The two techniques are complementary and comparison between the two can provide useful structural information. In an infrared spectrum the intensity of an absorption band is proportional to the derivative of the molecular dipole moment with respect to the normal coordinate. The intensity of Raman bands depends on polarizability.

Internal Coordinates

Internal coordinates are of the following types :

- **Stretching** : a change in the length of the bond.
- **Bending** : a change in the angle between 2 bonds.
- **Rocking** : a change in the angle between group of atoms.
- **Wagging** : a change in the angle between the plane of group of atoms and a plane through the rest of the molecule.
- **Twisting** : a change in the angle between the planes of two groups of atoms.
- **Out-of-plane** : a change in the angle between one of the bonds and the plane defined by the remaining atoms of the molecule.

In a rocking, wagging or twisting coordinate the bond lengths within the groups involved do not change while the angles do change. Rocking is distinguished from wagging by the fact that the atoms in the group

stay in the same plane. Figure 11 illustrates the vibrations of methelyne group CH_2 in a molecule. The illustration does not represent the *recoil* of C atoms, which, though necessarily present to balance the overall movements of the molecule, are much smaller than the movements of the lighter H atoms.

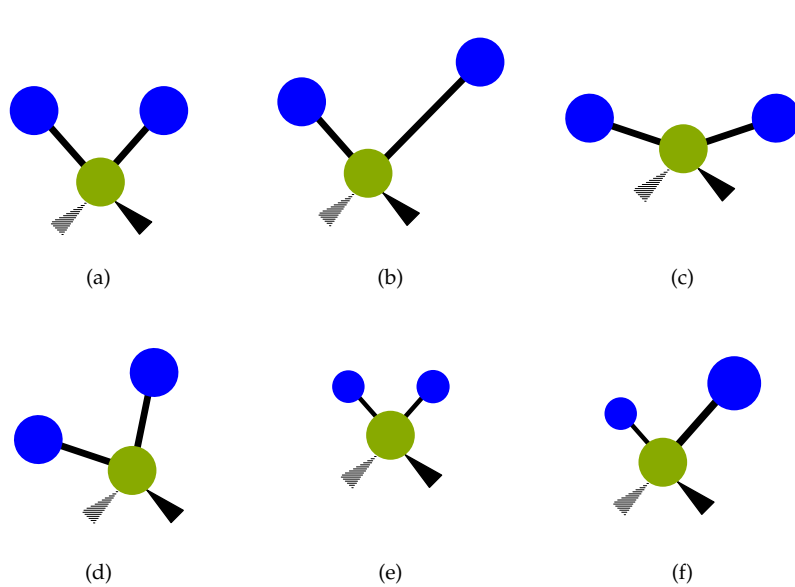


Figure 11: Types of Internal Co-ordinates

Measured Spectrum and Uncertainty

In absorption spectroscopy, the information sought for is the absorption of radiant power from a source by the sample. In infrared spectroscopy, this is done in practice by a spectrometer; the construction of this instrument will be dealt with in a later chapter. The idea behind the technique is to send radiation through (or interact with) a sample and measure the characteristics of the radiation emerging from the sample [24] [25].

Let us assume that monochromatic radiation (only one-frequency radiation) with sufficient intensity and of a frequency that matches the frequency of absorption is passed through a sample. A part of the radiation will be absorbed and the intensity of the radiation emerging from the sample, the transmitted radiation, will be of reduced intensity. If we plot the percent of the intensity of the transmitted relative to the source intensity against frequency, then the plot should contain a single line as shown in Figure 12a and absorption spectrum will be as shown in Figure 12b.

The real absorption spectrum of a diatomic molecule, which has only a single vibrational mode, is not a line spectrum, but an absorption spectrum containing a broad peak with a maximum at the frequency of absorption as shown in Figure 12. The line broadening in spectrometry arises because of characteristics adherent to molecules in different phases and uncertainty in the energy levels due to the limited residence time of the particle in the excited state. In solids, liquids and gases the particle velocities are different. The particles collide more frequently in the gas phase than in the liquid phase.

The vibrational and rotational energy levels are perturbed from their actual values and lead to small variations in the ground state energy levels. This implies that solids should give sharp bands. This is true, but the bands are split because of electronic interactions. Spectral line broadening arises also due to the Doppler effect. The infrared measurements are made in cells where the radiation is allowed to pass through or interact with the sample. Molecules that are in motion towards the source will absorb radiation of higher frequency compared with the molecules that are moving away from the source (lower frequency). One of the important effects that cause spectral line broadening is the uncertainty effect. The uncertainty principle proposed by Werner Heisenberg suggests that there is natural limitation on how precise a pair of physical parameters can be made. In vibrational spectrometry the uncertainty in the energy level of the excited state, ΔE , and uncertainty in the lifetime of the molecule at an excited vibrational state, Δt is related by the uncertainty relationship as follows.

$$\Delta E \Delta t \geq \frac{h}{2\pi}$$

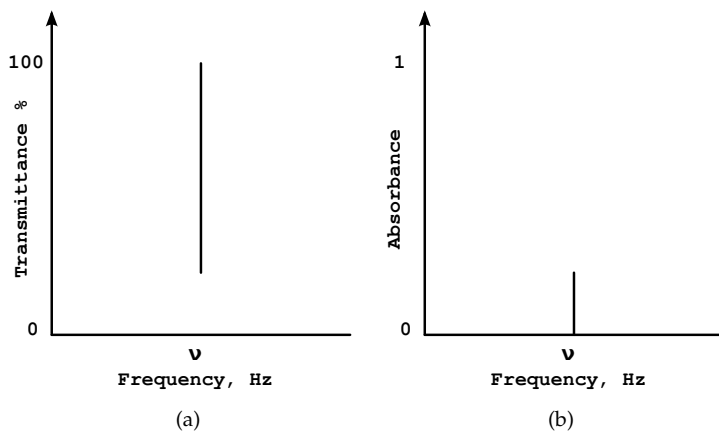


Figure 12: A line spectrum of Transmission and Absorption

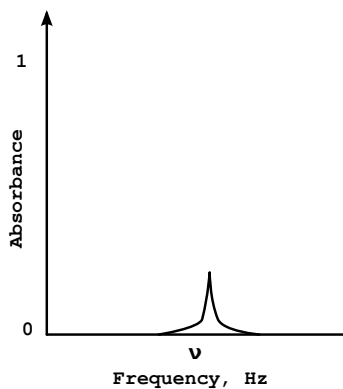


Figure 13: Line broadening phenomenon of Absorption Spectra

This can be rewritten to include frequency ν as follows

$$\Delta h\nu \Delta t \geq \frac{h}{2\pi}$$

i.e.

$$\Delta\nu\Delta t \geq \frac{1}{2\pi}$$

If the residence times at the excited vibrational states are infinite then the uncertainty in the frequency of absorption is zero and the frequency can be determined precisely. The molecules that undergo vibrational transitions have a finite time of residence of 10^{-8} s and this leads to an uncertainty in the frequency.

$$\Delta\nu \geq \frac{h}{2\pi\Delta t} = \frac{1}{2\times 3.14\times 10^{-8}} \text{ s} \approx 10^8$$

This uncertainty is small compared to the radiation frequency of infrared radiation $10^{12} - 10^{14}$. This leads us to conclude that absorption by a single vibrational mode will be a band spectrum with a finite frequency width as shown in Figure 13.

Beer-Lambert's Law

The basis of most quantitative spectroscopic analyses is Beer's law. This law relates the amount of light absorbed by a sample, a spectroscopically observable property, to the concentration of absorbing species in the sample. This relationship is what allows absorbance measurements to be used to predict concentrations [5]. To derive Beer's law, we assume the experimental setup shown in Figure 14.

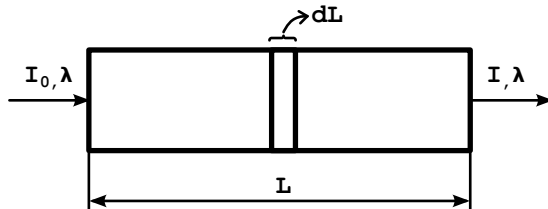


Figure 14: Beer's law experimental setup

We also assume that monochromatic light of wavelength λ , impinges upon the sample perpendicular to one of its faces. Before the light enters the sample, it has intensity I_0 . Light intensity is defined as the number of photons of light hitting a unit area per unit time. The thickness or pathlength of the material is denoted by L . An infinitesimally thin slab of the absorbing material is denoted by dL . When the light leaves the sample it has intensity $I < I_0$ due to absorbance of the light by the sample.

To study the interaction between the photon and the molecule we can consider them as particles and the interaction between them as collisions. When two particles collide, several different types of collision can occur. The particles may undergo an elastic collision, which is illustrated in Figure 15. Before the collision, the incoming photon has energy $E_P = h\nu$ as stated in equation, and imagine the methane molecule has no kinetic or vibrational energy, and can be considered at rest. By definition, an **elastic collision** results in no net energy exchange between the molecules. After the collision, the photon still has energy $h\nu$, and the methane molecule is still at rest. The only thing that has changed is the direction of travel of the photon, and to a lesser extent, the position of the methane molecule. Elastic collisions between photons and molecules result in a phenomenon called **Rayleigh scattering**, in which the direction but not the energy of the photon is changed.

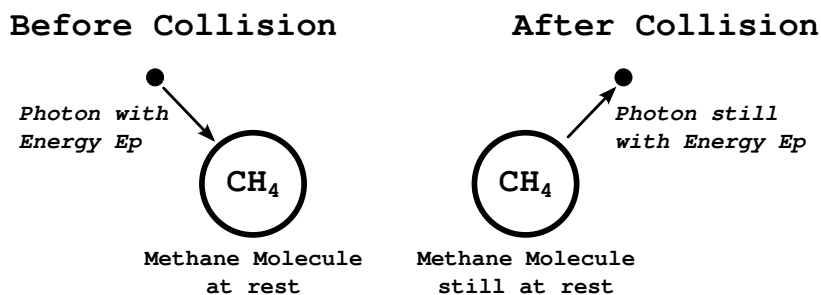


Figure 15: Elastic Collision between a Photon and a CH_4 molecule

Another type of photon/molecule collision are *inelastic collisions*. In this type of collision, energy is exchanged between the particles, and they leave the collision with different energies than before the collision. This is illustrated in Figure 16. Before the collision, the incoming photon has energy E_p , and the methane molecule is at rest. After the collision, some of the photon's energy is deposited into the molecule as vibrational energy, E_v . The photon's energy after the collision is E_i (i for inelastic). All processes must follow the law of conservation of energy, thus, $E_p = E_v + E_i$. The concentric circles in Figure 16 indicate that the methane molecule is vibrationally excited. Also, note that the direction of the photon has changed after the collision.

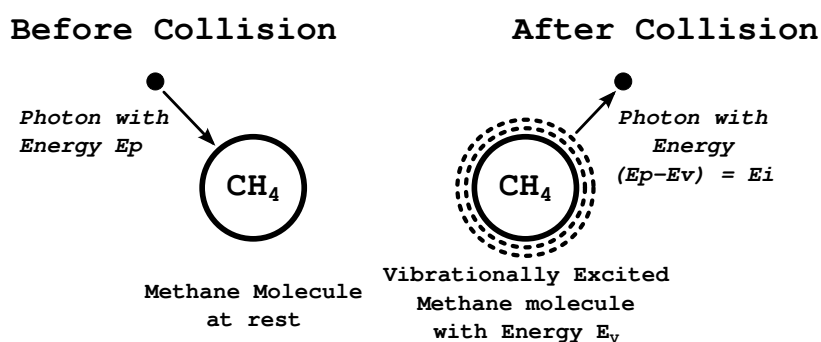


Figure 16: InElastic Collision between a Photon and a CH_4 with change in direction of photon

Inelastic collisions between molecules and photons give rise to a phenomenon called *Raman scattering*. The amount of energy lost by the photon, E_v , is characteristic of the molecule involved in the scattering. Thus, after the collision the inelastically scattered photon carries chemical information. When the intensity and the wavenumber of these photons are analyzed and plotted, one obtains a *Raman spectrum*. Raman spectra are similar to infrared spectra in that they measure the vibrational energy levels of a molecule.

A third thing that can occur when a photon encounters a molecule is a *totally inelastic collision*. This is illustrated in Figure 17. Before the collision, the photon has energy E_p , and the methane molecule is at rest. After the collision the photon has disappeared; all its energy has been absorbed by the molecule leaving it excited. This phenomenon is known as *absorbance*. The wavenumber of the light absorbed and the intensity

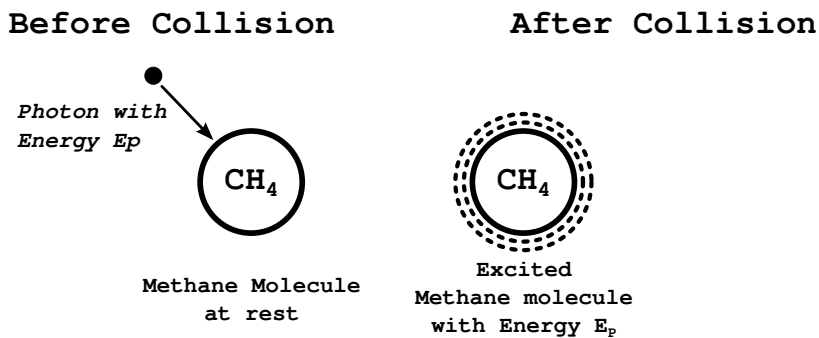


Figure 17: InElastic Collision between a Photon and a CH_4 with absorbance

with which it is absorbed depends upon the molecule involved in the collision. Thus, chemical information can be derived from a plot of absorbance intensity versus wavenumber, called an *absorbance spectrum*.

The total amount of light absorbed by a sample is simply equal to the total number of photons that undergo totally inelastic collisions with molecules. The decrease in the number of photons leaving the sample will give rise to an absorbance feature in the spectrum of the sample. Now, photons may also be scattered by macroscopic-size particles such as dust grains, leading to a decrease in photons exiting the sample as well. Experimentally, this will look like absorbance but it is not. Thus, we are tacitly assuming that our sample has no other species present other than molecules that will interact with the light beam.

In Figure 14, the change in light intensity across slab dL of the sample will be denoted by dI . The more photons and molecules there are in dL , the more collisions will occur. The number of molecules in dL is simply determined by the analyte concentration, c . The number of photons present is given by the intensity of light in dL , which is simply I . Additionally, the thicker the slab dL , the more photons will be absorbed because there are more molecules encountered. Thus, we can write a proportionality for the light absorbed in dL as

$$-dI \propto IcdL$$

where,

dI = amount of light absorbed in dL

I = intensity of light impinging on dL

c = concentration of absorbing species in dL

dL = thickness of an infinitesimally thin slab of sample

The negative sign of dI means that the intensity of the light beam decreases as it traverses dL . This proportionality assumes that the change in I across the width of dL is negligible because dL is infinitesimally thin. Thus, we assume that I is the same at all points in dL . Note that the amount of light lost simply depends on the number of analyte molecules present (c), the number of photons present (I), and the sample thickness (dL). It tells us what parameters determine the total number of photon-molecule collisions.

Molecules and photons can undergo several different types of collisions. Only some percentage of these collisions will be totally inelastic. It is the number of *totally inelastic collisions that determines the amount of light absorbed*. To calculate the number of these collisions, we must multiply the right-hand side of equation by the fraction of collisions that are totally inelastic. This number is called the *absorptivity*, and is denoted with ϵ . The absorptivity can also be thought of as a probability, it is the probability that a photon-molecule collision will be totally inelastic. The absorptivity depends upon the identity of the molecule absorbing the light, and the wavelength of light being absorbed. By inserting the absorptivity into the above equation, it functions as a proportionality constant making the formerly qualitative relationship between dI and concentration quantitative. We can then remove the proportionality sign to obtain

$$-dI = \epsilon IcdL$$

where,

ϵ = the absorptivity of the analyte molecule at wavelength λ

$$\frac{-dI}{I} = \epsilon cdL$$

$$-\int_{I_0}^I \frac{dI}{I} = \epsilon c \int_0^L dL$$

$$\ln\left(\frac{I_0}{I}\right) = \epsilon c L$$

Dividing both sides of the equation by 2.303 yields:

$$\log\left(\frac{I_0}{I}\right) = \epsilon c L$$

This new quantity $\log\left(\frac{I_0}{I}\right)$ is called as *Absorbance*.

$$A = \log\left(\frac{I_0}{I}\right)$$

This allows to establish Beer's law :

$$A = \epsilon c L$$

where,

A = Absorbance

ϵ = absorptivity

l = pathlength

c = concentration

This equation tells us is that the amount of light absorbed by a sample depends on the concentration of the analyte, the thickness of the sample, and the sample's absorptivity. Also, note that the relationships in Beer's law are linear [26]. For example, doubling the pathlength or concentration of a sample doubles its absorbance. Many spectrometers are capable of measuring spectra with the Y-axis in absorbance units. Because the relationship between absorbance and concentration is linear, the peak height or area of an analyte's absorbance band will vary linearly with concentration.

Acousto-Optics

IN OPTICS, a diffraction grating is an optical component with a periodic structure, which splits and diffracts light into several beams traveling in different directions. The directions of these beams depend on the spacing of the grating and the wavelength of the light so that the grating acts as the dispersive element. The relationship between the grating spacing and the angles of the incident and diffracted beams of light is known as the grating equation. According to the Huygens-Fresnel principle, each point on the wavefront of a propagating wave can be considered to act as a point source, and the wave-front at any subsequent point can be found by adding together the contributions from each of these individual point sources. Gratings [27] may be of the *reflective* or *transmissive* type, analogous to a mirror or lens respectively. A grating has a *zero-order mode* (where $m=0$), in which there is no diffraction and a ray of light behaves according to the laws of reflection and refraction the same as with a mirror or lens respectively.

An idealized grating is considered here which is made up of a set of slits of spacing d , that must be wider than the wavelength of interest to cause diffraction. When a plane wave of wavelength λ with normal incidence, (perpendicular to) the grating, each slit in the grating acts as a quasi point-source from which light propagates in all directions (although this is typically limited to a hemisphere). The diffracted light is composed of the sum of interfering wave components emanating from each slit in the grating. At any given point in space through which diffracted light may pass, the path length to each slit in the grating will vary. Since the path length varies, generally, so will the phases of the waves at that point from each of the slits, and thus will add or subtract from one-another to great peaks and valleys, through the phenomenon of additive and destructive interference.

When the path difference between the light from adjacent slits is equal to half the wavelength, $\frac{\lambda}{2}$, the waves will all be out of phase, and thus will cancel each other to create points of minimum intensity. Similarly, when the path difference is λ , the phases will add together and maxima will occur. The maxima occur at angles \hat{y}_m , which satisfy the relationship $\frac{d \sin \theta_m}{\lambda} = |m|$ where θ_m is the angle between the diffracted ray and the grating's normal vector, and d is the distance from the center of one slit to the center of the adjacent slit, and m is an integer representing the propagation-mode of interest. Thus, when light is normally incident on the grating, the diffracted light will have maxima at angles θ_m , given by:

$$d \sin(\theta_m) = m\lambda$$

It is straightforward to show that if a plane wave is incident at any arbitrary angle θ_i , the grating equation becomes:

$$d(\sin \theta_i + \sin \theta_m) = m\lambda$$

When solved for the diffracted angle maxima, the equation is:

$$\theta_m = \arcsin\left(\left(\frac{m\lambda}{d}\right) - \sin \theta_i\right)$$

The light that corresponds to direct transmission (or specular reflection in the case of a reflection grating) is called the zero order, and is denoted $m = 0$. The other maxima occur at angles which are represented by non-zero integers m . Note that m can be positive or negative, resulting in diffracted orders on both sides of the zero order beam. This derivation of the grating equation is based on an idealised grating. However, the relationship between the angles of the diffracted beams, the grating spacing and the wavelength of the light apply to any regular structure of the same spacing, because the phase relationship between light scattered from adjacent elements of the grating remains the same.

The detailed distribution of the diffracted light depends on the detailed structure of the grating elements as well as on the number of elements in the grating, but it will always give maxima in the directions given by the grating equation. Gratings can be made in which various properties of the incident light are modulated in a regular pattern; these include

- transparency (transmission amplitude gratings)
- reflectance (reflection amplitude gratings)
- refractive index (phase gratings)
- direction of optical axis (optical axis gratings)

The grating equation applies in all these cases.

Acousto-Optic Theory

It was found that some specific form of crystals, when excited at certain specific wavelengths of electromagnetic wave and incident angles, produced intense peaks of reflected radiation (known as Bragg peaks). As a result, re-emitted wave fields interfere with each other either constructively or destructively producing a diffraction pattern on a detector [28] [29]. This forms the basis of diffraction analysis which is called as Bragg diffraction [30]. The result is explained, by modeling the crystal as a set of discrete parallel planes separated by a constant parameter d . It was proposed that the incident radiation would produce a Bragg peak if their reflections off the various planes interfered constructively. The interference is constructive when the phase shift is a multiple of 2π ; this condition can be expressed by Bragg's law,

$$n\lambda = 2d \sin \theta$$

Where,

n is an integer

λ is the wavelength of incident wave, d is the spacing between the planes in the atomic lattice,

θ is the angle between the incident ray and the scattering planes.

All the results are explained with X-ray radiation.

Bragg diffraction

Two beams with identical wavelength and phase approach a crystalline solid and are scattered off two different atoms within it [31]. The lower beam traverses an extra length of $2d \sin \theta$. Constructive interference occurs when this length is equal to an integer multiple of the wavelength of the radiation as shown in Figure 18.

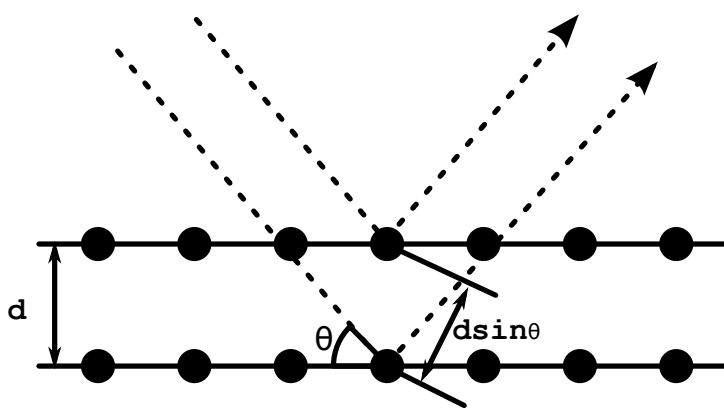


Figure 18: Interaction of light and solid material

BRAGG CELL [31] is a device using a bulk acousto-optic(AO) interaction, built using the frequency shifting optics using a piezoelectric crystal and signal driver. Although acoustic interactions can be observed in liquids, practical devices use crystals or glasses as the interaction medium, with RF frequencies in the MHz to GHz range [32] [33]. A piezoelectric transducer generates the acoustic wave when driven by an RF signal. The transducer is placed between 2 electrodes.

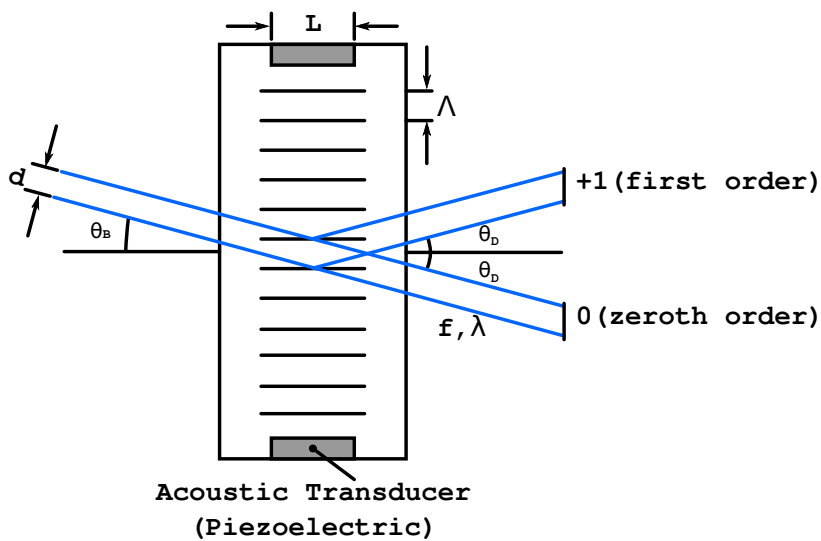


Figure 19: Diffraction in Bragg Cell

The top electrode determines the active limits of the transducer. The ground electrode is bonded to the crystal. The transducer thickness is chosen to match the acoustic frequency to be generated. The height of the electrode H depends on the type of application, and must exceed the laser beam diameter. For a deflector, it is selected in order to collimate the acoustic beam inside the crystal during propagation. The electrode length L is chosen to give the required bandwidth and efficiency. The shape of the electrode can be varied for impedance matching or to shape the acoustic wave [34].

The crystal will generally be AR(Anti Reflection) coated to reduce reflections from the optical surfaces. Alternatively, the faces can be cut to *Brewster's angle* for a specific wavelength. A variety of different materials can be used. All have their own advantages and disadvantages. An **apodization**(Apodization literally means "removing the foot". It is the technical term for changing the shape of a mathematical function, an electrical signal, an optical transmission or a mechanical structure) of the acoustic signal can be obtained by optimizing the shape of the electrode. An impedance matching circuit is added to couple the transducer to the driver. Indeed, this circuit is necessary to adapt the Bragg cell to the impedance of the RF source (in general 50 Ohms), to avoid power returned losses. The RF power return loss is characterized with the VSWR(*Voltage Standing Wave Ratio*) of the AO device.

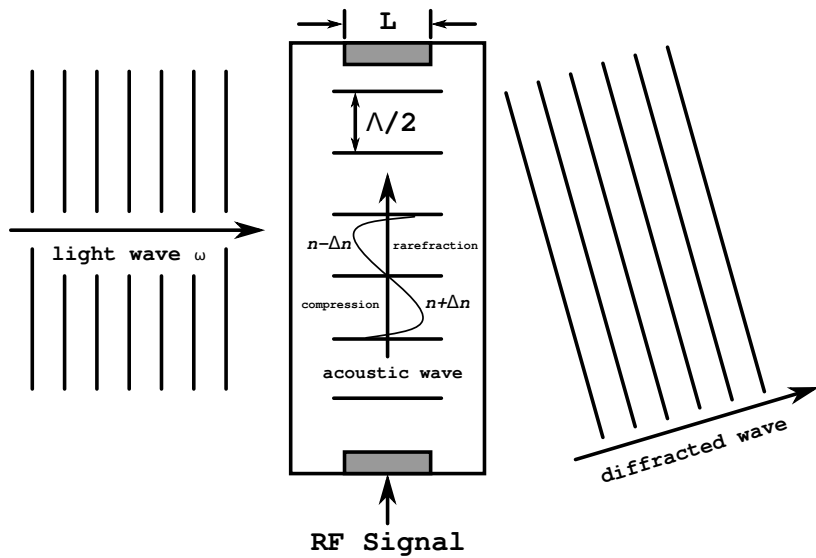


Figure 20: Variation of Refractive index in Bragg cell for an acoustic wave

Figure 20 depicts how the acoustic wave induces change in refractive index in the crystal medium [31] [35], which results in diffraction of the incident light wave. As the transducer is excited with RF signal it vibrates the crystal medium all along the volume producing periodic change in refractive index synonymous to the RF signal type. Figure 21 shows a refractive index profile [36] along the crystal following a sine wave pattern when the RF signal tends to be a sine signal. Period compression and rarefaction induced by the acoustic pressure in the crystal produces these periodic refractive index profile.

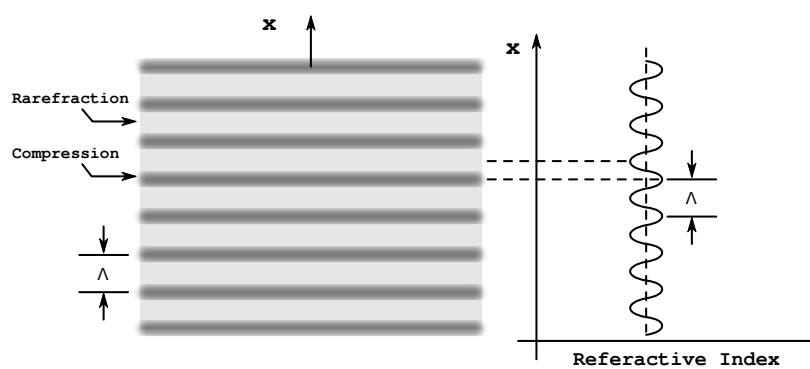


Figure 21: Refractive index profile in Bragg cell created by an acoustic wave

Characteristic Parameters

Acousto-optic(AO) interactions can be characterized with the following parameters :

BRAGG ANGLE (θ_B): The particular angle of incidence (between the incident beam and the acoustic wave) which gives efficient diffraction into a single diffracted order. This angle will depend on the wavelength and the RF frequency.

SEPARATION ANGLE (θ): The angle between the zero order and the first order.

RF BANDWIDTH (∇F): For a given orientation and optical wavelength there is a particular RF frequency which matches the Bragg criteria. However, there will be a range of frequencies for which the situation is still close enough to optimum for diffraction still to be efficient. This RF bandwidth determines, for instance, the scan angle of a deflector or the tuning range of an AOTF.

MAXIMUM DEFLECTION ANGLE ($\delta\theta$): The angle through which the first order beam will scan when the RF frequency is varied across the full RF bandwidth.

RISE TIME (T_R): Proportional to the time the acoustic wave takes to cross the laser beam and, therefore, the time it takes the beam to respond to a change in the RF signal. The rise time can be reduced by reducing the beams width.

MODULATION BANDWIDTH (δF_{mod}): The maximum frequency at which the light beam can be amplitude modulated. It is related to the rise time and can be increased by reducing the diameter of the laser beam.

EFFICIENCY (η): The fraction of the zero order beam which can be diffracted into the **1st** order beam.

EXTINCTION RATIO: The ratio between maximum and minimum light intensity in the **1st** order beam, when the acoustic wave is **on** and **off** respectively.

FREQUENCY SHIFT (F): The difference in frequency between the diffracted and incident light beams. This shift is equal to the acoustic frequency and can be a shift up or down depending on orientation.

RESOLUTION (N): The number of resolvable points, which a deflector can generate - corresponding to the maximum number of separate positions of the diffracted light beam - as defined by the Rayleigh criterion.

RF POWER (P_{RF}): The electrical power delivered by the driver.

ACOUSTIC POWER (P_a): The acoustic power generated in the crystal by the piezoelectric transducer. This will be lower than the RF power as the electro-mechanical conversion ratio is lower than 1.

QUALITY FACTOR (Q): Quality Factor Q determines the interaction regime. Q is given by:

$$Q = \frac{2\pi\lambda_0 L}{n\Lambda^2}$$

where,

λ_0 is the wavelength of the laser beam, n is the refractive index of the crystal,

L is the distance the monochromatic beam travels through the acoustic wave and

Λ is the acoustic wavelength.

RAMAN-NATH REGIME ($Q \ll 1$): The laser beam is incident roughly normal to the acoustic beam and there are several diffraction orders (...-2 -1 0 1 2 3...) with intensities given by Bessel functions.

BRAGG REGIME ($Q \gg 1$): At one particular incidence angle ϕ_B , only one diffraction order is produced the others are annihilated by destructive interference.

Acoustic-Optic Tunable Filter

The acousto-optic tunable filter (AOTF) is an electro-optical device that functions as an electronically tunable excitation filter to simultaneously modulate the intensity and wavelength of multiple laser lines from one or more sources. Devices of this type rely on a specialized birefringent crystal whose optical properties vary upon interaction with an acoustic wave. Changes in the acoustic frequency alter the diffraction properties of the crystal, enabling very rapid wavelength tuning, limited only by the acoustic transit time across the crystal [37] [38] [39]. An acousto-optic tunable filter consists of a tellurium dioxide or quartz anisotropic crystal to which a piezoelectric transducer is bonded. In response to the application of an oscillating radio frequency (RF) electrical signal, the transducer generates a high-frequency vibrational (acoustic) wave that propagates into the crystal. The alternating ultrasonic acoustic wave induces a periodic redistribution of the refractive index through the crystal that acts as a transmission diffraction grating or Bragg diffracter, in other words the crystal now behaves as phase grating to deviate a portion of incident electromagnetic beam into a first-order beam, (or two first-order beams when the incident light is non-polarized; as shown in Figure 19).

Changing the frequency of the transducer signal applied to the crystal alters the period of the refractive index variation, and therefore, the wavelength of light that is diffracted [40]. The relative intensity of the diffracted beam is determined by the amplitude (power) of the signal applied to the crystal [41].

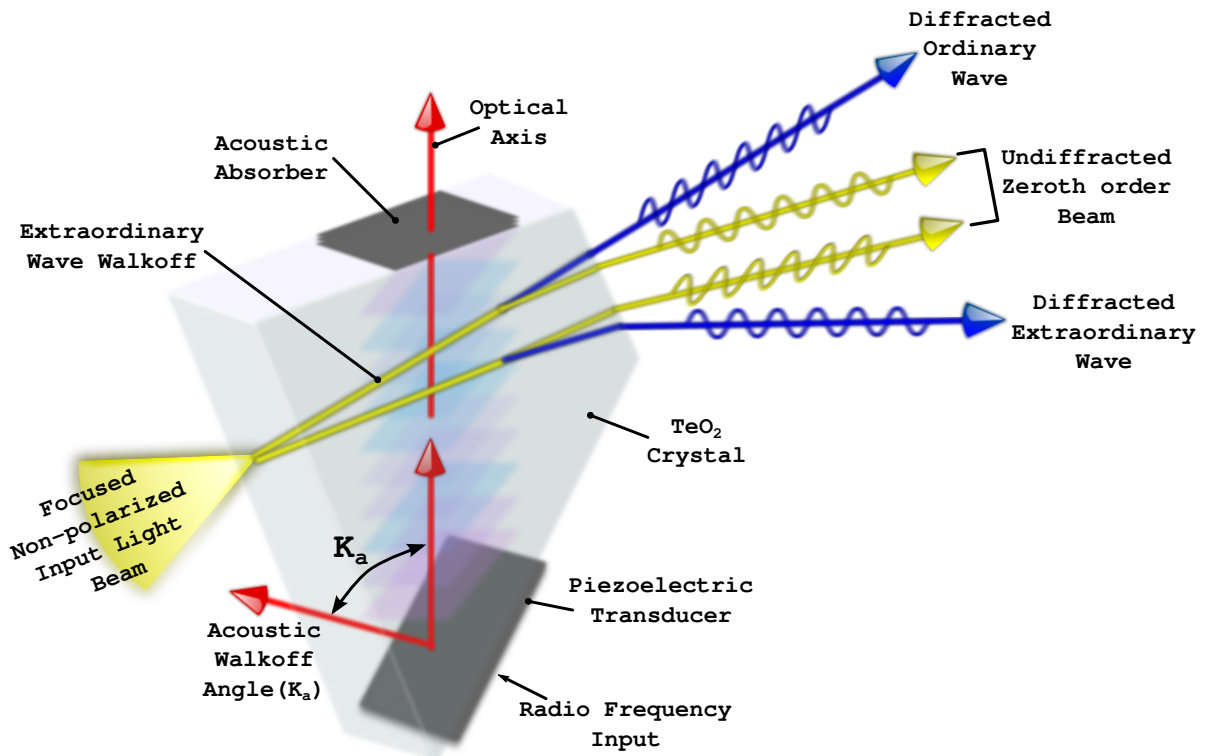


Figure 22: AOTF anatomy and Diffraction process

Working Principle

An acousto-optic crystal is defined as having optical properties that are altered in the presence of an acoustic wave. When an acoustic wave propagates through such a material, the crystal lattice structure is alternately compressed and relaxed in response to the oscillating wavefront. The basic mechanism responsible for this acousto-optic interaction is known as the *elasto-optic effect* [42] [43] [44].

Periodic regions of lattice compression and rarefaction throughout the crystal are manifested as refractive index fluctuations that can produce diffraction of incident light. Although the function of the acousto-optic tunable filter is similar to that of a diffraction grating, its behaviour differs in that diffraction occurs over an extended volume of the crystal rather than at a planar surface, and only a limited band of spectral frequencies are affected.

In this respect the AOTF performs more as a bandpass filter than a diffraction grating. The propagating acoustic waves generate a periodic modulation of the index of refraction throughout the crystal, effectively producing a mobile phase grating, which will diffract portions of the incident light that satisfy appropriate phase-matching (or momentum-matching) [45] conditions. For a particular acoustic frequency, only a limited

range (band) of spectral frequencies satisfies the phase-matching condition, and becomes diffracted. Varying the radio frequency driving the piezoelectric transducer changes the center of the spectral passband, as required to maintain the phase-matching condition. Appropriate selection of the drive frequency allows the crystal to be tuned to separate a particular wavelength band for diffraction, which then exits the crystal at a distinct angle relative to the undiffracted beam.

Additionally, the polarisation of the diffracted wavelength is rotated. For instance, if the incident radiation is an ordinary ray (o-ray), it will be converted into an extraordinary ray (e-ray) for the selected wavelength upon interaction with the acoustic wave. The incoming light can be imagined as a beam of photons while the acoustic wave moving through the crystal consists of phonons [34]. The sum of momentum of the incident light (M_i) and the acoustic wave (M_a) is equal to that of the diffracted radiation (M_d):

$$(M_i) \pm (M_a) = (M_d)$$

This relationship can be expressed in a vector form. If we denote the incident wave vector as k_i , the acoustic wave vector as k_a and the diffracted wave vector as k_d , the phase matching of the optical and acoustic beams requires that:

$$(k_i) \pm (k_a) = (k_d)$$

The magnitudes of the wave vectors are given by:

$$|k_i| = \frac{2\pi n_i}{\lambda},$$

$$|k_a| = \frac{2\pi f}{v},$$

$$|k_d| = \frac{2\pi n_d}{\lambda}$$

where f is the acoustic frequency, v is the acoustic speed in the crystal, λ is the optical wavelength, and $n_{i,d}$ is the crystal index of refraction for the incident and diffracted beams, respectively. This vector relationship is expressed on the wave-vector diagram shown in Figure 23, where θ_i and θ_d are the angles between incident and diffracted beam wave vectors and the optic axis, respectively; n_e and n_o are the extraordinary and ordinary refraction indices, respectively; and α is the angle between the acoustic wave vector, k_a , and the acoustic axis.

PHASE MATCHING CONDITION: The AOTF only diffracts one specific wavelength of light, so that it acts more like a filter than a diffraction grating. This is a result of the fact that the diffraction takes place over an extended volume, not just at a surface or plane, and that the diffraction pattern is moving in real time. The wavelength of light is diffracted is determined by the **Phase matching or momentum matching** [42] condition as described:

$$\lambda = \frac{v\Delta n}{f} \sqrt{\sin^4 \theta_i + \sin^2 2\theta_i}$$

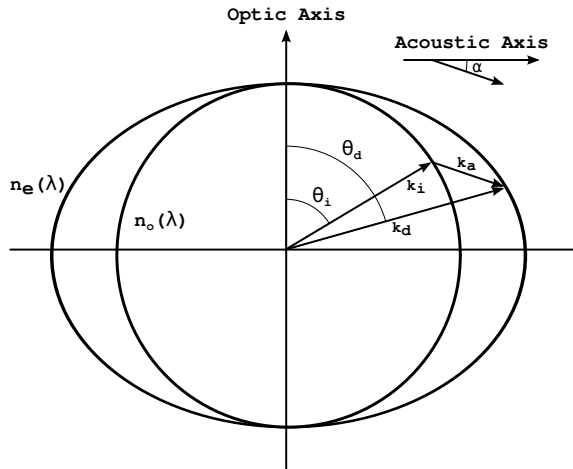


Figure 23: Wave-vector diagram of an Acousto-optic(AO) crystal

Where,

Δn is the difference in the refractive indices (birefringent) due to optical activity in crystals like TeO_2 ,
 θ_i is the incident angle of an ordinary ray,
 v and f are the velocity and frequency of the acoustic wave,

The wavelength of the light that is selected by this diffraction can therefore be varied simply by changing the frequency of the applied RF. As indicated in Figure 22, the diffracted light intensity is directed into two first order beams. These beams are orthogonally polarized, which is utilized in certain applications. To use the AOTF as a tunable filter, a beam stop is used to block the undiffracted, broadband light and the two first order monochromatic light is directed as the output.

The angle between the beams is a function of device design, but is typically a few degrees. The bandwidth of the selected light depends on the device and the wavelength of operation, and can be as narrow as 1nm FWHM. Transmission efficiencies are high (up to 98%), with the intensity divided between the first-order beams. Another useful and unique feature of the AOTF is its ability to precisely and rapidly adjust the intensity of the diffracted (filtered) light by varying the RF power.

Advantages of Acousto-optic Tunable Filter

- AOTF is a rugged and compact device, with no moving parts. AOTF is solid-state device and is both compact and rugged [46]. Just as important, short of actually breaking the device, vibrations and shocks will not affect the wavelength calibration or the alignment.
- AOTF naturally has two orthogonal polarization state outputs. AOTF can have two orthogonal linear polarization states as its outputs. Used with an achromatic waveplate, it is ideal for dichroism/birefringence measurements.
- AOTF has a built-in solid-state chopper which can serve as a lock-in amplifier. The intensity of the selected light is controlled electronically and can be rapidly modulated by changing the RF power that is supplied

to the AOTF crystal. This makes the AOTF ideal for use with a lock-in (phase and frequency sensitive) amplifier for low-level light detection in the presence of strong ambient light.

- AOTF is extremely fast and can provide random access. The limiting factor for changing the wavelength is the time it takes for the acoustic wave to fill the optical aperture - typically several to several tens of a nanosecond. The entire spectra can be scanned at very high speed, or discrete wavelengths may be accessed at rates of tens to hundreds of kHz, even when separated by hundreds of nanometers.
- AOTF has high efficiency. AOTF is highly efficient with transmission at the selected wavelength as high as 98%. Unlike a **classical** monochromator in which the entrance/exit slits define the spectral resolution and limit the overall optical throughput, the spectral resolution of an AOTF is independent of the optical aperture. Therefore, optical throughput can be high. High efficiency translates directly into lower operating power, higher sensitivity and faster data acquisition system ([DAQ](#)).
- AOTF can be easily calibrated. For a given device geometry, the transmitted wavelength is determined only by the frequency of the applied RF signal, which can be generated with digital precision. Thus, an AOTF based spectrometer can be easily self-calibrated by changing the RF frequency. Since fluorescent spectroscopy applications usually require measurements at multiple wavelengths, short and long term wavelength repeatability are highly advantageous [38].
- AOTF can be easily computer controlled/integrated. AOTF has a high degree of controllability or programmability. In AOTF, the RF synthesizer is interfaced directly to a microprocessor or computer. This enables an AOTF based spectrometer to be programmed to scan or access different wavelengths very rapidly, and even to change the output intensity at those wavelengths. In use, therefore, it is easily integrated into almost any computer controlled measurement system.

Mechanical Issues

Traditional spectrometers require careful handling and frequent calibration. Because an AOTF is an all solid-state tunable filter with no moving parts, it is a compact and rugged device. Thus, it is relatively immune to orientation changes or even severe mechanical shock and vibrations [46]. Just as important, short of actually breaking the device, vibrations and shocks will not affect the wavelength calibration or the alignment.

Temperature Issues

Standard AOTF devices are not able to withstand and operate in very low temperature [46] because of the thermal expansion mismatch that exists between the transducer and the **AO** crystal. Thus, the technique for bonding the transducer to the AO crystal is crucial in constructing an AO device for low temperature operation. In the existing AO device technology, the transducer is bonded to the AO crystal by the use of an adhesive layer. The bonding techniques fall into two groups. In the first group (hard bonding), rigid adhesive layers such as metals or epoxy resins are employed. One major problem with hard bonding is that it results in thermal stress concentrated at the bonding interface due to the large thermal expansion mismatch between the transducer and AO crystal. For AO devices with an X-cut $LiNbO_3$ bonded on TeO_2 AO crystal, the thermal stress will fracture a hard-bonded device at a temperature no lower than $-100^{\circ}C$. Also, driving the transducer with RF power makes the device more susceptible to fracture.

AOTF System Integration - I

This chapter elucidates the various subsystems of the instrumentation chain of an integrated AOTF based NIR spectrophotometer. We can understand how the subsystems such as optical frontend, analog signal processing unit, microcontroller unit, data acquisition system work together in tandem to form the whole instrument. The interfaces between the subsystems and how they tend to produce a whole instrument will be explained from different points of view. For ease of understanding the system and its subsystems, as shown in Figure 24 is reduced into four essential blocks each dedicated for a particular functionality, with proper interfacing between them.

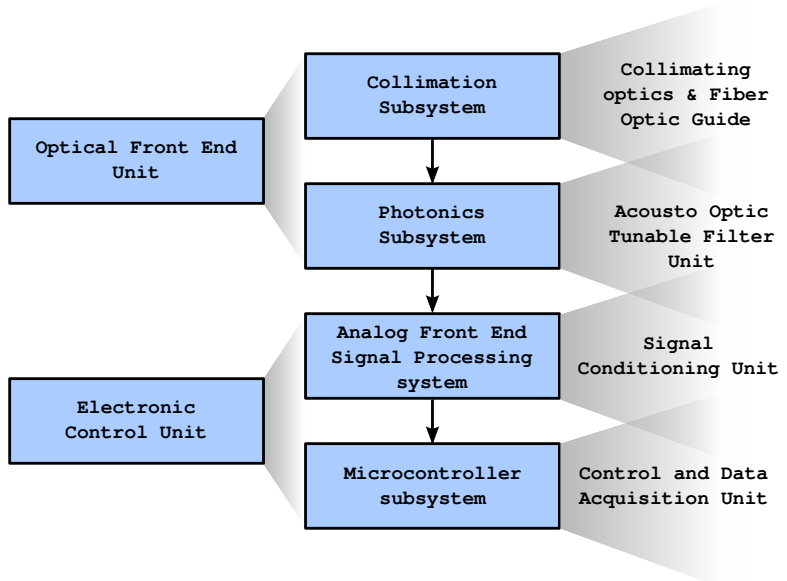


Figure 24: Layered abstract view of the Spectrophotometer system

The functionality with each subsystem is associated with the signals each system process and to propagate the result further down the path which will be again processed by another subsystem. With such a construction, the optical signal which is provided at the input port of the system, gets converted into electrical energy and then again into numerical data that can be processed by a microcontroller or by a computer at the farther end. The following list conveys an overall idea of how the subsystems interact to measure a spectrum.

- The collimation system will take care of generating the stimuli for the system consisting of a NIR source, and the set-up needed to focus it and guiding the same using respective fiber optic wave guide.

- The Photonics system comprises the electrically controllable optical components, that can replace the plane diffraction grating, which is an acousto optic tunable filter in our case.
- The Analog Front end system comprises the signal conditioning functions and interfacing circuits to match the signals from the photonics system and provide conditioned signals for forthcoming Digital system.
- The Digital (Numerical processing) system comprises the microcontroller, signal processing and control units, and a supervisory system by which the user is facilitated to command the system effectively.

The following block diagram illustrates how actually the instrumentation system are connected together while at the same time drills down further down the verticals of each subsystem in the instrument.

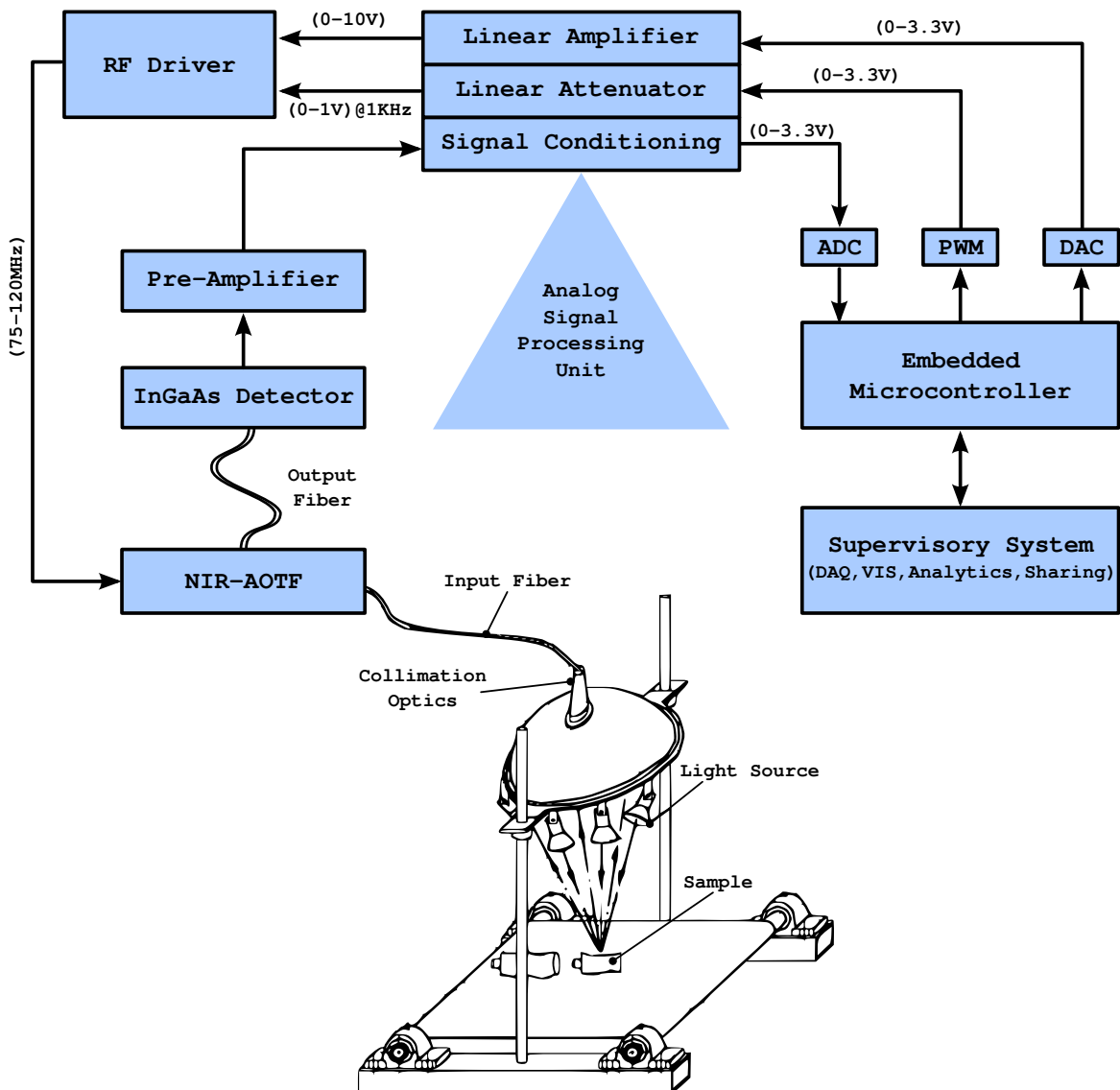


Figure 25: Block Schematic of NIR-AOTF Spectrophotometer

Figure 25 can be effectively understood on the basis of systems instrumentation point of view. The functionalities assigned with each block and its interface with its immediate block are listed and explained below:

- The sample/material under test is kept in the Light source and collimation assembly (Optical Front End System). Then the reflected or transmitted optical signal from the collimator is transmitted using the Fiber optic Transmission Line (Multi mode Fiber Optic Wave guide of 600μ), to the AOTF set-up.
- The AOTF set-up consisting the AOTF crystal and the other electronically controllable units, accepts the optical signal guided by the Fiber optic wave guide. The AOTF crystal is controlled electronically by the piezoelectric crystal which in turn is controlled by the RF Driver. The output optical signal is then again guided by the Fiber optical wave guide from the AOTF crystal output to the InGaAs detector. The modulated optical signal helps discriminate itself from the additive ambient and background noises.
- The InGaAs(Indium Gallium Arsenide) detector which receives the optical signal, converts it into equivalent electrical signal(current form). The InGaAs detector is Thermoelectrically cooled to compensate for the non-linearity effects due to Temperature rise in the detector(Reduces dark currents due to Thermal Noise), because of the high current densities. Then it is converted into voltage and sent to the pre-amplifier.
- The impedance matched pre-amplifier receives the electrical signal from the detector, then amplifies the voltage to the required level, reduces the offset voltage (couples the AC signal), increases the SNR(Signal to Noise Ratio), and then again the signal is sent to the Analog signal processing unit.
- The Analog signal processing unit, performs the linear signal conditioning functions such as, amplification, filtering, and series of other functionalities to improve the SNR to a significant level. It is the bridge between the sensor(Detector) / Actuator(RF Driver) system and the Computing system. It is connected to the Analog to Digital Converter(ADC), Digital to Analog Converter(DAC), and Pulse width Modulator(PWM), with suitable impedance matching conditions and voltage regulation units.
- The ADC converts the voltage signal representing the detected photon count, into numerical symbols, depending upon its conversion time, resolution, range, least count and linearity. Then the Algorithm implemented in the programmable memory of the Microcontroller takes the ADC quantized values as input, process it and the produces the suitable control outputs, in numerical form which in turn is converted into Analog signal using DAC. The modulation signal required by the AOTF is generated from the microcontroller using its PWM module.
- The microcontroller is in turn connected to a supervisory system, responsible for firing commands, as requested by the user of the system. In turn the microcontroller sends the data back to the supervisory system, where visualization, and online or offline analysis would be performed.
- The PWM signal and the control signal from the DAC is processed in the Analog signal processing unit (ASPU)for suitable impedance matching and voltage regulations. Then the PWM signal and the Control signal is applied to the Radio Frequency(RF) Driver. The RF driver which is very basically a voltage controlled oscillator (VCO) produces the continuously changing RF signal and drives the piezo-electric crystal driving the AOTF crystal, thereby responsible for producing suitable diffraction pattern(phase grating mechanism). The Diffraction efficiency of the AOTF is controlled by the magnitude of PWM signal or Modulation signal from the RF driver, also serves suitable segregation between optical signal of interest from the background noise.

Thus from the systems integration point of view, one can see that there are two most important abstraction, the hardware abstraction of the concept and the software abstraction for computing and control. The Hardware here includes, the mechanical, electrical, optical, electronic specifications which forms the basis for building the system. The Software part mainly concentrates on the use of control algorithm, employed to actuate the RF driver as per the user requirement, and to visualize and analyze the acquired data.

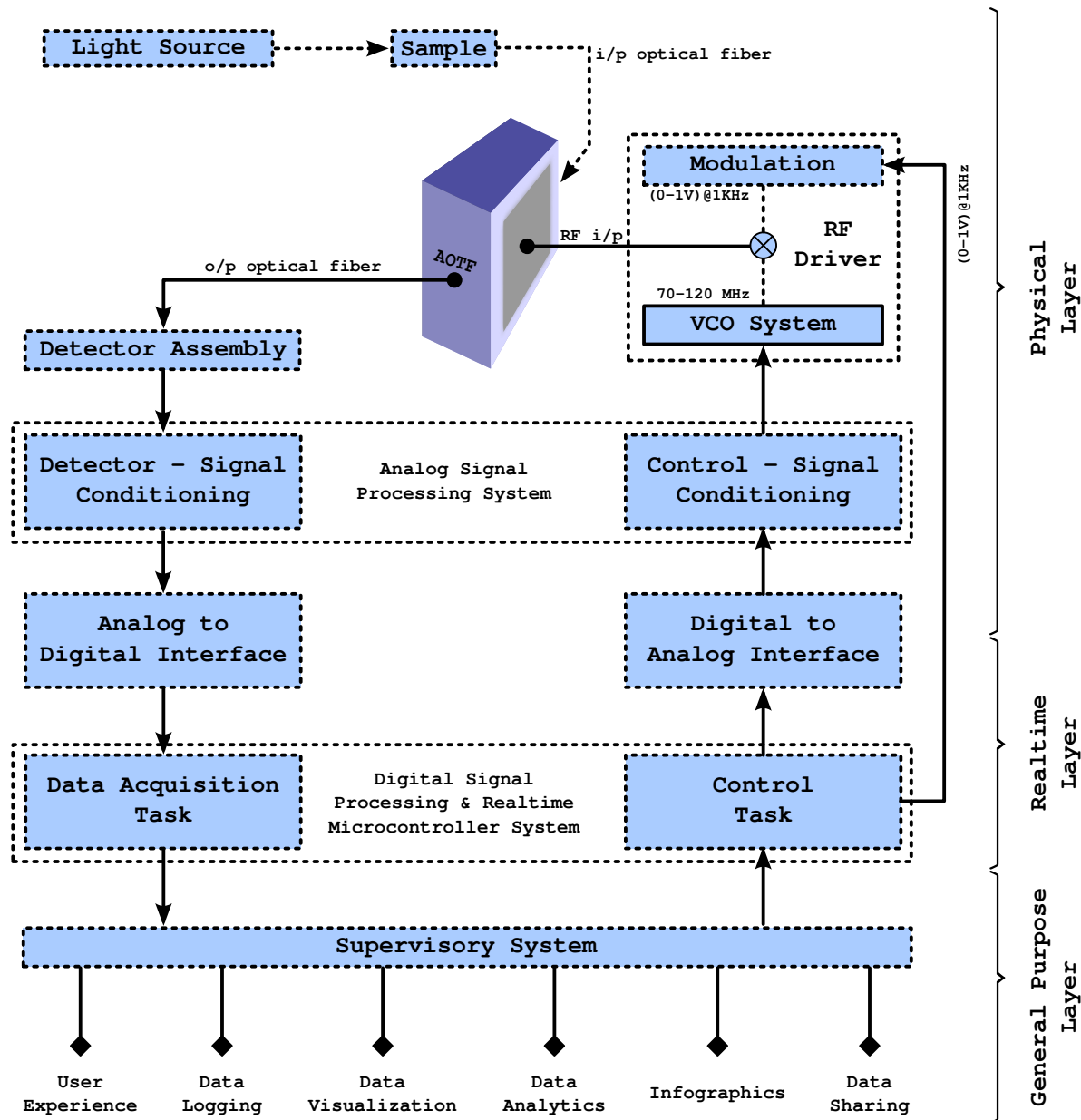


Figure 26: Signal flow Schematic of NIR-AOTF Spectrophotometer

The signal flow schematic as depicted in Figure 26, helps one to easily understand, the system's working mechanism based on Signals that are handled by the subsystems, at each layer providing necessary abstract functionalities(Signals and Systems point of view). This signal flow schematic is also helpful in isolating glitches which arise due to underpinning mistakes that are implemented between the abstraction layers. The signal flow graph emphasizes the importance of type of signals handled and about the subsystems each of specific type to handle the signals received from other subsystems.

This allows one to design the data acquisition([DAQ](#)) algorithms and control algorithms, effectively, because the algorithm designer is given enough information about the nature of the signals being handled, which necessitates the timing and deterministic relationship between the input and output of each subsystems. For instance, the DAQ algorithm must be aware of the state of the signal to be acquired, and its parametric nature : Amplitude, frequency, phase. Depending on this the sampling rate and the gain factor can be decided for better accuracy of the Sampled data representing the physical phenomenon.

One has to note, that deploying intelligence (algorithm) by software into the Realtime embedded target, should not anyway affect the deterministic requirement of the application. Obviously, the software part implemented in the embedded target, should not consume much resource like memory and processor. Even though missing the deadline may not result any catastrophe in this case, it will lead to misunderstanding of information extracted from the collected data.

Similarly the Analog signal processing unit, which are mostly linear systems, are used to perform the linear operations like amplifying, attenuating, filtering. Some non- linear operations may also be implemented, like modulation (generalized non-linearity). But application specific non-linear functions should be implemented using the software methodology. The voltage to frequency relationship of the RF driver (VCO operation), have a non-linear characteristic, and thus it is implemented with the help of look up table using the software, which is very vital for actuating the AOTF.

Non-linear characteristics of AOTF & Radio Frequency Driver

The desired non-linear characteristic behavior of the RF driver, is implemented in the software part. The lookup table is constructed from interpolating the characteristic curve of the voltage - frequency - wavelength relationship from the data-sheet of the RF driver. From the interpolation, the required voltage values are produced from the Realtime control hardware/software system.

The software maps the frequency required at the actuator end (AOTF-Piezoelectric) by pumping desired voltage to the RF driver in a sequential manner. The voltages which are pumped follow the non-linear characteristic curve as depicted in the voltage - frequency relationship given in the data-sheet shown in Figure 27.

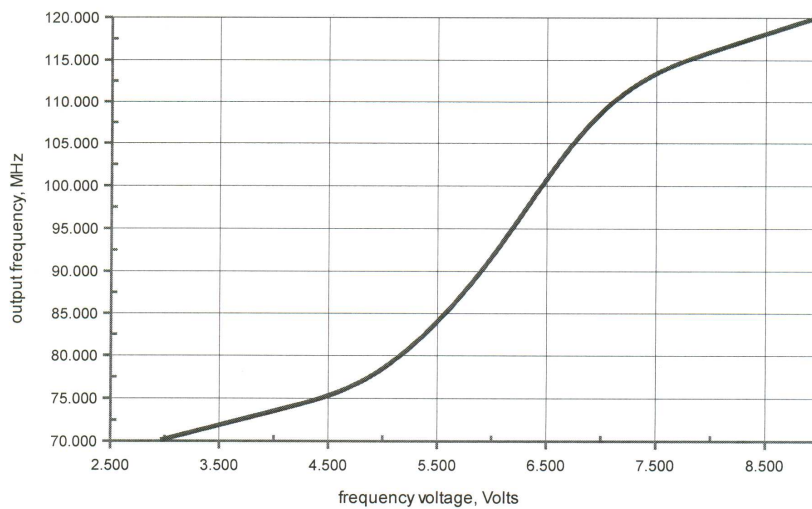


Figure 27: Voltage - Frequency characteristic curve of RF Driver

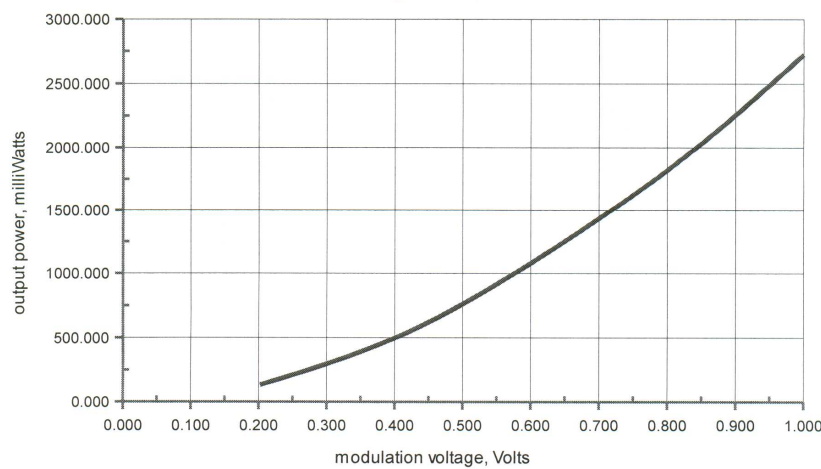


Figure 28: Output Power characteristics of RF Driver

As illustrated in the signal flow schematic in Figure 26, the AOTF crystal unit is controlled by the RF Driver unit, producing modulated RF output that drives the piezoelectric crystal bonded with the AOTF which in turn decides the diffraction efficiency of the spectrophotometer. Figure 28 shows the output RF power produced by the RF driver characteristics based upon the input modulation voltage.

Based upon the pumped RF power generated at a specific frequency AOTF selects a particular wavelength subjected to its own wavelength resolution. Figure 29 illustrates the nonlinear characteristic curve representing the filtering functionality of the AOTF subsystem.

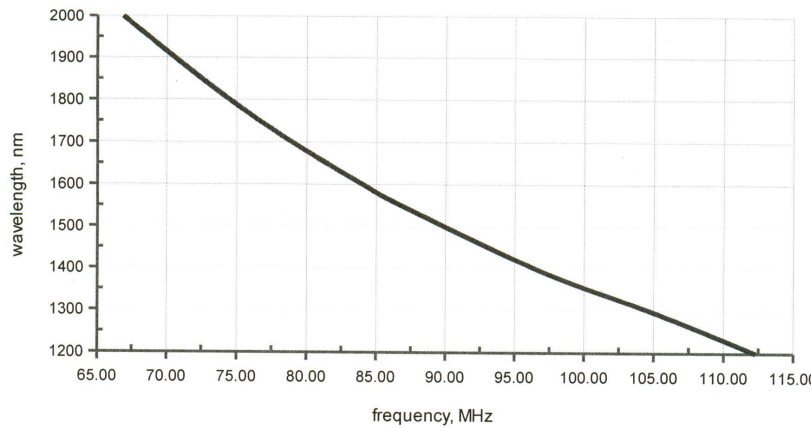


Figure 29: Frequency - Wavelength tuning characteristics of AOTF

Thus from the above characteristics we can clearly understand that the filtering phenomena actually reduces into three stage process as shown in Figure 30.

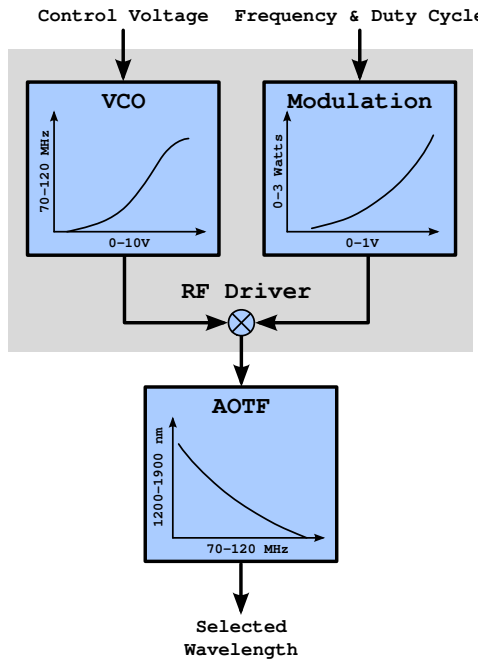


Figure 30: Filtering process involved with RF Driver and AOTF

The AOTF based wavelength scanning phenomenon can simply be viewed as a two part filtering mechanism operating in sequence with each other as shown in Figure 30. The wavelength scanning mechanism is actually a selection of sequence of wavelength under the spectral bandwidth of 1200-1900nm. Thus repeating a wavelength selection mechanism until reaching 1900nm will manifest the instruments behavior as a wavelength scanner. This also facilitates the system to be programmed to select a particular wavelength instead of scanning the whole spectral bandwidth when targeted for investigating only few specific wavelengths.

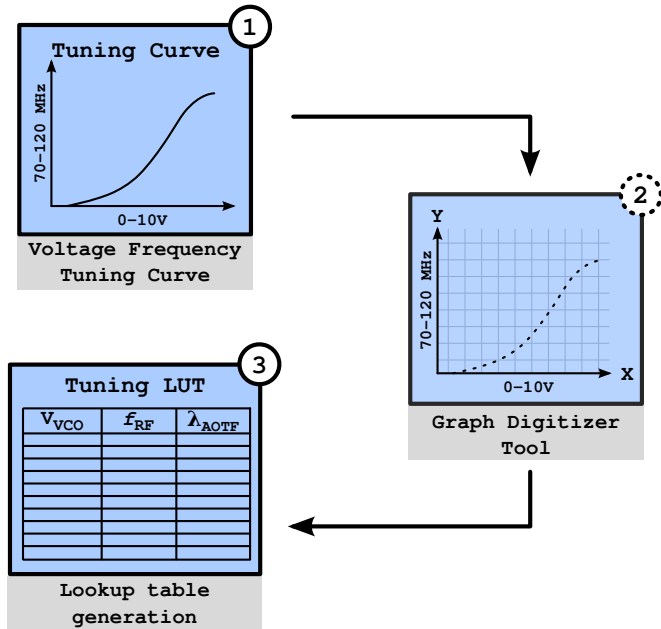


Figure 31: Interpretation of Tuning curve into lookuptable(LUT) involved with filtering process

In order to select a particular wavelength a modulated signal with specific radio frequency has to be pumped out from the RF driver. This requires two signals to be given to the RF driver. A control voltage(0-10V) for the voltage controlled oscillator and an analog modulation signal(0-1V) for controlling the RF power to be delivered to the AOTF. As depicted in Figure 30, the RF driver voltage-frequency tuning curve is completely nonlinear and thus requires to setup a complete lookup table representing it. This is accomplished by digitizing the tuning curve and converting the digitized curve into lookup table using the graph digitization tool[47] as shown in Figure 31.

The constructed lookup table consists of list of voltages necessary to control VCO operation (V_{VCO}) mapped to corresponding RF output frequencies (f_{RF}). The RF frequencies are then again mapped to corresponding list of wavelengths (λ_{AOTF}) as depicted by the AOTF wavelength selection characteristics. The lookup table representing the voltage-frequency tuning curve of the RF driver, was then used in constructing a microcontroller based data acquisition and control system interfaced with suitable dedicated analog signal processing unit. Such signal processing and control stack facilitates wavelength selection and provide better operational stability.

Implementation of Prototype Analog Signal Processing Unit

ANALOG SIGNAL PROCESSING UNIT(*ASPU*) is the bridge between the digital signal processing system and the physical units (sensors and actuators) of the system. In that way, it is a necessary abstraction layer between the two ends. It takes care of linearization, noise removal, and if any non-linear signal processing involved. It interfaces the numerical quantity provided by the digital system to the actuator by processing the signal provided by DAC. Similarly it provides electrical signal to ADC, by conditioning the signal from the sensor/detector system with low SNR. Functional schematic of the analog signal processing chain is shown in Figure 32. Usually, the design goal of this very vital system is :

- To ensure good signal integrity.
- To ensure signal isolation from each other.
- To ensure safety for the personnel, and protection of the circuit components.
- To provide necessary test points for glitch isolation.
- To provide good Signal to Noise Ratio (SNR) by following generalized signal conditioning rules, suitable for the application.
- To numerically compute and verify the SNR by using mathematical transfer functions of the functionality expressed by a circuit block, formed by set of circuit components.
- To implement the unit to produce as precise measurement as possible.

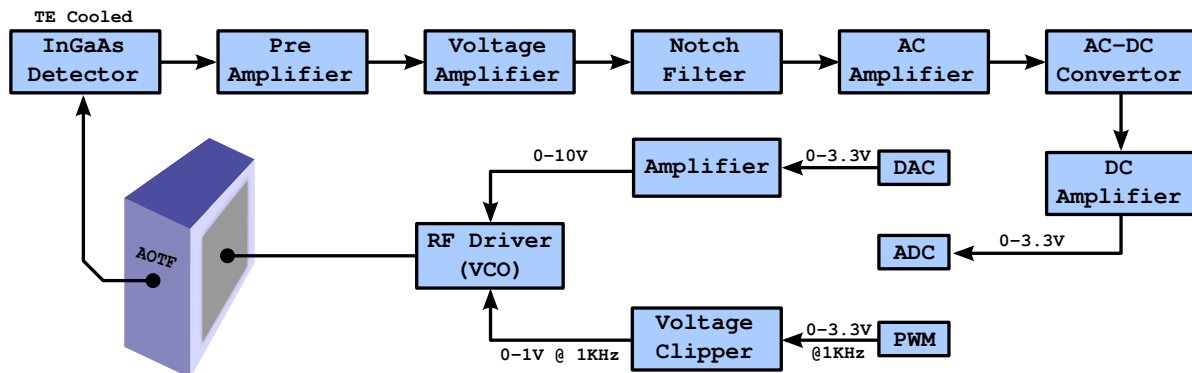


Figure 32: Analog Signal Processing Chain Block Schematic

The following section describes each of the sub units in the analog signal processing system in detail along with their designed circuit schematic and possible tested signal outputs probed at required points in the whole circuit. The analog signal processing unit is fabricated upon a perforated board, which was designed with the circuit design as shown in Appendix G. The circuit is also designed with KiCAD Circuit design tool [48]. The sub modules of the *ASPU* was tested individually and verified for its functionality. After testing the modules sequentially one after the another, the *ASPU* chain is formed as proposed in Figure 32. The corresponding design values for the circuit components such as Resistors, capacitors are shown in following subsections and in Appendix G.

InGaAs Detector: InGaAs detectors [49] [50] [51] operate over the spectral range from 0.8μ to 2.6μ . These detectors provide fast rise time, uniformity of response, excellent sensitivity, and long term reliability for a wide range of applications. The used InGaAs detector: *J23TE2 – 66C – R01M – 2.2* have a Full Width Half Maximum (FWHM) bandwidth range of 1.2μ to 2.2μ .

Thermoelectric Cooler (TEC): For enhanced performance or temperature stability of response near the cutoff wavelength, detector is cooled thermoelectrically. The *CMAMP – T066 – PA7* Thermoelectric cooler (TEC) has been integrated with Heat sink amplifier and Temperature controller, thus the functionalities of detector signal amplification, heat sinking, temperature control can be attained in a single package [52].

Pre-amplifier: The Pre-amplifier is a Transimpedance amplifier [53], that converts the current generated by the photodetector to voltage. The used pre-amplifier (PA) is *PA – 7 – 70*, which is designed to give best performance for InGaAs detectors. The bandwidth of the pre-amplifier operation depends upon the detector resistance and capacitance. The pre-amplifier is impedance matched, so that it offers a 50Ω impedance for transmission of voltage signal through the coaxial transmission line.

Voltage Amplifier: This is the first sub unit in the fabricated analog signal processing system. The impedance matched voltage amplifier, improves the gain of the pre-amplified signal. The first version of the analog signal processing unit is designed with a gain of 38 (approx.). The output of the gain stage is then driven to the filter stage. Designed Voltage amplifier at the measurement side is shown in Figure 33.

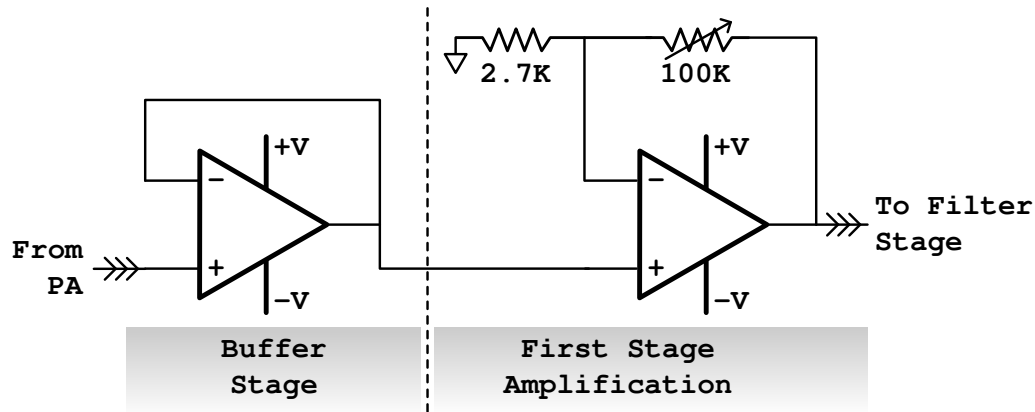


Figure 33: First Stage - Voltage Amplifier Unit

Notch Filter: Here due to difference in the reference voltages, a line cycle noise appears in the input signal, thus lowering the SNR. The designed Notch Filter at the measurement side is shown in Figure 34. In order to remove the fundamental line cycle noise of approximately 50 Hz , a notch filter is designed with cutoff frequency of 50 Hz , with high Q . It has to be noted, that even though 50 Hz (fundamental) notching is achieved with this technique, we have not achieved eradicating the harmonics of 50 Hz , which causes little variations in the signal level. Usage of Isolation amplifier can eradicate the problem.

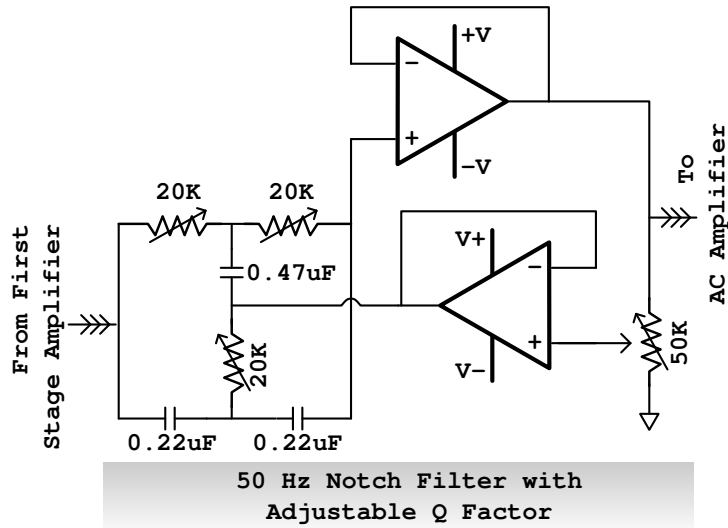


Figure 34: Notch Filter Unit

AC Amplifier: After removing the fundamental line cycle noise from the signal, it is experienced that the signal appears with a DC offset, which must be avoided. Thus a AC coupling stage with **AC** amplification, will aid us to minimize the DC offset voltage effectively. The designed amplifier at the measurement side is shown in Figure 35. Now the resultant AC voltage signal, found to be matched with the modulation frequency applied to the AOTF crystal, which is in turn the frequency generated from the PWM controller. This typical 1 KHz signal conforms the system functionality.

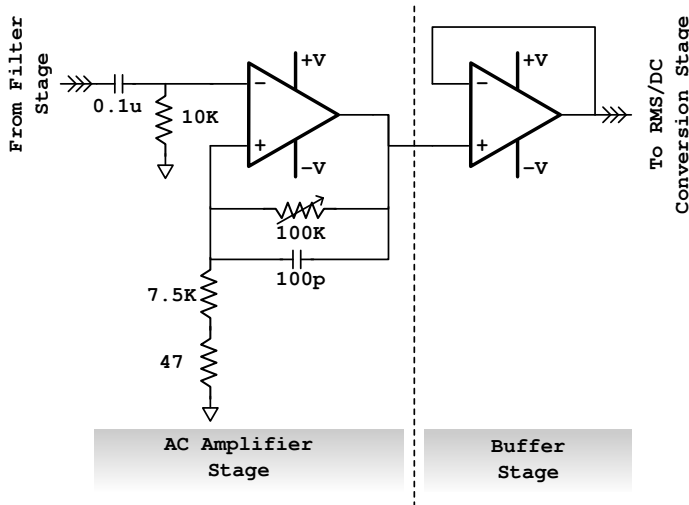


Figure 35: AC - Voltage Amplifier Unit

AC-DC Converter: The **AC** signal @ 1 KHz, cannot be used to represent the physical phenomena. Thus the energy contained in the AC signal (information of the physical phenomena), has to be extracted. This can be attained by using a **AC to DC** converter, and the resultant DC signal confirms to change the voltage level when there is a change in the amplitude of AC signal. The AC to DC converter used here is a monolithic RMS to DC converter [54] having its own analog computation unit built into a single package. The configured AC-DC converter at the measurement side is shown in Figure 36.

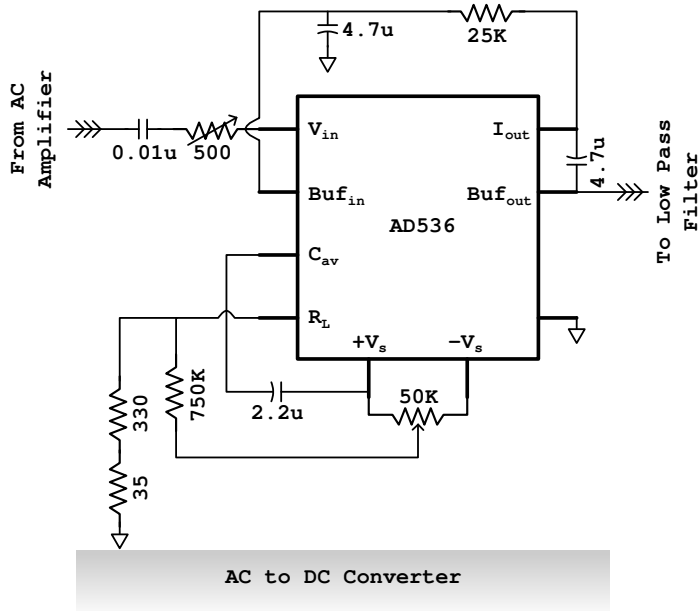


Figure 36: RMS to DC Converter Unit

DC Amplifier: The significant **DC** voltage is amplified linearly, to send it to the Analog to Digital Converter, of the microcontroller. The signal is impedance matched to avoid reflection. Similarly, the analog signal from the Digital to Analog Converter has to be impedance matched and amplified linearly to cover the full range of the RF driver input voltage requirement(0 – 10 V) DC, so that it pumps the RF signal to AOTF crystal, to produce the diffraction phenomena. The final stage amplifier designed at the measurement side is shown in Figure 37.

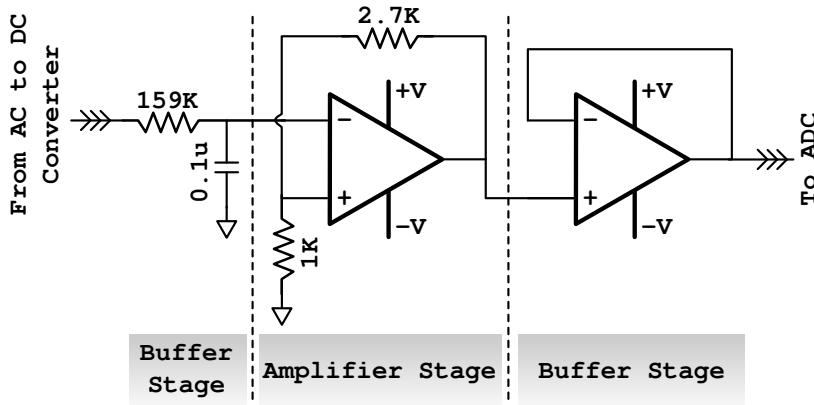


Figure 37: Final Stage DC Amplification before ADC

PWM Generator: The **PWM** signal is solely, responsible for controlling the diffraction efficiency, and improving the SNR by applying the modulation voltage to the crystal, along with the RF signal. The PWM is generated with the PWM controller module integrated within the microcontroller. The frequency and the Duty cycle can be changed through software.

Voltage Clipper: The voltage clipper shown in Figure 38 is interfaced with the PWM generator from the microcontroller, in order to clip the voltage level of the PWM signal to a maximum of 1 V. This limitation is due to the requirement, of the RF driver, stating that the modulation voltage cannot be more than 1 V at maximum.

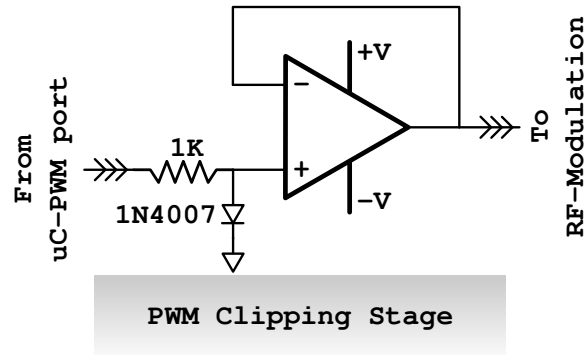


Figure 38: PWM Clipper Stage

Control Signal Conditioning: The generated voltage from the DAC varies from 0 to 3.3V which has to be applied at the *Frequency* port of the RF Driver that requires 0 to 10V. This voltage is the required for the VCO in the RF Driver generating from 70MHz to 120MHz RF signal which in turn will be applied to the AOTF electrical input.

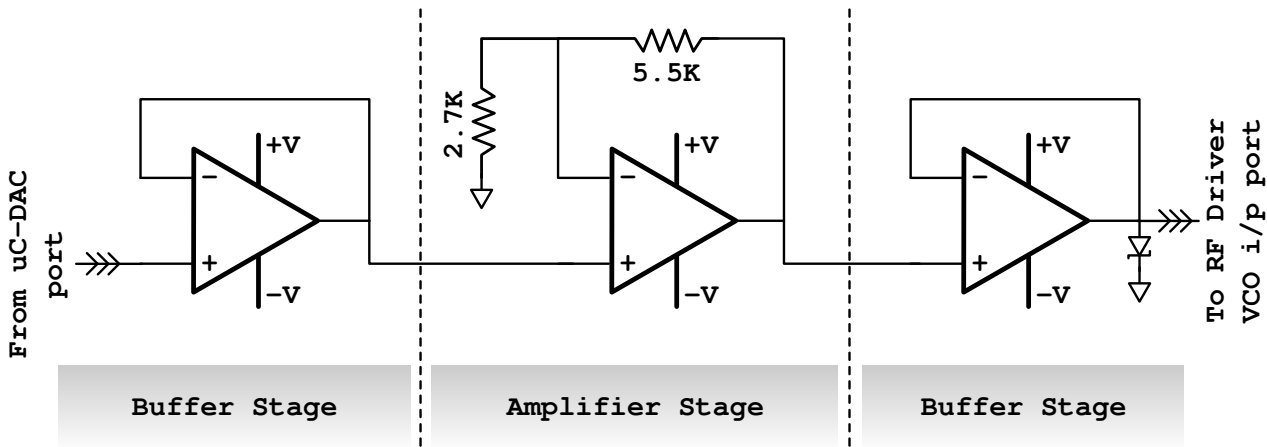
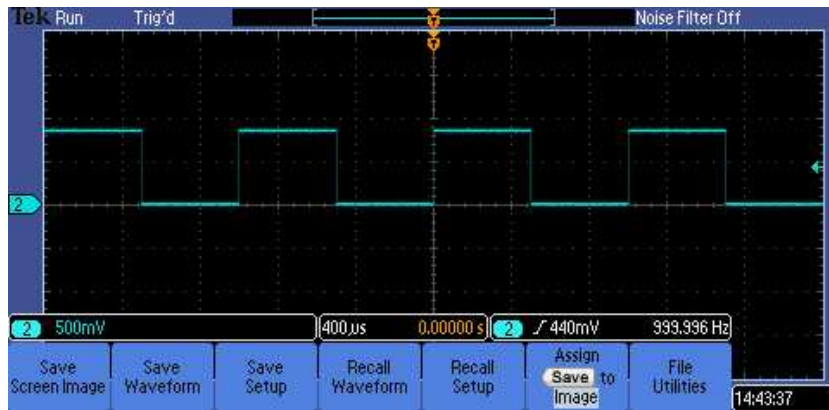
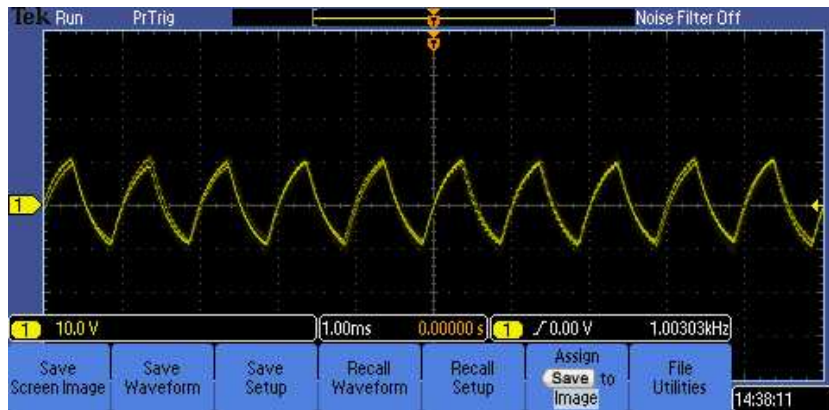
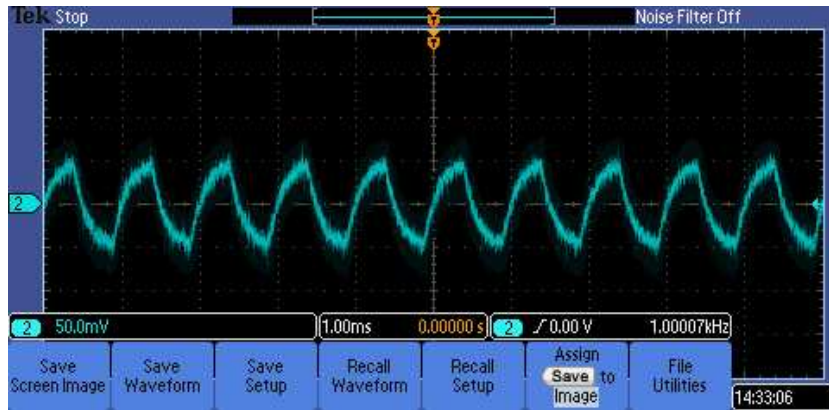


Figure 39: DAC to VCO Signal Conditioning Unit

After making the complete fabrication on the board, it was integrated with the microcontroller system and the AOTF system. Input and output voltages were completely verified for the non-linear relationship, depending upon the tuning curve. The necessary test points were pulled out through a DB – 9 port. This DB – 9 test port provides the accessibility for understanding the circuit behaviour, fault isolation thereby rapidly replace the damaged components if any. The test signals at various outputs were shown in CRO waveforms (Figure 40, 41, 42, 43). The fabricated unit is shown in Figure 44.



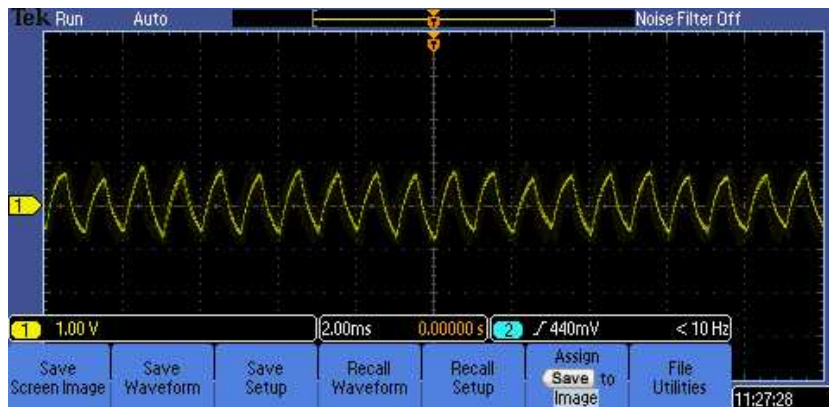


Figure 43: Amplified AC component of the **Sample** signal with $10 \times$ CRO probe setting during scan

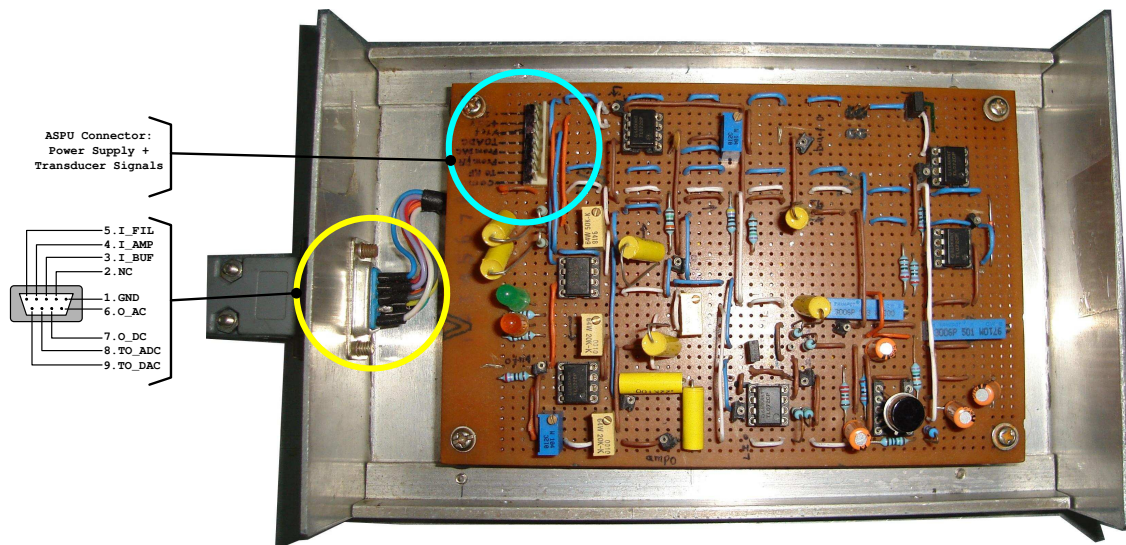


Figure 44: Fabricated electronic **ASPU** board

AOTF System Integration - II

Prototyping Microcontroller based Embedded System

Implementing a Signal to Data conversion, & Transmission functionality with a microcontroller based system follows a generic embedded system approach in the instrumentation chain. Regardless of its implementation philosophy and policy that governs its functionality this unit expresses the core control mechanism. Figure 45 represents the necessary functionality and its interface with the adjacent systems(ASPU & Supervisory system) similar to the analog signal processing chain.

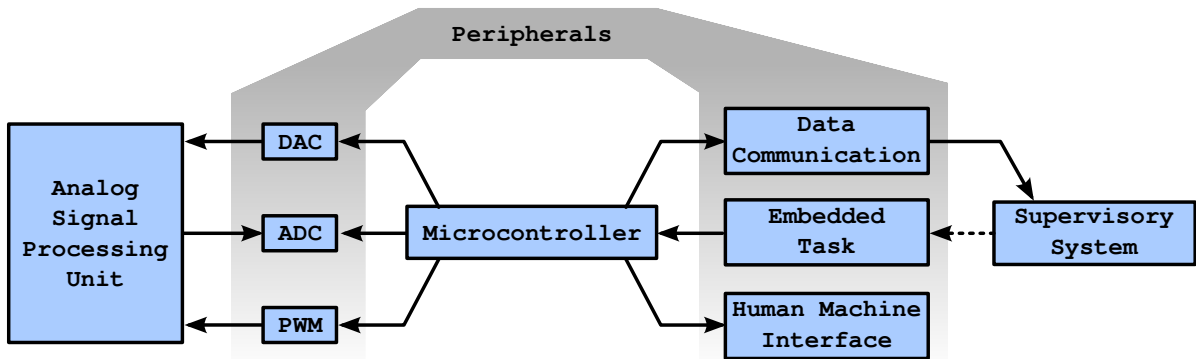


Figure 45: Generic Microcontroller with an embedded task interfaced with ASPU and Supervisory system

Its vital role manifests its functionality as an essential part of the whole instrumentation chain which cannot be stripped off the integrated system. In particular, associated with the spectrophotometer the embedded system share its function not only in producing the pulse width modulation signal (with adjustable duty cycle & frequency), driving the Digital to Analog Convertor but can also generate a lookup table instead of manually feeding it through an embedded task. However for prototyping the microcontroller is now equipped with manually generated non linear lookup table. Automated lookup table generation is readily possible only when the mathematical model for the required driving profile is devised and programmed as an embedded task.

Apart from its core functionality of controlling and collecting the data routinely, based on the requirement and the peripheral availability such as storage, human machine interface and communication the means of configuring and controlling the embedded system through supervisory system varies. So depending upon the features required the number of peripherals increases proportionately around the microcontroller when not available as an built in unit. Thus based upon the number of peripherals and features the code density required to access their functinoalities increases which directly impacts the systems performance [55]. This requires in optimizing the code generation, programming, testing and debugging cycle during the development time.

Without any difference in the implementation mechanism, the philosophy and policy decides the implementation methodology [56] [57] [58] that influences the process of integration. In the following sections we will demonstrate and discuss how the same mechanism was implemented proprietary tool chain and free tool chain respectively.

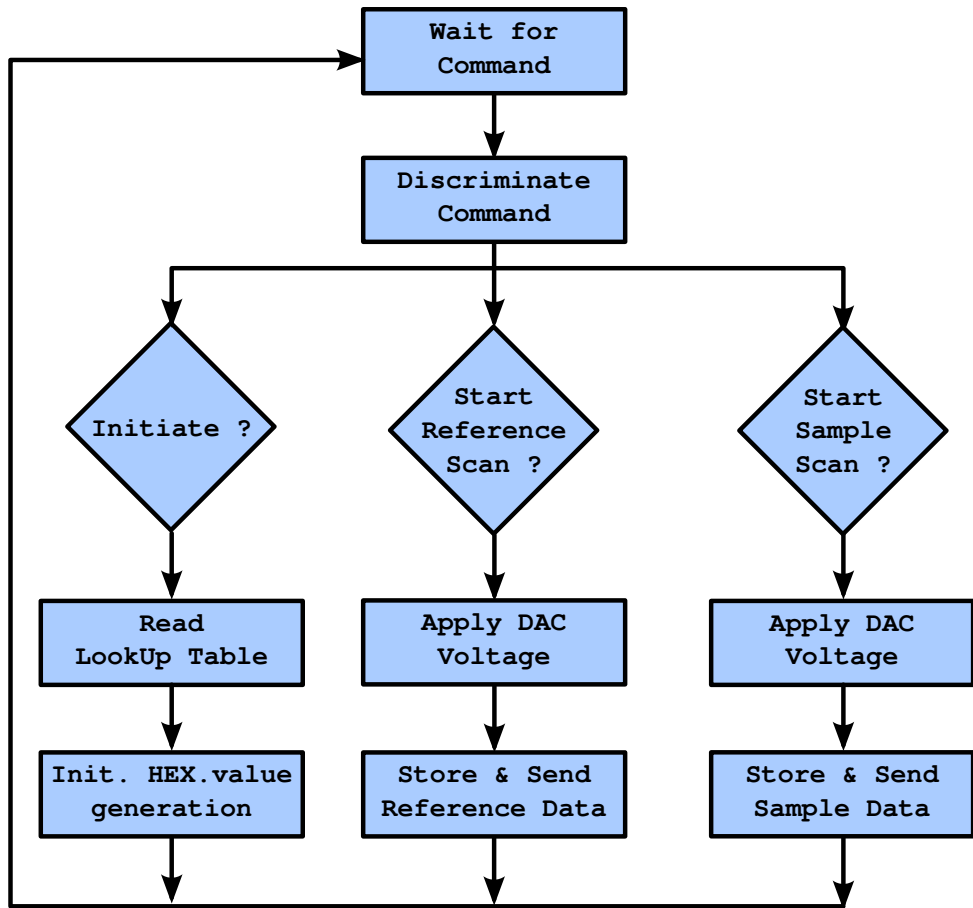


Figure 46: Flowchart of the em-
bedded task

The Mechanism : Embedded Task

As explained previously, any embedded system designed in generic manner will then be targeted for a specific application by developing software which provides some intelligence for the bare hardware. In our case, the targeted application i.e., developing a software controlled NIR-AOTF based spectrophotometer requires a specific task which had to be burned or embedded within the microcontroller of interest that performs three vital functions. First is the generation of DC voltages from 0 to **FSV** which will then be amplified by the ASPU matching the range required by the RF driver. Second, generating a continuous PWM signal which could be configured while the instrument is online for controlling the applied RF power which again has to be applied to RF driver. And finally, the response from the AOTF after passing through **ASPU** has to be collected properly and transmitted to the supervisory system. Figure 46 illustrates the flowchart explaining the control and data flow in the implemented mechanism.

Implementation through Proprietary System

The microcontroller based embedded system platform selected for implementing the designed mechanism is a KEIL - 16bit - **ARM7** belonging to LPC214X family of microcontroller. Figure 46 shows how the system is integrated together with this microcontroller and what are all the peripherals used along while integrating the system. For programming the microcontroller development board a KEIL μ Vision Integrated Development Environment and its proprietary tool chain was used. The lookup table generated to match the **AOTF** tuning characteristics as listed in the Appendix E was calculated specifically for the DAC resolution available in this microcontroller. Many other signle board instruments were avaialable with different implmentation strategies [57] that helped visualize the functionality of the embedded system.

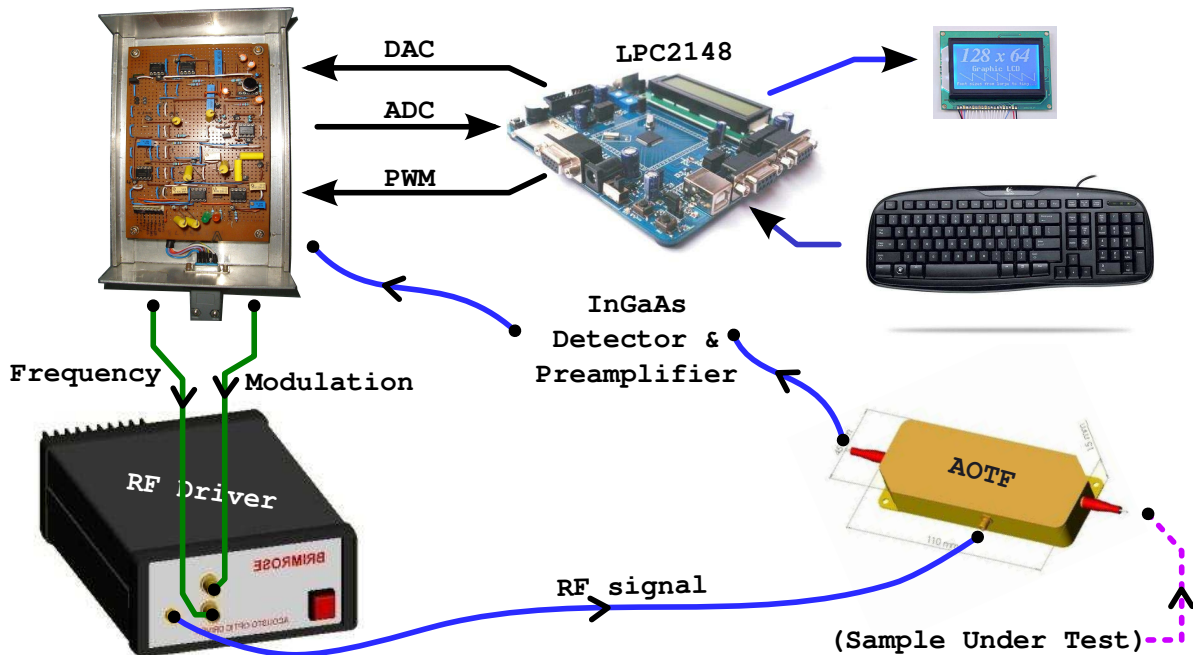


Figure 47: Integration using proprietary embedded microcontroller

Implementation through Free System

Ease of prototyping, transparency, collaborative development, freedom and generic nature of democratically licensed tools help not only design a system with minimal footprint but vitally helps propagate the scientific/engineering knowledge associated with the project it is involved. Furthermore the designed system was aimed to keep it simple and stupid as much as possible and distribute the workload depending upon the subsystems performance. In that way the whole system can stay modular that eases isolation from each other while keeping the interfacing clear and transparent.

We used Arduino based microcontroller platform constituting AVR 16 bit microcontroller. The microcontroller is serially programmed using the Arduino IDE that uses the GNU-AVR tool chain to compile the programs and generate the executable file. Adopting the basic mechanism to be devised the microcontroller is programmed and integrated as shown in Figure 48.

The program does the calculations to generate the required hexadecimal values from the sequence of voltages required that matches AOTF tuning characteristics. The required sequence of voltages were generated using a modular DAC board(MCP4725) interfaced with arduino through I₂C interface. This setup is tested and corresponding output is shown in Figure 49 for consecutive scans.

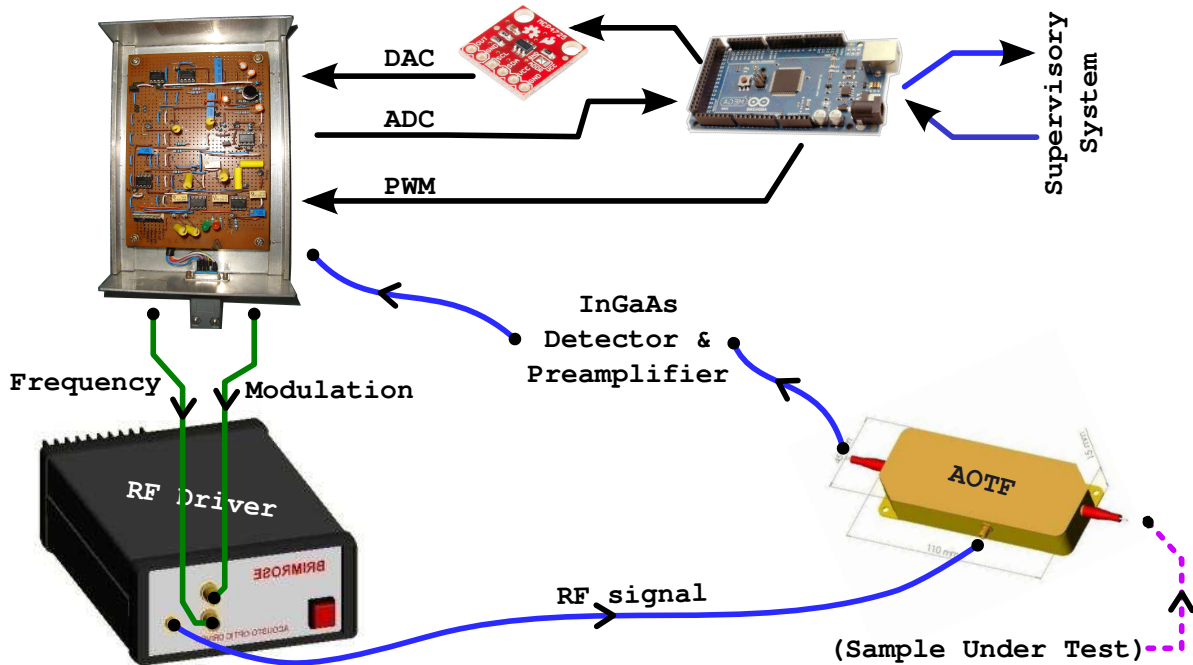


Figure 48: Integration using free microcontroller platform

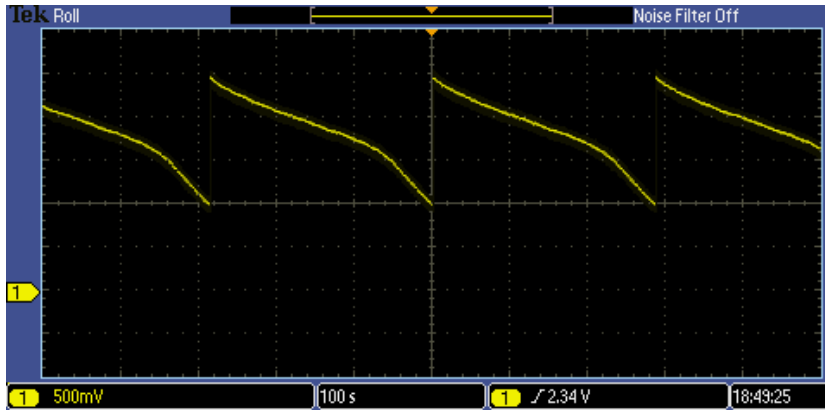


Figure 49: DAC output from MCP 4725 interfaced with Arduino

Prototyping Supervisory System

Supervising an embedded system in order to acquire the collected data, to store & analyze and produce the report based upon the information achieved so that it can be shared and further explored to attain theoretical or experimental knowledge is necessary. It is supervisory system that manages, configures and controls the underlying embedded layer which in turn takes care of all physical activities of the spectrophotometer. It abstracts (with transparency) all the physical processes and complex functionalities of instrument from the user.

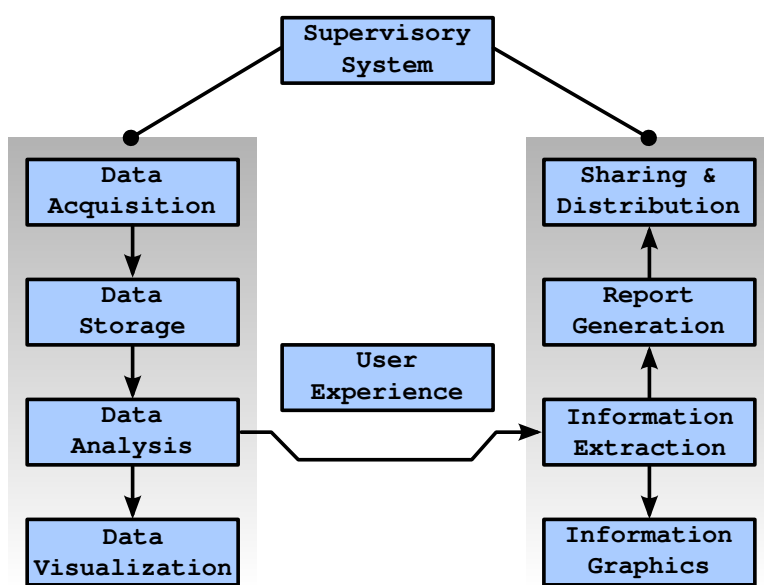


Figure 50: Supervisory system designed for the spectrophotometer

In general a supervisor system must be simple with graphical experience, management and configuration options specific for the targeted application. It is essentially a nice bridge between the embedded layer and the user interacting with the instrument. The user expects the instrument to do something based on the experience he/she gains from the supervisory layer. The design should not be based on providing all the options by default but only on request. Moreover developing a dedicated software instead of a generic library would further limit the propagation of the software architecture which can later be customized based upon the requirement.

The features to be offered by the system in general are data acquisition, data storage, data analysis(offline & online), data visualization([VIS](#)), information extraction, infographics and report generation, distribution and sharing of data/information/reports to the peer using distributed communication medium. It is not necessary to include all of these features in the designed software, but the idea is to make it more generic - so that the user can use at ease as well as more specific - so that the user can use their knowledge to exploit the internal workings of the instrument. Figure 50 shows how the supervisory system's mechanism was devised to target the functionalities of the NIR-AOTF spectrophotometer. However the system designed as described in the following sections does not include all of the features listed in the Figure 49. But the implementation consists provisions that enables most of the required functionalities to operate the spectrophotometer completely.

Implementation through Proprietary System

To implement a supervisory system based on a proprietary model, the microsoft visual basic programming [IDE](#) was selected with visual basic as the programming language that enables the interface and communication with the proprietary KEIL embedded platform.

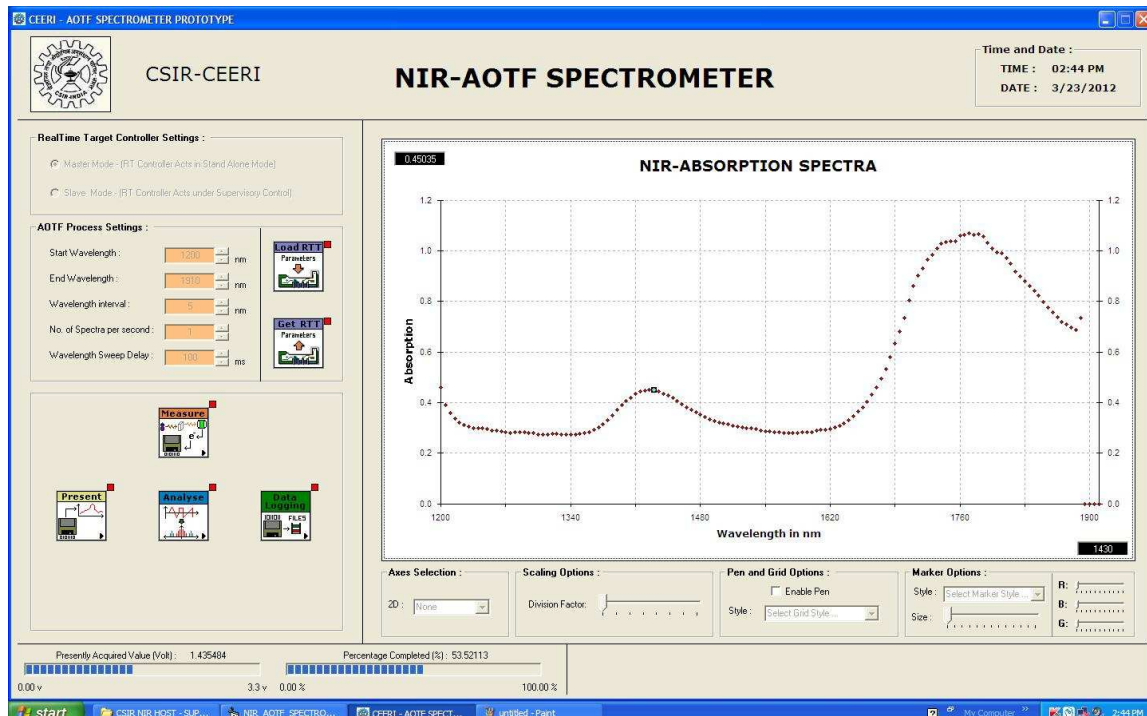


Figure 51: [GUI](#) based on Visual Basic

Similar other implementations was already done for AOTF based imaging spectrometers [58], which gave a general idea about the supervision strategy. Operating in tandem they facilitate the acquisition of NIR spectra and store them in spread sheets. The programming is event driven and is not asynchronous. This drawback have made the programming complex for which a super loop have to be executed polling the user execution and reject it while spectral scanning takes place. However, a working prototype have been devised and integrated together with the instrumentation chain. The designed application is shown in Figure 51.

As far as the code density, modularity and abstractness it does not qualify the quality scores. As the number of user interface elements increased to provide more flexibility and features to ease the access of instrument functionalities, managing the development become cumbersome. Figure 51 shows the graphical user interface of the supervisory system designed with Microsoft Visual Basic while collecting the spectra through the KEIL microcontroller embedded platform.

Implementation through Free System

With the availability of number of free systems we have chosen a trilayer approach to change the considerable part of the system to better increase the isolation and modularity of the software part. This trilayer approach as shown in Figure 52. It aims at distributing the work to respective subsystem which can perform that function alone and performs it better rather than all in one approach.

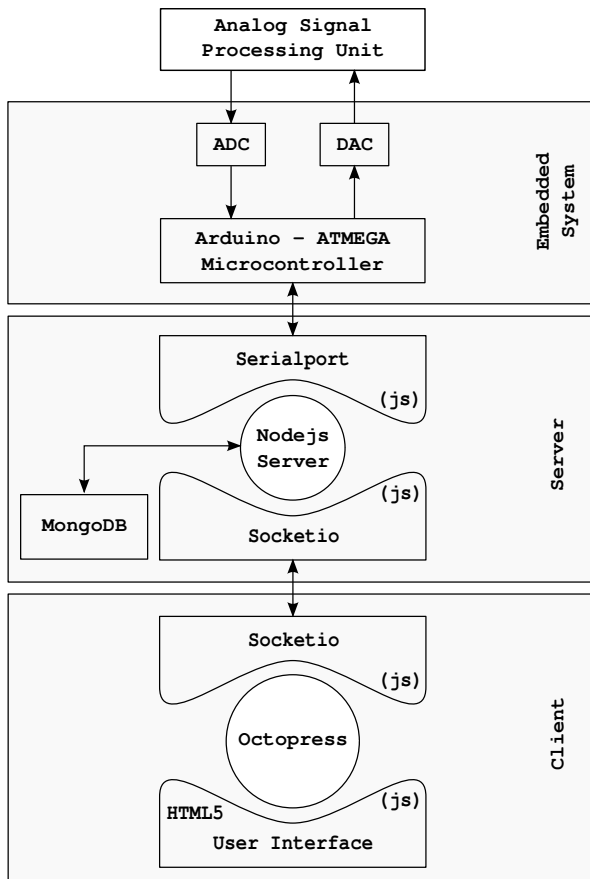


Figure 52: Trilayer approach of integrating embedded and supervisory layers

This embedded system-client-server – trilayer architecture provide a better understanding of the software implementation of the instrument which facilitates future updates to the system to be drilled down and classified with ease without disturbing other modules of the system. This trilayer approach involves Desktop, Embedded System and Web technologies integrated together to provide optimal usability by overlaying the advantages and minimizing the limitations of each system to a minimum which enabled us to push the operating boundaries of the system much further than the traditional approach of software development associated with instrumentation. Figure 53 shows the graphical user interface designed during the early stage of prototyping the supervisory system designed based on the trilayer approach.

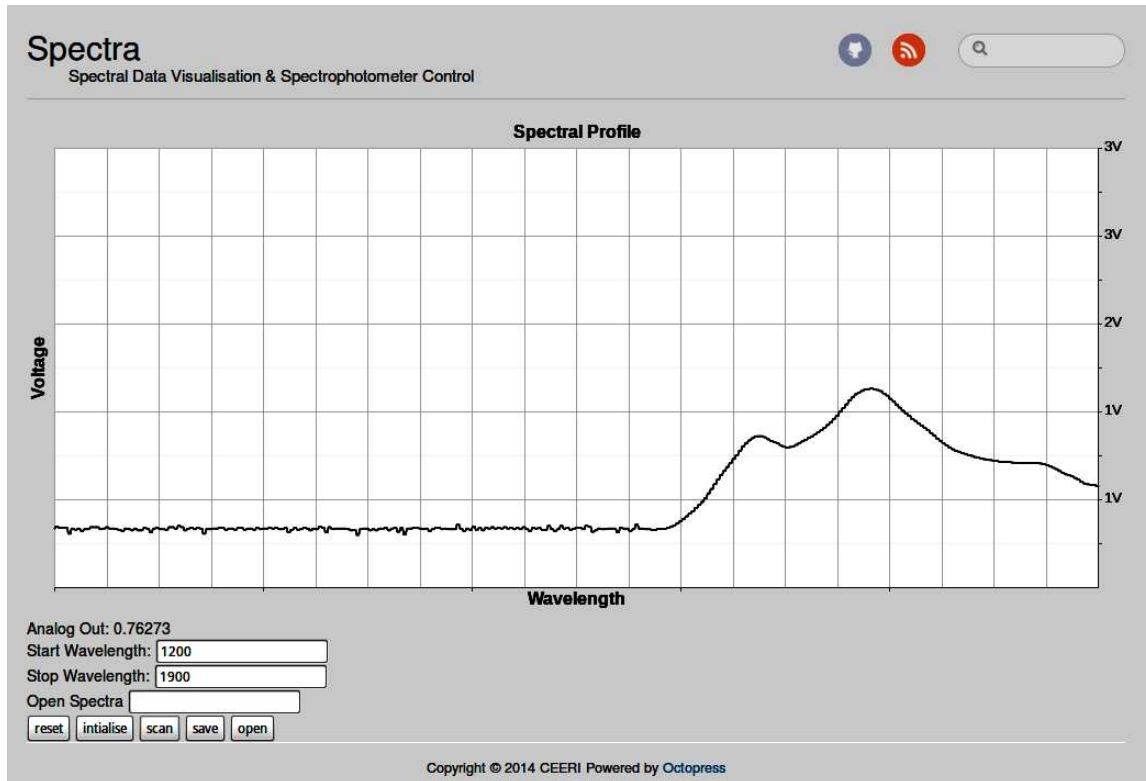


Figure 53: [GUI](#) based on [HTML5](#) & [JavaScript](#)

As shown in Figure 53, the [HTML5](#) based user interface which can be easily customized using web designing technologies like [CSS](#), helps the user to access it through any web browser(client) and feed in the required configuration and command to control and acquire data from the spectrophotometer. The events triggered by the user interface propagates down towards the server which may be running on its dedicated system or else in a general purpose computer transforms them to commands that can be understood by the microcontroller system. After taking necessary action, the microcontroller sends back the acknowledgement or data to the server which again propagates up towards the user interface to visualize the data acuired to the user.

Testing

RF Driver Test

After integrating the analog signal processing unit, microcontroller and the supervisory human machine interface into the spectrophotometer, the actuator end (RF Driver) is tested for conformance of its operating functionality. The RF driver as explained in beginning of this chapter has a nonlinear behavioural characteristic matched to that of the wavelength tuning curve of the AOTF. The necessary interpolation of the RF tuning curve into RF tuning lookup table and embedding the same in the microcontroller program is a vital part of the spectrophotometer's control functionality. The interpolated nonlinear lookuptable based on the understanding of the AOTF filter process has limited resolution ruled by the spectral resolution depicted by the AOTF (TeO_2) crystal.

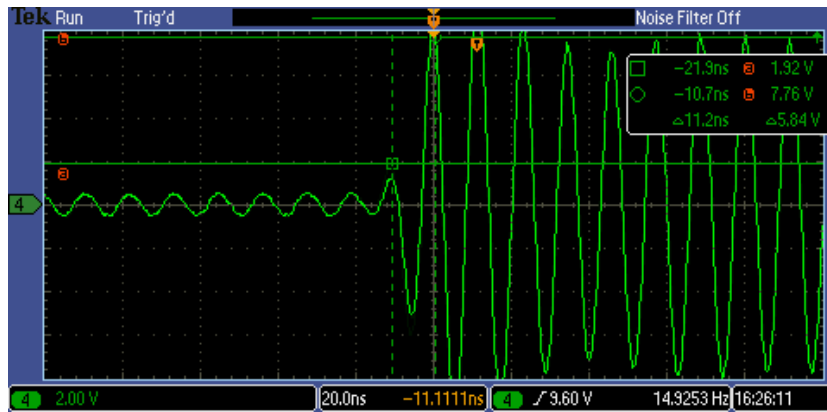


Figure 54: RF rise time test output captured with MSO

The constructed lookup table is provided in Appendix.H. Since the spectral resolution as provided by the manufacturer's test data is at 5nm(max)@1550nm, the quantization of the RF driver tuning characteristic curve is also set to 5nm interval. This produces a lookup table with spectral range of 1200nm to 1900nm with a step change of 5nm, which quantizes the tuning radio frequency generated by the RF driver accordingly. This lookup further quantizes to generate only 140 voltage values generated by the DAC interfaced with the microcontroller. The generated RF signal for tuning around 1550nm is shown in Figure 54 & 55 each representing the risetime and falltime involved with the analog modulated RF signal respectively. The modulation signal is a pulse width modulation signal with modulation voltage of 850mV and modulation frequency of 1KHz, with 50% dutycycle.

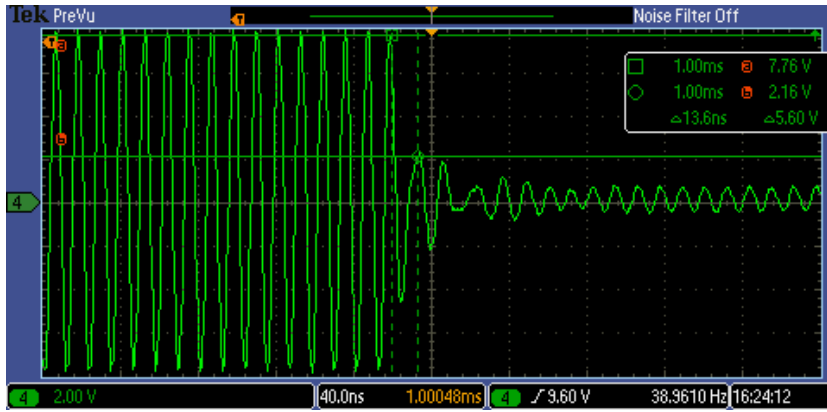


Figure 55: RF fall time test output captured with MSO

The plot shown in Figure 56 represents the constructed values of RF output power by digitizing the modulation voltage - RF output power curve from the datasheet supplied by the manufacturer. The experiment to understand the functionality of RF driver is done by exciting it with a voltage(VCO input) corresponding to 1550nm as dictated by the lookup table generated (**LUT**) (Refer – Figure – 30).

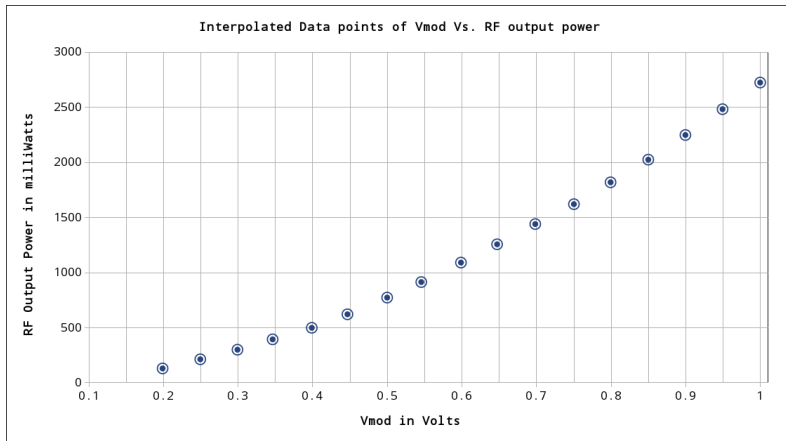


Figure 56: Constructed plot of RF power for change in modulation voltage

The pulse width modulation frequency is maintained at 1KHz@50% duty cycle, while the modulation voltage is gradually increased with a step voltage of 50mV from 0V to 1V. The observed RF power is plotted against the modulation voltage as shown in Figure 57. It consists of four additional data points observed between 0V and 200mV which is not provided by the manufacturer as in Figure 56. The above two plots were compared by calculating the correlation between them. Thus the correlation is taken for RF power data sets corresponding to modulation voltage within the range of 200mV to 1V. The correlation results in 0.9976, as the observed RF power has a positive offset of about 500mW for minimum input modulation voltage.

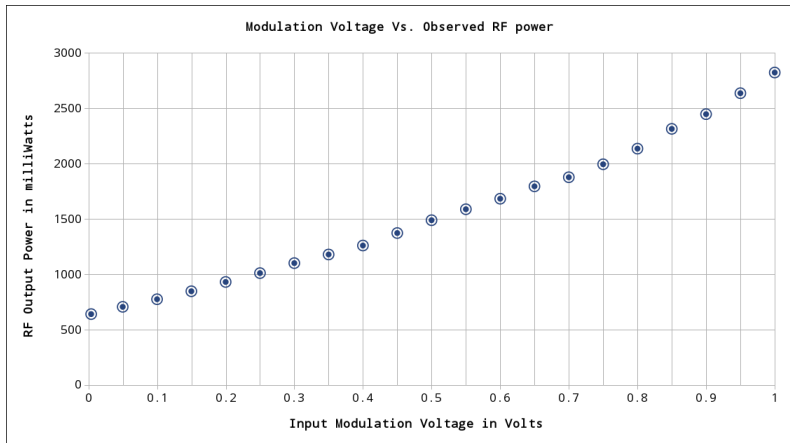


Figure 57: Experimental observation of RF power Vs. modulation voltage

Spectral Test Output from the Spectrophotometer

Shortly after completing a working prototype of the NIR-AOTF spectrophotometer, a collaborative experimentation on the AOTF characteristics was performed by CEERI, Chennai and SAG/ISAC ISRO team, Bangalore. The spectral output were acquired and stored with changes in different system parameters. Figure 58 - 63 shows the test output acquired with various kinds of samples with different configuration parameters for the instrument. A joint report : **Experimental understanding and functional behavior of Near Infrared AOTF Spectrometer** [59] was also prepared for the same.

Application of Chemometric pre-processing algorithms on the acquired data [60], and discriminating the data based on the pattern matched with the available standard spectral database and classifying them based on the target application necessitates the implementation of a good machine learning tool that integrates the chemometric specific algorithms which facilitates the users to undergo the spectrometric data analysis consuming less time and computing resources. Upon building the data bank, constituting an array of organic and inorganic materials and their associated meta data in the data base helps us to easily target analytical applications [61] [62] in food science, process control systems, storage and refrigeration, non-invasive biomedical engineering, antique document identification, etc.,.

Calibrating the instruments built or commercially purchased instrument is an essential part to be learned by the spectroscopist. Now with the advances in the machine learning, pattern recognition and their applications in chemometrics have made calibration not only better but also simple to use so that data collected from different instruments can be standardized and stripped off from their measurement non-linearities and its corresponding error contribution [63] [64].

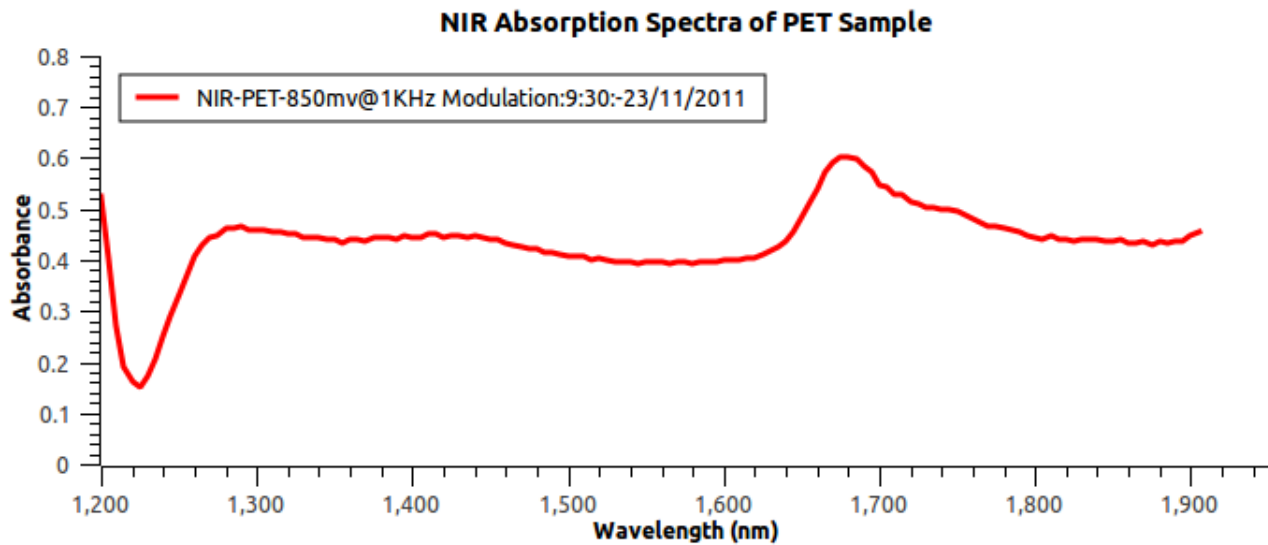


Figure 58: Single scan NIR-spectra of PET sample

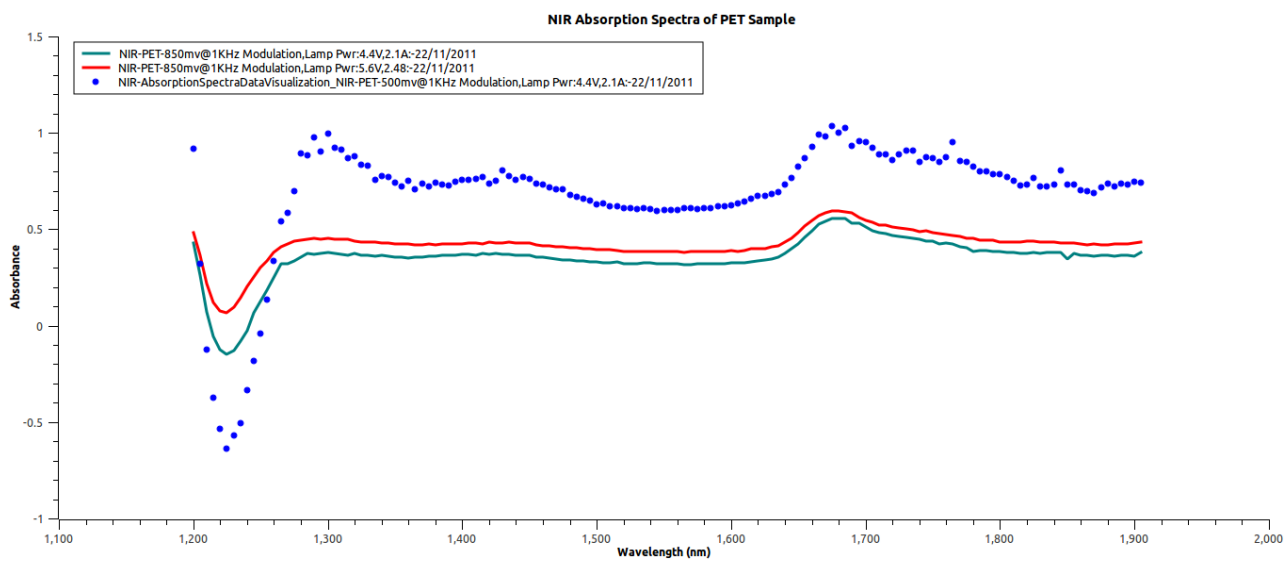


Figure 59: Overlaid spectral scan of PET sample with different lamp power

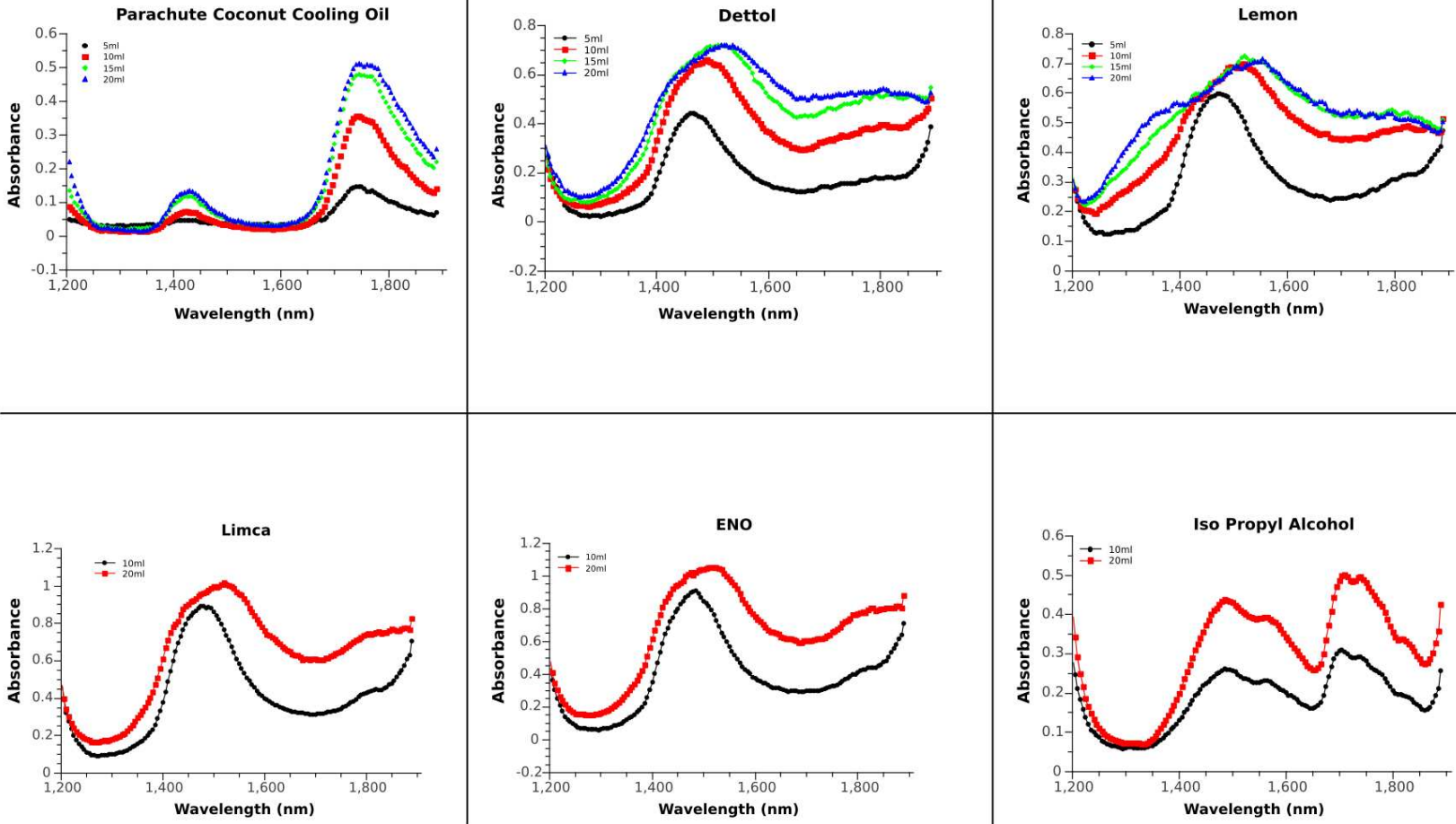


Figure 6o: Spectral test output of NIR-AOTF Spectrophotometer with different samples

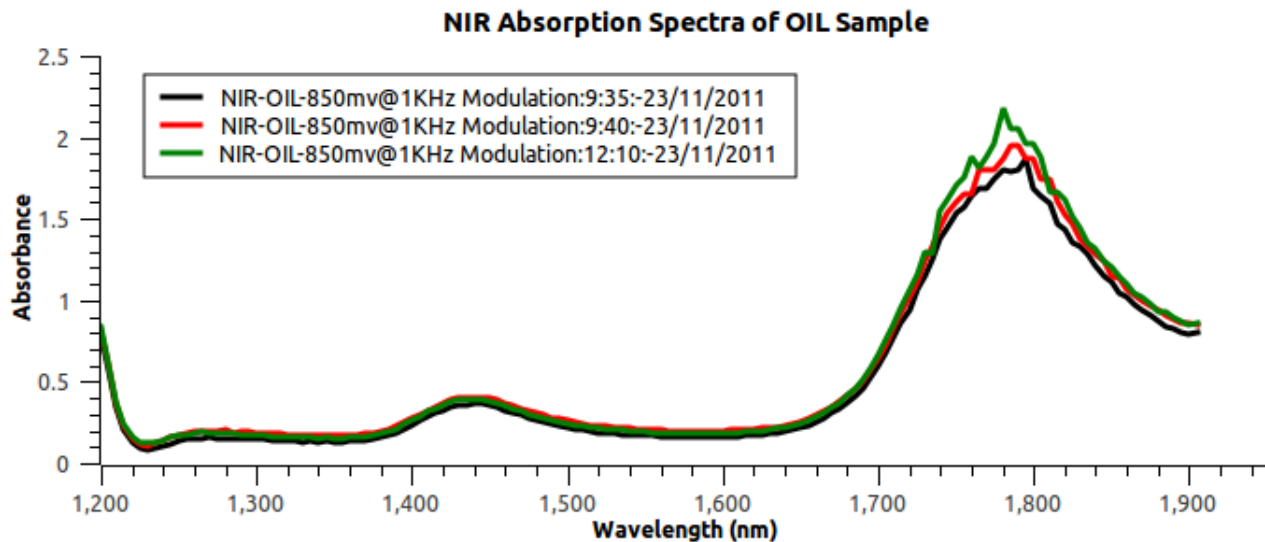


Figure 61: NIR spectra of Oil sample with no change in modulation voltage and frequency

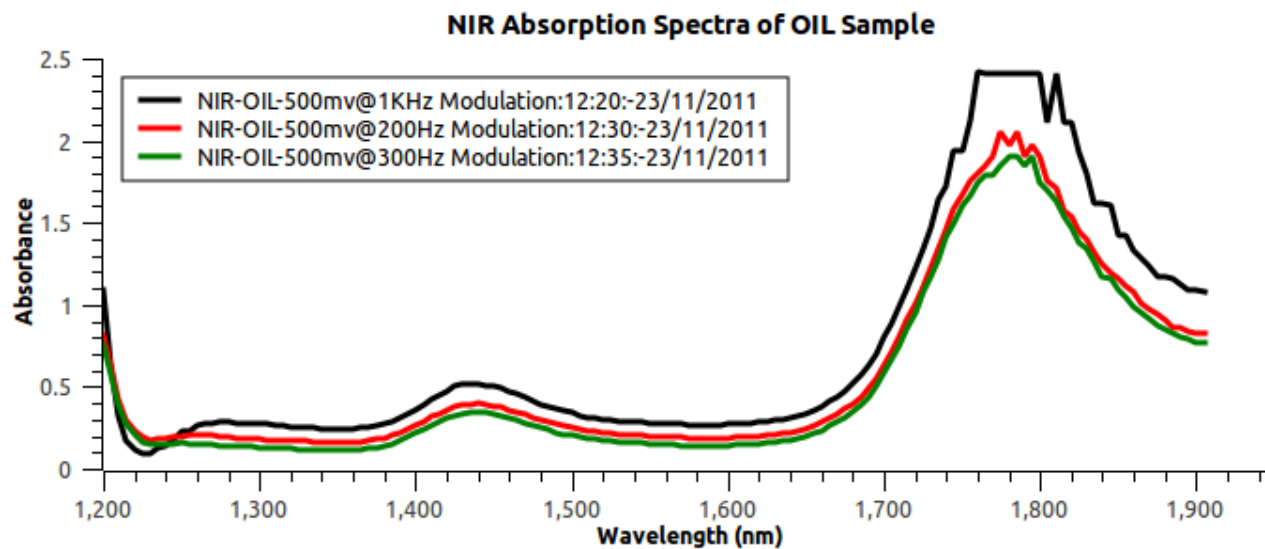


Figure 62: NIR spectra of Oil sample with change in modulation frequency

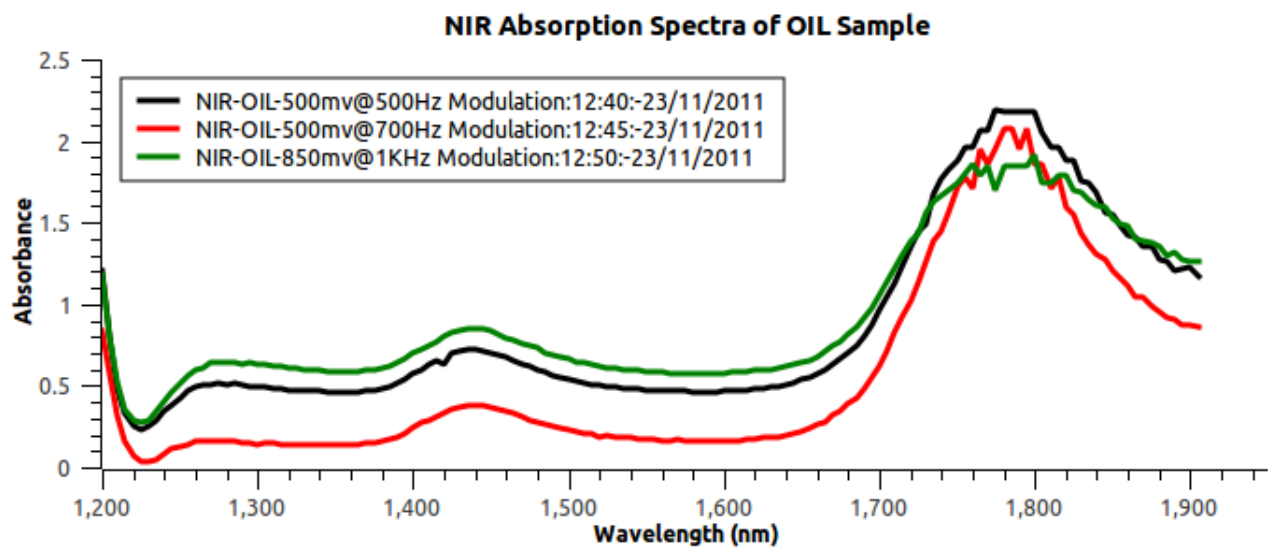


Figure 63: NIR spectra of Oil sample with change in both modulation voltage and frequency

List of Necessary Conceptual/Implementation Updates

As stated previously in *About the report* chapter, this report will be continued to record the development history of AOTF based NIR Spectrophotometer, that will guide the new comers in the experimentation for better and intuitive understanding of the underlying principles, mastering the mechanisms and policies that govern the functions of the spectrophotometer. After realizing the freedom, flexibility, self retention and life propagating capacity of the Free model Ecosystem this project is further hoped to be enhanced and updated using the tools, and technologies with Free Hardware and Free Software design philosophy adapting the Free model Ecosystem. There are a lot of enhancements that can be built upon the existing spectrophotometer such as:

Generalized Instrumentation Platform Specification & Updates

Updating the Analog Signal Processing System

Using gEDA/KiCAD [65; 66; 67; 68; 69] for Designing and Implementing ASPU and microcontroller platform. Signal integrity is mainly concentrated when designing the Printed Circuit Board for the ASPU, such that it can be immunized from far field and near field EMI(Electromagnetic Interference) noises. Error budgeting for the ASPU need to be completed to quantify the total error originated and propagated from the system. Such a quantitative analysis results in specifying the quality of signal delivered by ASPU in terms of SNR, Measurement accuracy and precision. Next the flexibility of the system needs to be addressed for configuring the linear analog parameters such as gain and filter arguments. The RF part of the system can be designed from the scratch using VCO or DDS operation.

Hardware that supports simple firmware and whole operating system

The present prototype contains a separate x86 based workstation acting as a server, and an Arduino performing the data acquisition and control tasks. The same system can be compressed together in a single platform that contains a GNU/Linux handling hardware interfaced with suitable microcontroller platform that performs all the deterministic low end tasks like data acquisition and control. The platforms that can makeup such facility is listed below:

- Using Beagle Bone/CHIP Hardware Platform
- Using Arduino Tre Hardware Platform
- Using Parallela [70; 71; 72] Hardware Platform

Software platform that completely covers Desktop, Embedded and Web Technologies

As stated earlier, while implementing DEW based systems, targeting the computing platforms with appropriate operating systems. The following is a non-exhaustive list of software platforms which in principle can be used with complete freedom and customized according to the requirement.

- Using TinyOS [73] or FreeRTOS as firmware for Small scale Embedded Systems
- Using AELBS for deploying General purpose Embedded Systems
- Using GNU/Linux in General purpose Hardware platforms
- Using Julia/C/Phyton/JavaScript at appropriate layers of Software Implementation

The study of determinism, jitter and power Vs performance needs to be handled here to understand the performance impact on the whole instrument when using the above platforms. This further helps us evaluate them for the complete operation.

Inclusion of Machine Learning, Data Analytics and Visualization Capability

Collecting spectral data and creation of spectral bank of different kinds of references and samples is one of the main task after completing the instrument testing. For this interfacing with data base system with little delay is need. Furthermore, with the availability and accessibility of free machine learning and data analysis libraries/tools help develop data analytics platform that performs complex mathematical and statistical computation, which demands significant computing power that can be supplemented with parallel computing hardware platforms.

Recognizing fundamental features and abstracting them to the targets we need, has gained the global research much traction in cognitive research, machine learning & deep learning communities. With the availability of graph based data base systems, open data systems and policies, availability of open designs, such spectroscopy projects can be made much more transparent and democratic than ever before.

- Using Machine Learning frameworks and libraries
 - SScikit Learn
 - Theano/Tensor Flow
 - RadioML
- Using Spectral Phyton(SPy) for Spectral data processing
- Developing Free Chemometrics library with GPL license
- Using Free(dom) libraries like VTK and tools like Visit, ScaVis, Veusz, D3, Snap, Gadfly for Visualization
- Developing User Interaction/Experience with Simplicity and Portability using Free(dom) software libraries such as ncurses, GNOME, Qt, Wx, Kivy, OF, Processing, OpenGL, OpenVG.

Development of simple visualization platform is another challenging task, when system is scaled to web based control by multiple peers. However sharing among multiple peers is only an experimental feature for the implementation. However, powerful visualization tools as listed above can provide scalable and efficient data and information visualization capabilities aiding in data analysis.

Attempting to form Instrument Grid

With the completion of the projected updates, this stage enables the instrument to be a node in the instrument grid, that allows remote operation and control, distributed sharing of the instrument's spectral data. The following list of systems help learn how the networking capabilities with the sensor based nodes to implement a web or grid architecture that becomes resilient and transparent.

- Learn and adapt Sensor Web and Sensor Grid [74; 75] Architecture
- Implement Mesh Networking in Instrument Grid by using GNU/Linux based distributions such as OpenWrt
- Implement Peer to Peer and Distributed architecture

With BOINC, distributed computing, sensing can be made possible. However, for now making a reliable instrument (of similar kind) in a democratic (Transparent and Open) way is a challenge. Once such critical requirement is surpassed, then this step would be inevitable.

Spectroscopy Specific Updates

The following requirements are to be completed to create a complete Spectrophotometer instrument which is enabled with necessary software intelligence. These essential updates ensure the integrated spectrophotometer to work based on standards specification. Many of the following requirements point to necessary features to be functionally implemented with either the hardware or software part of the system.

Spectral Manipulation

- Zap spectral regions, with zeros or interpolated lines, with the capability of adding noise back into the zapped regions
- Manual Baseline Correction
- Automatic Baseline Correction
- Manual Spectral Subtraction
- X-Axis Shift and Stretch
- Take derivatives of spectral data
- Ratio, absorbance, transmittance conversions
- Convert data between Absorbance, Transmittance, and Diffuse Reflectance formats
- 5 to 99 point smoothing, with Savitsky-Golay, moving average, Hannig and Hamming window methods
- Interpolate / Decimate to change the resolution of the spectral data
- Manual Interactive Spectral Subtraction
- Automatic Spectral Subtraction optimized over a user-selected region
- Offset data by constant
- Scale data by constant
- Truncate to change the spectral data limits
- Kramers-Kroning transform using the Maclaurin method

- Advanced ATR Correction: Attenuated Total Reflectance corrects for dispersion and depth of penetration
- Normalizations: Normalize the data to a minimum, a range, or using Vector Normalization
- Match spectra: set a group of spectra to have the same starting and ending values and number of data points

Data Handling

- Built-in file browser with data preview
- Built-in file finder
- Full automatic audit trail support keeps track of and documents all changes to data
- The audit trail is automatically saved with the data
- Save and restore complete work sessions
- Workspaces (the data windows and all the data contained in them) can be saved to disk for later recall
- Spectral Search and user libraries
- Library Search: a library is simply a directory containing datafiles
- Search is performed in the background, allowing the user to continue with other tasks
- View and edit file header information
- Edit datapoints directly in a built-in spreadsheet and instantly preview the result
- Spectral data can be exported directly into Excel spreadsheets
- Spectral data can be exported to .csv (comma-separated value ASCII) files
- Infinite-level undo of all data changes

Data Analysis

- Compute integrated areas of spectral regions
- Peak Picking automatically tabulates the peaks in a spectrum
- Peak Measurement: computes peak height using user-supplied peak endpoints
- Signal-to-Noise: computes signal-to-noise ratio over user-defined limits
- Spectral Library Search: search unknown spectra against libraries of data.

Quantitative Analysis

- Beer's Law Quant
- Partial Least Squares (PLS) and Classical Least Squares (CLS) and other packages accompanying necessary chemometric machine learning tools.

Spectral Library Search

- Library Search can be included in the Core version
- Hundreds of thousands of Reference Spectra can be made available.
- Support for other library formats (which are open) – try including Grams Spectral ID, Perkin Elmer, Thermo Omnic, Sadtler, and Mattson.
- Easily build libraries from your own spectra.
- Full Spectrum and Multiple Region Searching.
- Fast, cutting-edge search algorithms.
- Incremental text search.
- Browse libraries of spectra like a reference book.

Scripting, Programming and Automation

- To embed the open-source Python programming language, which is widely used in scientific programs. Python includes modules for advanced numeric programming and data processing. Can accommodate custom data processing by its ability to execute scripts written in Python.
- Powerful built-in batch processing. Users can create sequences of processing steps without having to write any programming code. A sequence editor makes it easy to automate repetitive tasks.
- Remote control for integration in multi-instrument applications. Instrument can have a built-in network socket interface that is used to accept commands from remote programs. The remote program can be running on the same computer or any computer on the network.

Supported File Formats for Saving Data (Try only for which are open)

- Grams (Galactic, Spectra-Calc) (.spc)
- JCAMP-DX (.dx, .jdx) (**IUPAC standard**)
- ASCII (x,y) pairs (.csv)
- AIT (Analect) .asf
- Perkin Elmer (.sp)
- Excel (.xls) (Export only)
- Matlab (.mat) (Export only)

Appendix A

Complete AOTF instrument Integrated Setup

Figure 59 shows the current integrated status of the NIR-AOTF spectrophotometer. As shown in the diagram the light source (Tungsten Halogen Lamp working at +12V, 55Watts) is excited and the sample is exposed in reflection or transmission based optical setup. The collimating optics (84-UV-25) [76] placed on the parabolic dish to couple the larger free space beam (the optical signal transmitted through or reflected from the sample) to a laboratory grade patch cord (Multimode fiber wave guide T600-2-VIS/NIR - 600 μ low OH from Ocean Optics) [77] which guides the optical signal to the input optical port of the AOTF module.

The Acousto-optic Tunable filter(AOTF) is controlled through its coaxial electrical input port with modulated RF signal that determines the diffraction efficiency and spectral resolution. The diffracted light is then delivered to the optical ouput fiber which is connected to the Indium Gallium Arsenide (InGaAs) detector unit which is cooled Thermoelectrically. The thermoelectric cooling unit is controlled by a temperature control unit by sensing the temperature at the detector unit. The detected signal is then pre-amplified using a transimpedance amplifier with defined gain setting.

The amplified signal is then coupled to the analog signal processing unit (ASPU) that conditions the input signal and sends it to the Analog to Digital convertor of the AVR 2560 microcontroller system. The embedded firmware running in the microcontroller acquires the signal and sends it to the supervisory system. It also generates the required modulation signal to be applied to the RF driver's modulation input. The constructed lookup table generates the required digital value which is then applied to the modular Digital to Analog convertor. The Analog output signal is then amplified and conditioned to deliver it to the RF driver's frequency input so that the AOTF can be tuned to select the next wavelength of interest.

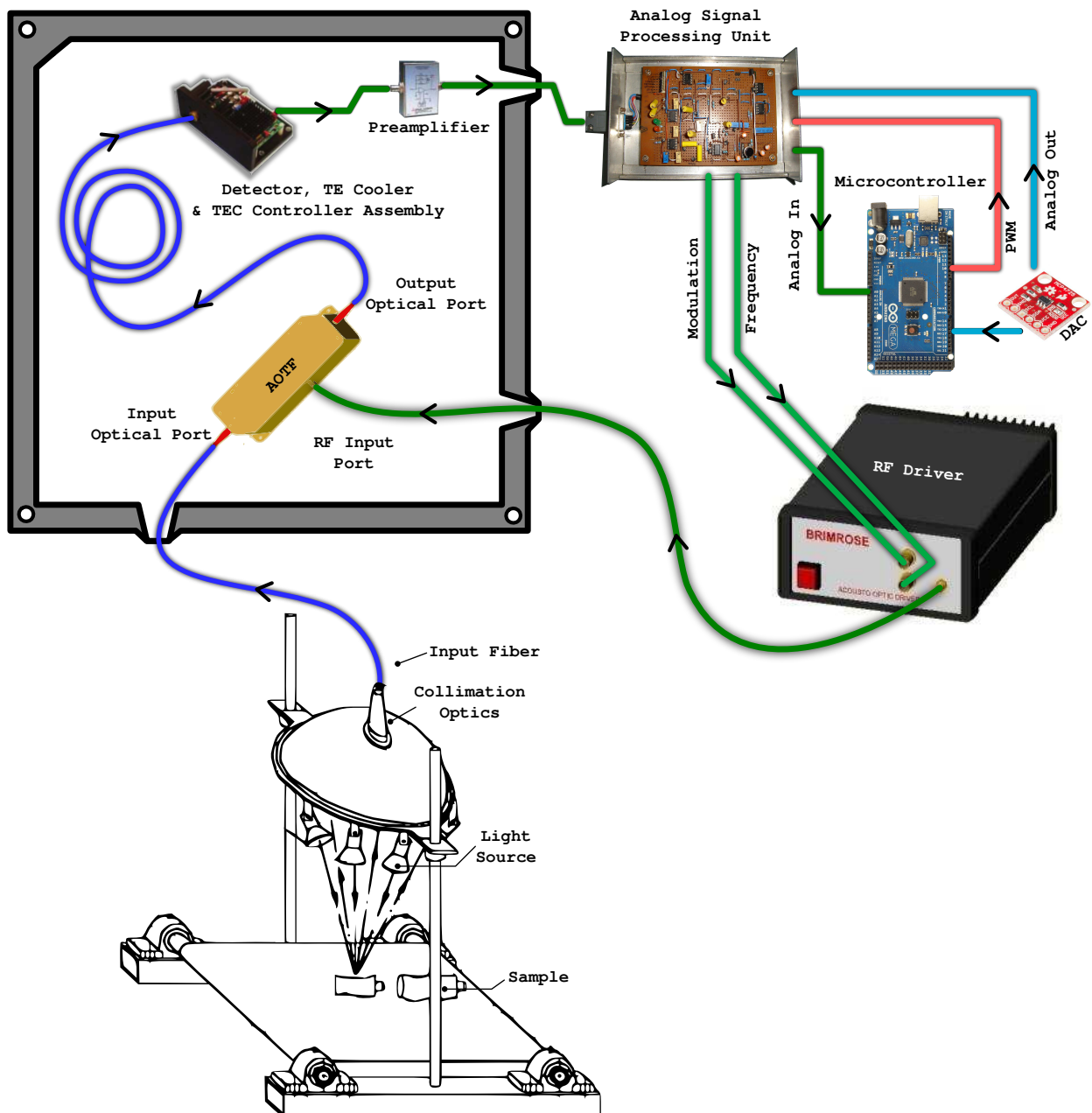


Figure 64: Completely Integrated NIR-AOTF Spectrometer Unit (Present Status)

Appendix B

Acousto Optic Tunable Filter Specification

PARAMETER	SPECIFICATIONS [78]	TEST DATA
Wavelength of Operation	1200 - 2000 nm	1200 - 2000 nm
Substrate	Tellurium Dioxide (TeO_2)	TeO_2
Spectral Resolution	2 - 0.5 nm	3.8 nm @ 1310nm ; 5.4 nm @ 1550 nm
RF Frequency	70 - 120 MHz	70 - 120 MHz
Acoustic Velocity	-	875 m/sec
Maximum RF Power [!]	3 Watts	3 Watts
Input Impedance	50 Ω	50 Ω
Voltage Standing Wave Ratio	2.1 : 1	2.1 : 1
Optical Polarization	-	Any
Sidelobes	- dB	\approx 12 dB
Wavefront Distortion	-	$\frac{\lambda}{10}$
Tuning Temperature Coefficient	-	-0.14 nm/ oC
RF Connector	SMB	SMB
Case Type	2port - Fiber Optically pigtailed; 150×45×15 mm	-
Type of Fiber(port 1 & 2)	600 μ core, 690 μ cladding, multimode	-
Polarization Dependent loss	-	\approx 1 dB
Fiber Connector Type	SMA	SMA
Polishing of the Fiber end	PC	PC
Fiber length	1 m	1 m
Fiber Jacket type	4.8 mm PVC tubing	4.8 mm PVC tubing
Total Insertion Loss*	6.0 - 7.0 dB	7 db @ 1550nm @ 86.8MHz

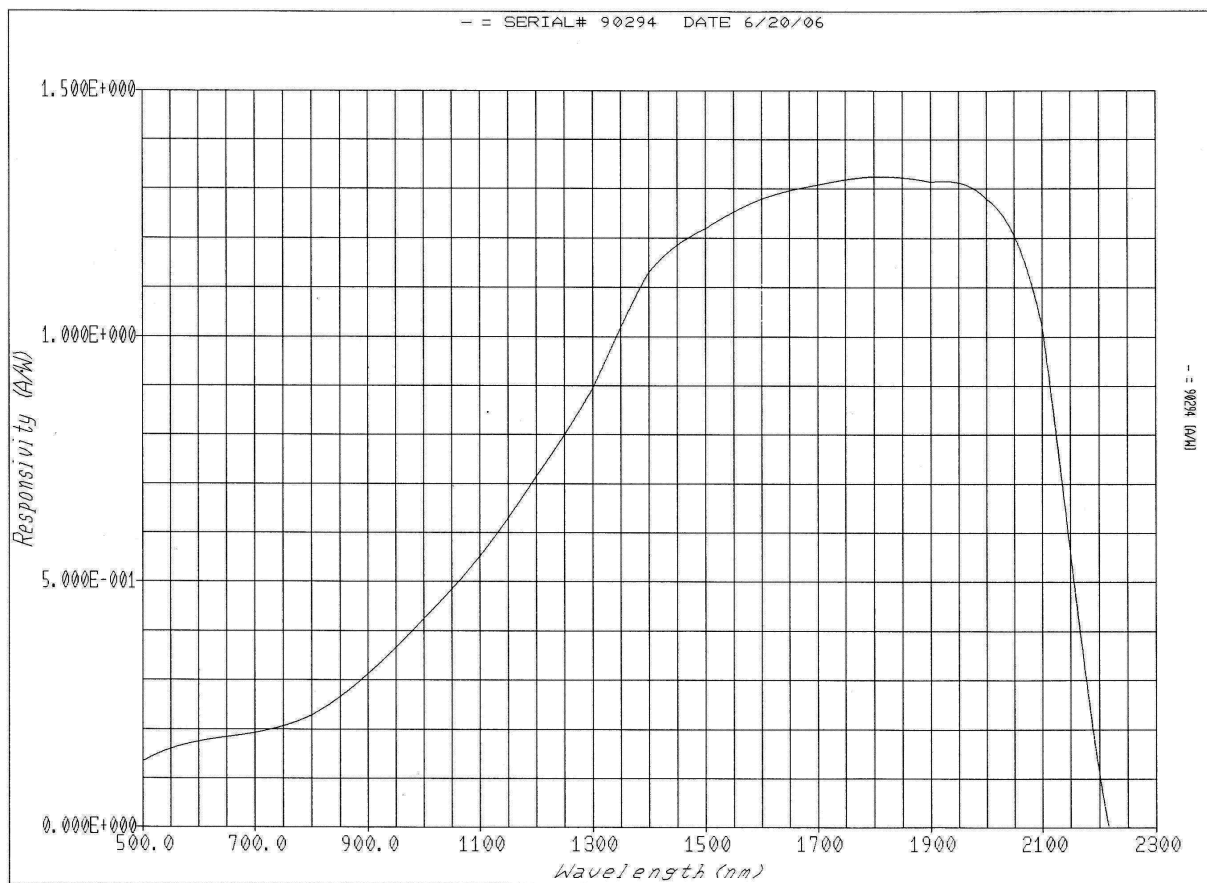
NOTE

- ! - Higher RF Powers can saturate the device, causing worse performance, or even damage the device.
- * - This specification includes: coupling losses, optical transmission through the crystal and Diffraction efficiency losses. Losses at the SMA connectors are not included. Because of core size and wavelength, Insertion Loss margin of error ≤ 1.0 dB.

Appendix C

InGaAs Detector Specification

PARAMETER [79]	VALUE
Model No.	J23TE2-66C-R01M-2.2
Active Size Diameter (mm)	1.00
Operating Temperature °C	-40
50 % cutoff wavelength (μ)	2.11+/-0.10
Peak Responsivity (A/W) min	1.1
Shut Impedance Ω	5.5E+06(min) 1.1E+07(typ)
Peak Detectivity (cmHz ^{1/2} /W) @1KHz	2.0E+12(min) 2.9E+12(typ)
NEP (W/rt - Hz) @ peak wavelength	4.4E-14(max) 3.1E-14(typ)
Capacitance (pF) @ 0V	1000

InGaAs Detector Spectral Response

Appendix D

TE Cooler Specification

PARAMETER [80]	VALUE
Model No.	CMAMP-T066-PA7
Part No.	490139
Heat Sink	CM1
Package Socket	9 pin T0-66 66X
Cables	12" RG174 SMA-BNC
Amplifier	PA-7-HYBRID
Temperature Controller	TC6
Power Requirements	+5V +/- .25 @ 2A +/-15V@10mA



Figure 65: TE cooler and its Heat Sink assembly

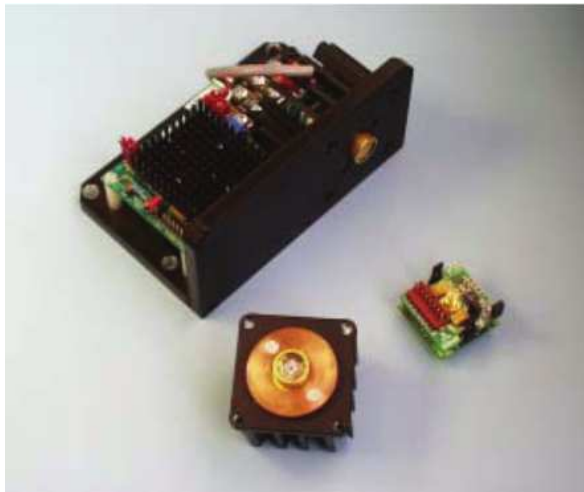


Figure 66: Complete Assembly of TE Cooler and its Controller

Appendix E

TE Cooling - Temperature Controller

The TC6 is a self contained Thermoelectric Cooler (TEC) Temperature Controller for single and multistage TEC cooled photodetectors [80]. Using a single 5 Volt power supply, the TC6 operates in conjunction with a thermistor, located in the detector assembly, to precisely measure and regulate the temperature of the cooled detector. The detector assembly temperature is set with a single resistor that is equal to the thermistor resistance at the desired set temperature. The detector manufacturer generally specifies the optimum detector operating temperature and corresponding thermistor value.

Electrical functionality of TEC controller

The various electrical inputs and outputs of the TC6 can be monitored and/or controlled through the connector as shown in Figure 57 if desired [80]. Making connection to the TC6 through this connector is not necessary to the operation of the controller. A Digital Volt Meter can be connected to the output of this fixture and a five position switch allows monitoring of the output of the thermistor bridge, the TEC current, the current through the temperature set resistor, the +5 Volt internal reference and the +5 Volt external power supply.

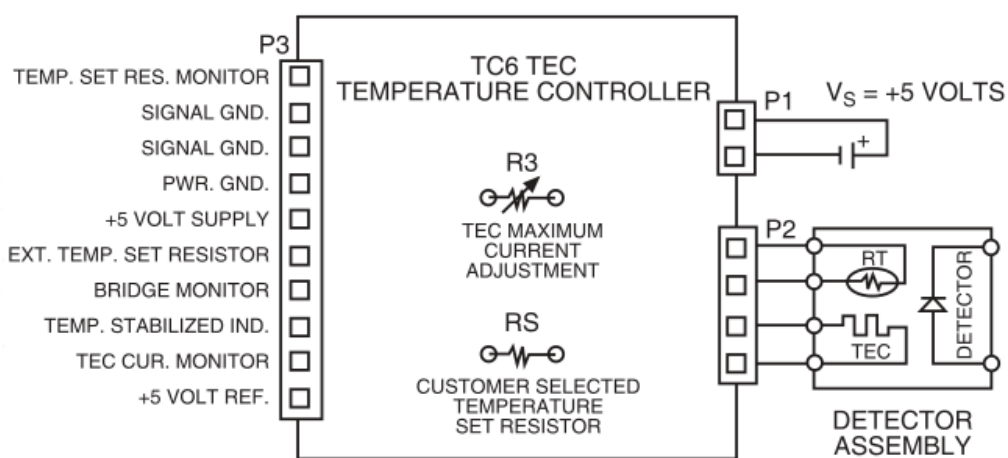


Figure 67: Electrical block diagram of TEC controller unit



Figure 68: TE cooling - Temperature Controller unit with its Heat Sink Assembly

Features

- Precise temperature control
- Temperature stability to $\pm 0.02^{\circ}\text{C}$
- Temperature set with a single resistor
- Single +5V operation
- Maximum TEC current adjustable to 2A
- **LED** Temperature stabilization indicator
- **TEC** current monitor
- Thermistor bridge monitor
- Small size

Appendix F

Pre Amplifier Specification

PARAMETER [80]	VALUES	
Model	PA-7-70	
Transimpedance Gain (Switched) (V/A)	High	10^7
	Medium	10^6
	Low	10^5
Bandwidth $R_D > 10K$, $C_D < 0.2nF$ (KHz)	@ High gain	8
	@ Medium gain	60
	@ Low gain	150
Input Offset Voltage (V_{OS}) μV	± 250	
Input Bias Current (I_B) nA	± 0.001	
Voltage Noise Density (e_N) @1KHz $Hz^{-\frac{1}{2}}$	12	
Voltage Noise from 0.1 to 10 Hz (μV_{pp})	1.5	
Current Noise Density (i_N) @1KHz @High gain $pA Hz^{-\frac{1}{2}}$	0.04	
Output Impedance	≤ 100	
Maximum Output Voltage	10	
Power Required (V_{pp})	+12V and -12V @10mA (or) +15V and -15V @10mA	

Equivalent circuit of Transimpedance Preamplifier

The PA-7 is an excellent general purpose preamplifier [80] for most high shunt resistance ($R_D > 25\text{K}\Omega$) detectors. It has extremely low current noise and current offset. For most applications, the PA-7-70 with high gain of 10^7 V/A offers best performance and versatility. However, for applications where 10^7 V/A gain is unusable (due to bandwidth or DC saturation), the PA-7- 60 or PA-7-50 are suitable alternatives.

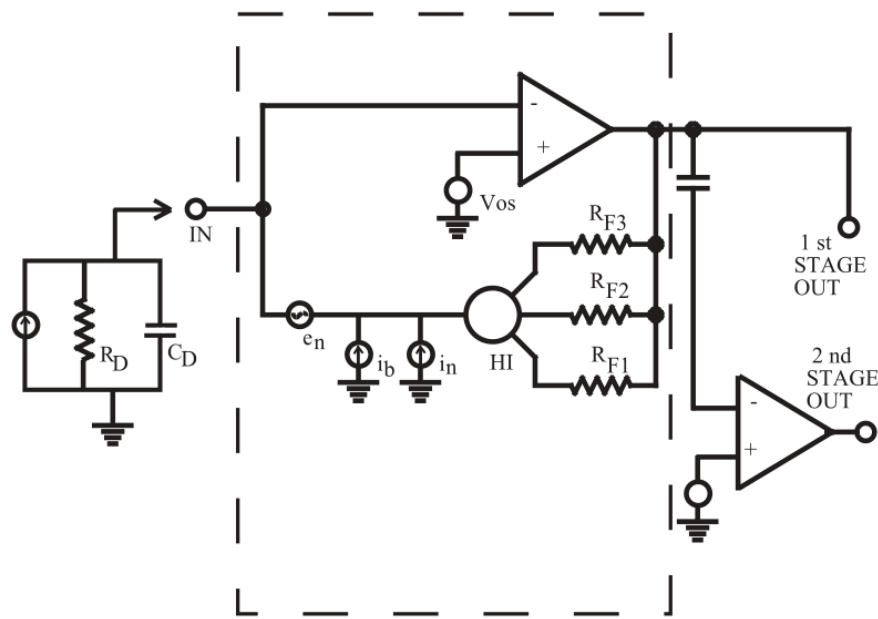


Figure 69: TE cooler and its assembly

Appendix G

Circuit Schematic for the Analog Signal Processing Unit

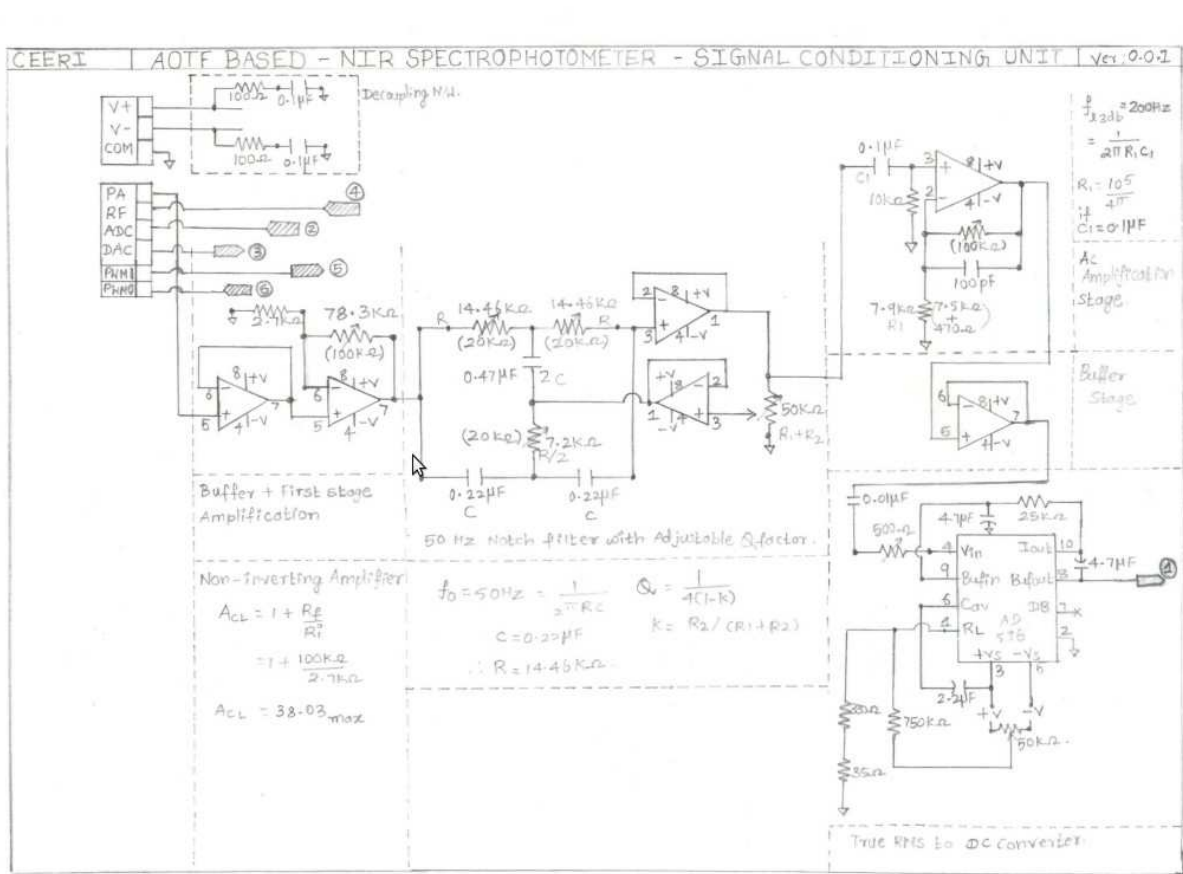


Figure 70: Circuit Schematic of designed ASPU - page 1

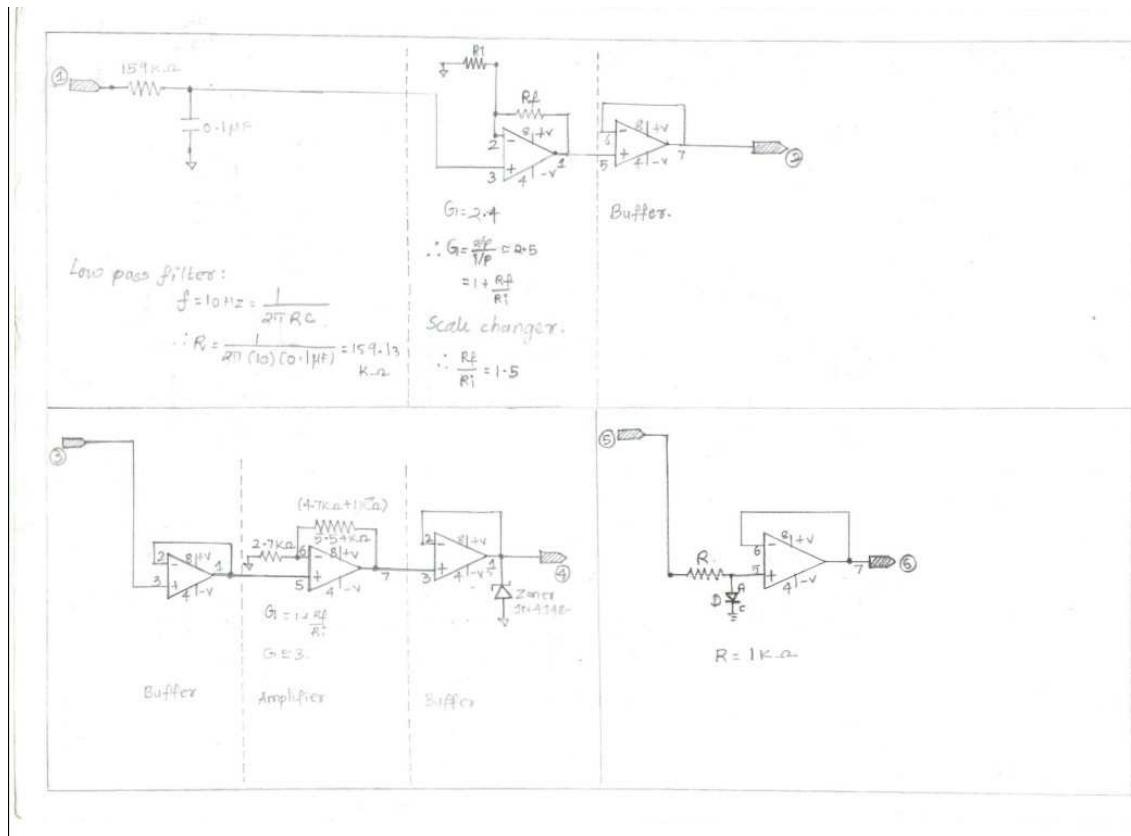


Figure 71: Circuit Schematic of designed ASPU - page 2

Appendix H

*LookUp Table(LUT) - Matched for Nonlinear Characteristics of
RF Driver-AOTF tuning curve*

Wavelength <i>nm</i>	Frequency <i>MHz</i>	Voltage <i>V_{Interpolated}</i>	True voltage <i>V_{RFDriver}</i>	DAC Voltage <i>V</i>	<i>V/V_{ref}</i>	Decimal Value	Hex. Value
1200	112.45657	4.864	7.364	2.454666667	0.743838384	48748	0XBEB6C
1205	112.09345	4.816	7.316	2.438666667	0.738989899	48430	0XBBD2E
1210	111.73001	4.771	7.271	2.423666667	0.734444444	48133	0XBBC05
1215	111.36595	4.73	7.23	2.41	0.73030303	47861	0XBBAF5
1220	111.00096	4.692	7.192	2.397333333	0.726464646	47610	0XB9FA
1225	110.6347	4.655	7.155	2.385	0.722727273	47365	0XB905
1230	110.26685	4.619	7.119	2.373	0.719090909	47126	0XB816
1235	109.89706	4.583	7.083	2.361	0.715454545	46888	0XB728
1240	109.52497	4.55	7.05	2.35	0.712121212	46670	0XB64E
1245	109.15019	4.518	7.018	2.339333333	0.708888889	46458	0XB57A
1250	108.7724	4.488	6.988	2.329333333	0.705858586	46259	0XB4B3
1255	108.39144	4.459	6.959	2.319666667	0.702929293	46067	0XB3F3
1260	108.00721	4.43	6.93	2.31	0.7	45875	0XB333
1265	107.61961	4.401	6.901	2.300333333	0.697070707	45683	0XB273
1270	107.22853	4.371	6.871	2.290333333	0.694040404	45485	0XB1AD
1275	106.83385	4.341	6.841	2.280333333	0.691010101	45286	0XB0E6
1280	106.43546	4.313	6.813	2.271	0.688181818	45101	0XB02D
1285	106.03322	4.289	6.789	2.263	0.685757576	44942	0XAFA8E
1290	105.62699	4.266	6.766	2.255333333	0.683434343	44790	0XAEF6
1295	105.21665	4.243	6.743	2.247666667	0.681111111	44637	0XAE5D
1300	104.80221	4.219	6.719	2.239666667	0.678686869	44478	0XADBE
1305	104.28552	4.19	6.69	2.23	0.675757576	44286	0XACFE
1310	103.96218	4.171	6.671	2.223666667	0.673838384	44161	0XAC81

Wavelength <i>nm</i>	Frequency MHz	Voltage <i>V_{Interpolated}</i>	True voltage <i>V_{RFDriver}</i>	DAC Voltage <i>V</i>	<i>V/V_{ref}</i>	Decimal Value	Hex. Value
1315	103.53728	4.145	6.645	2.215	0.671212121	43989	0XABD5
1320	103.1096	4.12	6.62	2.206666667	0.668686869	43823	0XAB2F
1325	102.67956	4.094	6.594	2.198	0.666060606	43651	0XAA83
1330	102.24757	4.069	6.569	2.189666667	0.663535354	43485	0XA9DD
1335	101.81407	4.044	6.544	2.181333333	0.661010101	43320	0XA938
1340	101.37951	4.02	6.52	2.173333333	0.658585859	43161	0XA899
1345	100.94437	3.996	6.496	2.165333333	0.656161616	43002	0XA7FA
1350	100.50937	3.972	6.472	2.157333333	0.653737374	42843	0XA75B
1355	100.07662	3.948	6.448	2.149333333	0.651313131	42684	0XA6BC
1360	99.64856	3.925	6.425	2.141666667	0.648989899	42532	0XA624
1365	99.22741	3.903	6.403	2.134333333	0.646767677	42387	0XA593
1370	98.81506	3.88	6.38	2.126666667	0.644444444	42234	0XA4FA
1375	98.41305	3.858	6.358	2.119333333	0.642222222	42089	0XA469
1380	98.02182	3.837	6.337	2.112333333	0.64010101	41950	0XA3DE
1385	97.6403	3.816	6.316	2.105333333	0.637979798	41811	0XA353
1390	97.26742	3.796	6.296	2.098666667	0.635959596	41678	0XA2CE
1395	96.90225	3.776	6.276	2.092	0.633939394	41546	0XA24A
1400	96.54399	3.756	6.256	2.085333333	0.631919192	41413	0XA1C5
1405	96.19193	3.736	6.236	2.078666667	0.62989899	41281	0XA141
1410	95.84544	3.717	6.217	2.072333333	0.627979798	41155	0XA0C3
1415	95.50395	3.698	6.198	2.066	0.626060606	41030	0XA046
1420	95.16697	3.679	6.179	2.059666667	0.624141414	40904	0X9FC8
1425	94.83403	3.661	6.161	2.053666667	0.622323232	40785	0X9F51
1430	94.50471	3.642	6.142	2.047333333	0.62040404	40659	0X9ED3
1435	94.17862	3.624	6.124	2.041333333	0.618585859	40540	0X9E5C
1440	93.8554	3.605	6.105	2.035	0.616666667	40414	0X9DDE
1445	93.53471	3.587	6.087	2.029	0.614848485	40295	0X9D67
1450	93.21618	3.569	6.069	2.023	0.613030303	40176	0X9CF0
1455	92.8994	3.552	6.052	2.017333333	0.611313131	40063	0X9C7F
1460	92.58399	3.534	6.034	2.011333333	0.609494949	39944	0X9C08
1465	92.26956	3.517	6.017	2.005666667	0.607777778	39831	0X9B97
1470	91.95575	3.5	6	2	0.606060606	39719	0X9B27
1475	91.64218	3.483	5.983	1.994333333	0.604343434	39606	0X9AB6
1480	91.32851	3.466	5.966	1.988666667	0.602626263	39494	0X9A46
1485	91.01436	3.449	5.949	1.983	0.600909091	39381	0X99D5
1490	90.69936	3.431	5.931	1.977	0.599090909	39262	0X995E
1495	90.38316	3.413	5.913	1.971	0.597272727	39143	0X98E7
1500	90.06535	3.394	5.894	1.964666667	0.595353535	39017	0X9869

Wavelength <i>nm</i>	Frequency MHz	Voltage <i>V_{Interpolated}</i>	True voltage <i>V_{RFDriver}</i>	DAC Voltage <i>V</i>	<i>V/V_{ref}</i>	Decimal Value	Hex. Value
1505	89.74553	3.374	5.874	1.958	0.593333333	38885	0X97E5
1510	89.42328	3.354	5.854	1.951333333	0.591313131	38752	0X9760
1515	89.09816	3.333	5.833	1.944333333	0.589191919	38613	0X96D5
1520	88.76971	3.312	5.812	1.937333333	0.587070707	38474	0X964A
1525	88.43849	3.29	5.79	1.93	0.584848485	38329	0X95B9
1530	88.1066	3.269	5.769	1.923	0.582727273	38190	0X952E
1535	87.77623	3.247	5.747	1.915666667	0.580505051	38044	0X949C
1540	87.44953	3.225	5.725	1.908333333	0.578282828	37898	0X940A
1545	87.12843	3.203	5.703	1.901	0.576060606	37753	0X9379
1550	86.81461	3.182	5.682	1.894	0.573939394	37614	0X92EE
1555	86.50938	3.161	5.661	1.887	0.571818182	37475	0X9263
1560	86.21272	3.14	5.64	1.88	0.56969697	37336	0X91D8
1565	85.92352	3.119	5.619	1.873	0.567575758	37197	0X914D
1570	85.6408	3.099	5.599	1.866333333	0.565555556	37064	0X90C8
1575	85.36373	3.079	5.579	1.859666667	0.563535354	36932	0X9044
1580	85.09155	3.059	5.559	1.853	0.561515152	36799	0X8FBF
1585	84.82361	3.04	5.54	1.846666667	0.55959596	36674	0X8F42
1590	84.55932	3.021	5.521	1.840333333	0.557676768	36548	0X8EC4
1595	84.29814	3.003	5.503	1.834333333	0.555858586	36429	0X8E4D
1600	84.03958	2.985	5.485	1.828333333	0.554040404	36310	0X8DD6
1605	83.78318	2.968	5.468	1.822666667	0.552323232	36197	0X8D65
1610	83.52851	2.95	5.45	1.816666667	0.550505051	36078	0X8CEE
1615	83.27516	2.932	5.432	1.810666667	0.548686869	35959	0X8C77
1620	83.02273	2.913	5.413	1.804333333	0.546767677	35833	0X8BF9
1525	82.77084	2.893	5.393	1.797666667	0.544747475	35701	0X8B75
1630	82.51929	2.872	5.372	1.790666667	0.542626263	35562	0X8AEA
1635	82.26813	2.851	5.351	1.783666667	0.540505051	35423	0X8A5F
1640	82.01741	2.829	5.329	1.776333333	0.538282828	35277	0X89CD
1645	81.76718	2.806	5.306	1.768666667	0.535959596	35125	0X8935
1650	81.51749	2.783	5.283	1.761	0.533636364	34972	0X889C
1655	81.26839	2.76	5.26	1.753333333	0.531313131	34820	0X8804
1660	81.01994	2.737	5.237	1.745666667	0.528989899	34668	0X876C
1665	80.77219	2.714	5.214	1.738	0.526666667	34516	0X86D4
1670	80.52517	2.69	5.19	1.73	0.524242424	34357	0X8635
1675	80.27895	2.667	5.167	1.722333333	0.521919192	34204	0X859C
1680	80.03356	2.643	5.143	1.714333333	0.519494949	34046	0X84FE
1685	79.78906	2.619	5.119	1.706333333	0.517070707	33887	0X845F
1690	79.54548	2.595	5.095	1.698333333	0.514646465	33728	0X83C0

Wavelength <i>nm</i>	Frequency MHz	Voltage <i>V_{Interpolated}</i>	True voltage <i>V_{RFDriver}</i>	DAC Voltage <i>V</i>	<i>V/V_{ref}</i>	Decimal Value	Hex. Value
1695	79.30287	2.57	5.07	1.69	0.512121212	33562	0X831A
1700	79.06127	2.544	5.044	1.681333333	0.509494949	33390	0X826E
1705	78.82072	2.517	5.017	1.672333333	0.506767677	33212	0X81BC
1710	78.58126	2.489	4.989	1.663	0.503939394	33026	0X8102
1715	78.34293	2.461	4.961	1.653666667	0.501111111	32841	0X8049
1720	78.10576	2.431	4.931	1.643666667	0.498080808	32642	0X7F82
1725	77.86978	2.401	4.901	1.633666667	0.495050505	32444	0X7EBC
1730	77.63503	2.369	4.869	1.623	0.491818182	32232	0X7DE8
1735	77.40154	2.336	4.836	1.612	0.488484848	32013	0X7D0D
1740	77.16934	2.302	4.802	1.600666667	0.485050505	31788	0X7C2C
1745	76.93846	2.266	4.766	1.588666667	0.481414141	31550	0X7B3E
1750	76.70892	2.229	4.729	1.576333333	0.477676768	31305	0X7A49
1755	76.48078	2.191	4.691	1.563666667	0.473838384	31053	0X794D
1760	76.25411	2.152	4.652	1.550666667	0.46989899	30795	0X784B
1765	76.02898	2.112	4.612	1.537333333	0.465858586	30531	0X7743
1770	75.80545	2.071	4.571	1.523666667	0.461717172	30259	0X7633
1775	75.58358	2.028	4.528	1.509333333	0.457373737	29974	0X7516
1780	75.36342	1.982	4.482	1.494	0.452727273	29670	0X73E6
1785	75.14504	1.932	4.432	1.477333333	0.447676768	29339	0X729B
1790	74.92848	1.879	4.379	1.459666667	0.442323232	28988	0X713C
1795	74.71379	1.821	4.321	1.440333333	0.436464646	28604	0X6FBC
1800	74.50101	1.761	4.261	1.420333333	0.43040404	28207	0X6E2F
1805	74.29017	1.698	4.198	1.399333333	0.424040404	27790	0X6C8E
1810	74.08119	1.633	4.133	1.377666667	0.417474747	27360	0X6AE0
1815	73.874	1.569	4.069	1.356333333	0.411010101	26936	0X6938
1820	73.66851	1.505	4.005	1.335	0.404545455	26512	0X6790
1825	73.46466	1.444	3.944	1.314666667	0.398383838	26108	0X65FC
1830	73.26237	1.383	3.883	1.294333333	0.392222222	25705	0X6469
1835	73.06157	1.322	3.822	1.274	0.386060606	25301	0X62D5
1840	72.8622	1.263	3.763	1.254333333	0.38010101	24910	0X614E
1845	72.66419	1.203	3.703	1.234333333	0.374040404	24513	0X5FC1
1850	72.46745	1.144	3.644	1.214666667	0.368080808	24123	0X5E3B
1855	72.27176	1.084	3.584	1.194666667	0.362020202	23725	0X5CAD
1860	72.07689	1.023	3.523	1.174333333	0.355858586	23322	0X5B1A
1865	71.88261	0.962	3.462	1.154	0.34969697	22918	0X5986
1870	71.6887	0.9	3.4	1.133333333	0.343434343	22507	0X57EB
1875	71.49492	0.84	3.34	1.113333333	0.337373737	22110	0X565E
1880	71.30106	0.781	3.281	1.093666667	0.331414141	21720	0X54D8

Wavelength <i>nm</i>	Frequency MHz	Voltage <i>V_{Interpolated}</i>	True voltage <i>V_{RFDriver}</i>	DAC Voltage <i>V</i>	<i>V/V_{ref}</i>	Decimal Value	Hex. Value
1885	71.1069	0.724	3.224	1.074666667	0.325656566	21342	0X535E
1890	70.91231	0.67	3.17	1.056666667	0.32020202	20985	0X51F9
1895	70.71776	0.619	3.119	1.039666667	0.315050505	20647	0X50A7
1900	70.52385	0.571	3.071	1.023666667	0.31020202	20329	0X4F69
1905	70.33119	0.525	3.025	1.008333333	0.305555556	20025	0X4E39
1910	70.14033	0.481	2.981	0.993666667	0.301111111	19734	0X4D16

NOTE

Although the AOTF is capable of functioning till 2000 nm , the Variable Frequency Driver has a limiting range of $70 - 120\text{ MHz}$. Thus values beyond 1910 nm are not mapped. Specifications given by the manufacturer include plots of wavelength vs. frequency and frequency vs. voltage. Thus the values of voltage for corresponding wavelengths are interpolated herein. These interpolated voltages have an offset of 2.5 V . Thus a new column of true voltage is added after the interpolated voltage column as understandable from the above table. This true voltage column ranges from 2.981 to 7.364 V .

However, DAC of the Microcontroller, can produce a maximum of 3.3 V . Thus the true voltage is scaled down by a factor of 3 and tabulated as the expected output of the DAC of Microcontroller. The digital input need be given to the DAC is a sixteen bit hex value corresponding to the input voltage, taking 3.3 V as the reference voltage (V_{ref}). Thus the corresponding decimal values and hexadecimal values are computed and tabulated. $16\text{bit} = 2^{16} = 65,536$. Therefore for a value of 0.30111111 V , the corresponding decimal value is $19,734(65,536 \times 0.30111111 = 19734)$.

One can able to extract a model which could fit the above look up table and the characteristic curve, using machine learning libraries for curve fitting. However the model has to be validated for the fit it provides.

Bibliography

- [1] Colin N Banwell and Elaine M McCash. *Fundamentals of molecular spectroscopy*. McGraw-Hill London, 1983.
- [2] Heinz W Siesler, Yukihiko Ozaki, Satoshi Kawata, and H Michael Heise. *Near-infrared spectroscopy: principles, instruments, applications*. John Wiley & Sons, 2008.
- [3] Douglas A Skoog and Donald M West. *Principles of instrumental analysis*, volume 158. Saunders College Philadelphia, 1980.
- [4] Phil Williams and Karl Norris. *Near-infrared technology in the agricultural and food industries*. American Association of Cereal Chemists, Inc., 1987.
- [5] Brian C Smith. *Quantitative Spectroscopy: Theory and Practice: Theory and Practice*. Academic Press, 2003.
- [6] Derek Steele. Infrared spectroscopy: theory. *Handbook of Vibrational Spectroscopy*, 2006.
- [7] Antibonding molecular orbital, . URL https://en.wikipedia.org/wiki/Antibonding_molecular_orbital.
- [8] Electromagnetic spectrum, . URL https://en.wikipedia.org/wiki/Electromagnetic_spectrum.
- [9] Arno Bohm and Mark Loewe. *Quantum mechanics: foundations and applications*. Springer-Verlag New York, 1986.
- [10] Wavefunction, . URL <http://hyperphysics.phy-astr.gsu.edu/hbase/quantum/wvfun.html#c1>.
- [11] Hans Dekker. Classical and quantum mechanics of the damped harmonic oscillator. *Physics Reports*, 80(1):1–110, 1981.
- [12] Schrodinger equation, . URL <http://hyperphysics.phy-astr.gsu.edu/hbase/quantum/schr.html#c1>.
- [13] Properties of wavefunction, . URL <http://hyperphysics.phy-astr.gsu.edu/hbase/quantum/wvfun.html#c2>.
- [14] Constraints on wavefunction, . URL <http://hyperphysics.phy-astr.gsu.edu/hbase/quantum/qm.html#c4>.
- [15] Morse potential, . URL https://en.wikipedia.org/wiki/Morse_potential.
- [16] S Flügge, P Walger, and A Weiguny. A generalization of the morse potential for diatomic molecules. *Journal of Molecular Spectroscopy*, 23(3):243–257, 1967.
- [17] E Bright Wilson, John Courtney Decius, and Paul C Cross. *Molecular vibrations: the theory of infrared and Raman vibrational spectra*. Courier Corporation, 2012.

- [18] Quantum harmonic oscillator, . URL <http://hyperphysics.phy-astr.gsu.edu/hbase/quantum/hosc.html>.
- [19] Paul Geerlings, Didier Berckmans, and HP Figeys. The influence of electrical and mechanical anharmonicity on the vibrational transition moments of diatomic and polyatomic molecules. *Journal of molecular structure*, 57:283–297, 1979.
- [20] E Marechal and S Bratos. Infrared and raman spectra of hydrogen bonded liquids. effect of electrical anharmonicity on profiles of hydrogen-stretching bands. *The Journal of Chemical Physics*, 68(4): 1825–1828, 1978.
- [21] Kent Wiberg. Multivariate spectroscopic methods for the analysis of solutions. 2004.
- [22] Molecular vibration, . URL https://en.wikipedia.org/wiki/Molecular_vibration.
- [23] Degrees of freedom, molecular vibrations & infrared radiaition, . URL https://en.wikipedia.org/wiki/Raman_scattering.
- [24] Barbara Stuart. *Infrared spectroscopy*. Wiley Online Library, 2005.
- [25] Joyce A Wahr, Kevin K Tremper, Satwant Samra, and David T Delpy. Near-infrared spectroscopy: theory and applications. *Journal of cardiothoracic and vascular anesthesia*, 10(3):406–418, 1996.
- [26] J Rud Nielsen, V Thornton, and E Brock Dale. The absorption laws for gases in the infra-red. *Reviews of Modern Physics*, 16(3-4):307, 1944.
- [27] Christopher A Palmer, Erwin G Loewen, and RGL Thermo. *Diffraction grating handbook*. Newport Corporation Springfield, OH, 2005.
- [28] Acousto optics - physical principles. URL <http://www.acoustooptic.com/acousto-optic-principles.html>.
- [29] Acousto optics, . URL <http://en.wikipedia.org/wiki/Acousto-optics>.
- [30] Katherine Creath. Phase-measurement interferometry techniques. *Progress in optics*, 26(26):349–393, 1988.
- [31] Robert D Guenther, Duncan G Steel, and Leopold Bayvel. *Encyclopedia of modern optics*. Elsevier, 2005.
- [32] Acousto optic modulator, . URL http://en.wikipedia.org/wiki/Acousto-optic_modulator.
- [33] Dennis R Pape, Akis P Goutzoulis, and Sergei Viktorovich Kulakov. *Design and fabrication of acousto-optic devices*. M. Dekker, 1994.
- [34] IC Chang. Acoustooptic devices and applications. *IEEE transactions on sonics and ultrasonics*, 23(1):p2, 1976.
- [35] Norman J Berg and John N Lee. Acousto-optic signal processing: theory and implementation. In *New York, Marcel Dekker, Inc. (Optical Engineering. Volume 2)*, 1983, 496 p. No individual items are abstracted in this volume., volume 2, 1983.
- [36] MALVIN CARL Teich and BEA Saleh. Fundamentals of photonics. *Canada, Wiley Interscience*, page 3, 1991.
- [37] Acousto optic effect. URL http://www.mt-berlin.com/frames_ao/descriptions/ao_filters.htm.
- [38] Chieu D Tran. Acousto-optic devices: optical elements for spectroscopy. *Analytical chemistry*, 64(20): 971A–981A, 1992.

- [39] Aotf introduction. URL <http://www.olympusfluoview.com/theory/aotfintro.html>.
- [40] Gordon S Kino. *Acoustic waves: devices, imaging, and analog signal processing*, volume 107. Prentice-Hall Englewood Cliffs, NJ, 1987.
- [41] Jieping Xu and Robert Stroud. *Acousto-optic devices: principles, design, and applications*, volume 12. Wiley-Interscience, 1992.
- [42] Joan Vila Francés et al. Use of acousto-optic filters in imaging applications. a contribution to the smartspectra project. 2009.
- [43] ADRIANUS KOWEL. Acousto-optics-a review of fundamentals. *Proceedings of the IEEE*, 69(1), 1981.
- [44] Adrian Korpel. *Acousto-optics*, volume 57. CRC Press, 1996.
- [45] Non-linear optics, . URL http://en.wikipedia.org/wiki/Nonlinear_optics.
- [46] Narasimha S Prasad, Edward W Taylor, Sudhir Trivedi, Sue Kutcher, and Jolanta Soos. Space qualification issues in acousto-optic and electro-optic devices. In *Optical Engineering+ Applications*, pages 67130F–67130F. International Society for Optics and Photonics, 2007.
- [47] Mark Mitchell. Engauge digitizer-digitizing software. <http://digitizer.sourceforge.net/> [retrieved 2007], 2010.
- [48] Jean-Pierre Charras. " kicad: Gpl pcb suite".
- [49] Infrared detector, . URL http://en.wikipedia.org/wiki/Infrared_detector.
- [50] Antoni Rogalski. Infrared detectors: status and trends. *Progress in quantum electronics*, 27(2): 59–210, 2003.
- [51] Indium gallium arsenide, . URL http://en.wikipedia.org/wiki/Indium_gallium_arsenide.
- [52] Thermoelectric cooling, . URL https://en.wikipedia.org/wiki/Thermoelectric_cooling.
- [53] Transimpedance amplifier, . URL http://en.wikipedia.org/wiki/Transimpedance_amplifier.
- [54] True rms to dc converter. URL <http://pdf.datasheetcatalog.com/datasheet/analogdevices/AD536AKH+.pdf>.
- [55] Vitaly B Voloshinov, Konstantin B Yushkov, and Bogumil BJ Linde. Improvement in performance of a teo₂ acousto-optic imaging spectrometer. *Journal of Optics A: Pure and Applied Optics*, 9(4):341, 2007.
- [56] Joan Vila-Frances, Javier Calpe-Maravilla, Luis Gomez-Chova, and Julia Amoros-Lopez. Design of a configurable multispectral imaging system based on an aotf. *Ultrasonics, Ferroelectrics, and Frequency Control, IEEE Transactions on*, 58(1):259–262, 2011.
- [57] Joel Mobley, Brian M Cullum, Alan L Wintenberg, S Shane Frank, Robert A Maples, David L Stokes, and Tuan Vo-Dinh. Single-board computer based control system for a portable raman device with integrated chemical identification. *Review of scientific instruments*, 75(6):2016–2023, 2004.
- [58] Javier Calpe-Maravilla, Joan Vila-Frances, Emilio Ribes-Gomez, Vicente Duran-Bosch, Jordi Munoz-Mari, Julia Amoros-Lopez, Luis Gomez-Chova, and Enrique Tajahuerce-Romera. 400-to 1000-nm imaging spectrometer based on acousto-optic tunable filters. *Journal of Electronic Imaging*, 15(2): 023001–023001, 2006.
- [59] Govindaraj.R, Anil P.K, Ganesh.G, Anuj Nandi, and Prince Agarwal. An internal report of ceeri - experimental understanding and functional behavior of near infrared aotf spectrometer. June 2012.

- [60] Bismin Nisha, Ganesh.G, and Govindaraj.R. Aotf spectral data processing, principal component analysis on selected food and polymer samples a programming approach. 2013. URL <http://www.csirmadrascomplex.gov.in/JJ13.PDF>.
- [61] Celio Pasquini. Near infrared spectroscopy: fundamentals, practical aspects and analytical applications. *Journal of the Brazilian Chemical Society*, 14(2):198–219, 2003.
- [62] Paul Antony Gass. Acousto-optic devices and applications. 1991.
- [63] E Bouveresse and DL Massart. Standardisation of near-infrared spectrometric instruments: A review. *Vibrational Spectroscopy*, 11(1):3–15, 1996.
- [64] Yan Liu, Wensheng Cai, and Xueguang Shao. Standardization of near infrared spectra measured on multi-instrument. *Analytica chimica acta*, 836:18–23, 2014.
- [65] Andrei Drumea. Education in development of electronic modules using free and open source software tools. *HIDRAULICAĂI Magazine of Hydraulics, Pneumatics, Tribology, Ecology, Sensorics, Mechatronics*, (3-4):54–60, 2012.
- [66] Stuart Brorson. Circuit design on your linux box using geda. *Linux Journal*, 141(7), 2006.
- [67] C Medrano, I Plaza, M Castro, Francisco GarcíAa-Sevilla, JD Martínez-Calero, Josep Pou Felix, and M Corbalán. A review of electronic engineering design free software tools. In *Education Engineering (EDUCON), 2010 IEEE*, pages 1867–1871. IEEE, 2010.
- [68] John C Luciani Jr. Automated copying of schematics and pcb layouts. 2005.
- [69] Richard BALOGH. Using an open software for electronics and robotics.
- [70] G Goavec-Mérou and JM Friedt. Gnuradio as a general purpose digital signal processing environment. *FOSDEM (Bruxelles, 2014)*, 2014.
- [71] Attila Hidvégi. *FPGA-based Instrumentation for Advanced Physics Experiments*. Department of Physics, Stockholm University, 2011.
- [72] Shenghou Ma, Vuk Marojevic, Philip Balister, and Jeffrey H Reed. Porting gnu radio to multicore dsp+ arm system-on-chip—a purely open-source approach.
- [73] Yajie Ma, Mark Richards, Moustafa Ghanem, Yike Guo, and John Hassard. Air pollution monitoring and mining based on sensor grid in london. *Sensors*, 8(6):3601–3623, 2008.
- [74] Hock Beng Lim, Yong Meng Teo, Protik Mukherjee, Vinh The Lam, Weng Fai Wong, and Simon See. Sensor grid: integration of wireless sensor networks and the grid. In *Local Computer Networks, 2005. 30th Anniversary. The IEEE Conference on*, pages 91–99. IEEE, 2005.
- [75] M Pallikonda Rajasekaran, S Radhakrishnan, and P Subbaraj. Sensor grid applications in patient monitoring. *Future Generation Computer Systems*, 26(4):569–575, 2010.
- [76] Collimation optics,. URL <http://oceanoptics.com/product/84-uv-25-collimating-lens/>.
- [77] Laboratory grade fiber patch cord,. URL <http://oceanoptics.com/product/lab-grade-patch-cords/>.
- [78] Technical support manual of aotf & rf driver, 2011. URL <http://www.brimrose.com>.
- [79] Teledyne judson - specification of ingaas detector. Website, 2004. URL http://www.judsontechnologies.com/files/pdf/ingaas_shortform_dec2004_rev2.pdf.
- [80] Teledyne judson - specifications of preamplifier, thermoelectric cooler & temperature controller. Website, 2004. URL http://www.judsontechnologies.com/files/pdf/preamp_cooler_shortform_Feb2004.pdf.

Index

- About the Report, v
- Absorbance, 17
- Absorbance Spectra, 18
- Acoustic Power, 26
- Anti-bonding, 4
- AOTF Anatomy, 27
- AOTF Specification, 71
- Arduino, 50
- ASPU, 39
- Beer-Lambert's Law, 16
- Bragg Angle, 25
- Bragg Cell, 23
- Bragg Diffraction, 23
- Bragg Regime, 26
- Bragg's law, 22
- Chemical Bonds, 4
- Collisions, 19
- Degrees of Freedom, 12
- Democratic License, 50
- Disassociation Energy, 7
- Dual nature of light, 1
- Efficiency, 25
- Elasto-Optic Effect, 27
- Electrical Anharmonicity, 11
- EM Spectrum, 5
- Embedded Task, 48
- Energy Levels, 11
- Extinction Ratio, 25
- Frequency Shift, 26
- InGaAs Detector, 40
- InGaAs Specification, 73
- Integrated Instrument, 69
- License, i
- LUT Generation, 38
- Matter & Energy interaction, 3
- Mechanical Anharmonicity, 10
- Modulation Bandwidth, 25
- Molecular Vibration, 12
- Morse Potential, 7
- Notch Filter, 41
- Origin of EM Radiation, 3
- Oscillators, 3
- Perturbation, 10
- Phase-matching, 28
- Pre-amplifier Specification, 79
- Quality Factor, 26
- Quanta, 6
- Quantum Anharmonic Oscillator, 10
- Quantum Harmonic Oscillator, 9
- Raman-Nath Regime, 26
- Resolution, 26
- RF Bandwidth, 25
- RF Power, 26
- Rise Time, 25
- Schrodinger Equation, 6
- Separation Angle, 25
- Signal Flow, 35
- Spectrophotometer, 1
- Spectroscopy, 1
- Supervisory System, 52
- TE Cooler Specification, 75
- Thermoelectric Cooler, 40
- Transimpedance Amplifier, 40
- Wave Vector, 28
- Wavefunction, 6
- Wavelength Selection, 37
- Wavelength selection LUT, 83
- Web Technologies, 54

Published Works

- R.Govindaraj et al, AOTF based spectrometer for industrial measurement application, Proceedings (abstract) of The 2nd Asian NIR Symposium (ANS2010), p40-41, 2010, China.
- N.Bismin Nisha, G.Ganesh & R.Govindaraj, AOTF spectral data processing, principal component analysis of selected food & polymer samples – a programming approach at the National conference on Emerging Trends in Modern Electronics & Biomedical Engineering, held at Jerusalem Engineering College, Chennai on 3rd May 2013.
- R.Govindaraj, invited talk on Role of Tellurium-Dioxide (TeO_2) Crystal in Acousto-Optics for Wavelength Tuning, XVII National Seminar on Crystal Growth (NSCG-2013), Organized by Department of Physics, Anna University, 9-11th January 2013, Chennai.
- R.Govindaraj and G.Ganesh, Experimental Characterization of Fiber coupled NIR-AOTF for Wavelength Tuning, [Communicated to Springer Journal of Optics]
- R.Govindaraj and G.Ganesh, Development and Integration of an AOTF based NIR Spectrophotometer, [Communicated to Springer Journal of Optics]
- G.Ganesh and R.Govindaraj, Design and Development of an Analog Signal Processing Unit for AOTF based NIR Spectrophotometer, [Communicated to Journal of Circuits, Systems & Computers - WSP]
- Debanjum Singh Solanky, G.Ganesh & R.Govindaraj, Integration of Web and Embedded Technologies for AOTF Spectrophotometer Control and Data Acquisition, [Communicated to Journal of Circuits, Systems & Computers - WSP]
- G.Ganesh, Debanjum Singh Solanky & R.Govindaraj, Collaborative peer production as an alternative to hierarchical internet based business systems, [Communicated to arXiv]
- G.Ganesh, Debanjum Singh Solanky & R.Govindaraj, Knowledge ecosystem for creative commons and communities using free & distributed technologies, [Communicated to arXiv]

About the Authors

Govindaraj Rajamanickam received his M.Sc. degree in Physics from St.Joseph's College(Autonomous), Trichy, Tamil Nadu, India in 1984. He then received his Ph.D degree from University of Madras, Tamil Nadu, India in the year 1996. He worked as Project Scientist in CSIR-Central Electronics Engineering Research Institute (CEERI), CSIR Madras Complex, Taramani, Chennai-600113, between March 1989 and July 1994. Since August 1994, he is working in CEERI as Scientist in the field of Electronic Instrumentation. His current research interests include optical sensors, imaging spectroscopy, image processing and machine vision systems for industrial applications.



Research Work Details:

Arxiv Author Identifier: http://arxiv.org/author_id

ORCID ID : 0000-0002-6389-7826

Public Record URL: <http://orcid.org/0000-0002-6389-7826>

Email ID: rajagovind@hotmail.com

Contact no.: +919444227199



Ganesh Gopal received his B.E. degree in Electronics & Communication Engineering from Pallavan College of Engineering(Affl. to Anna University), Kancheepuram, Tamil Nadu, India in 2009. He then received his P.G diploma in Industrial Automation from DOEACC, Calicut, Kerala, India in the year 2010. He worked as Assistant Engineer in DOEACC between September 2010 and March 2011. He worked as Project Assistant Level II in CSIR-Central Electronics Engineering Research Institute CEERI-CMC, India, between 2011 and 2012. He then served his position as Research Intern in CEERI-CMC, India, between 2012 and 2014.



Research Work Details:

Arxiv Author Identifier: http://arxiv.org/a/gopal_g_1

ORCID ID : 0000-0002-7282-694X

Public Record URL: <http://orcid.org/0000-0002-7282-694X>

Email ID: 31gane@gmail.com

Contact no.: +919952524267

